ALIANA CARVALHO VAIRINHOS

HOW DOES THE PRESENCE OF NANOPLASTICS AFFECT HUMAN LUNG AND GUT CELL LINES?

UNIVERSIDADE DO ALGARVE

Faculdade de Ciências e Tecnologia

2023

ALIANA CARVALHO VAIRINHOS

HOW DOES THE PRESENCE OF NANOPLASTICS AFFECT HUMAN LUNG AND GUT CELL LINES?

Mestrado em Biotecnologia

Trabalho realizado sobre a orientação de:

Professora Doutora Deborah M. Power

Doutora Rute C. Félix

UNIVERSIDADE DO ALGARVE

Faculdade de Ciências e Tecnologia

2023

How does the presence of nanoplastics affect human lung and gut cell lines?

Declaração de autoria de trabalho

Declaro ser a autora deste trabalho, que é original e inédito. Autores e trabalhos consultados estão devidamente citados no texto e constam da listagem de referências incluída.

_____

(Aliana Carvalho Vairinhos)

Acknowledgements

I would like to specially thank to my supervisors Doutora Rute C. Félix and Professora Doutora Deborah M. Power for all the dedication and time given throughout this journey.

I'm also thankful to my lab colleagues, Maoxiao Peng and Youssef Elamine, for introducing me to the laboratory and all the help in the experiments.

A special thanks to my lab partner and friend, Lelde Hermane, for all the support and friendship.

I would also like to thank to my family and friends, particularly my parents and siblings, for all their love, support, and patience during my academic journey.

Resumo

Os plásticos são materiais sintéticos que resultam da combinação de polímeros e têm inúmeras aplicações na indústria farmacêutica, alimentar, automóvel, tecnológica e outras. Estes materiais estão presentes em todas as atividades do nosso dia-a-dia, e a sua produção tem vindo sempre a aumentar, atingindo as 390,7 milhões de toneladas métricas em 2021. Os plásticos mais comumente produzidos incluem polietileno, polipropileno, polivinilcloreto, polietileno tereftalato, poliuretano e poliestireno. Após serem descartados, os produtos plásticos ficam expostos a diversos fatores ambientais, como a radiação ultravioleta, precipitação, vento, oxidação, fatores mecânicos e biológicos que causam a sua degradação em partículas mais pequenas. Estas partículas são classificadas em microplásticos quando possuem uma dimensão entre 1 μm e 5 mm, ou como nanoplásticos quando têm um tamanho entre 1 e 1000 *n*m. Estas partículas são conhecidas como micro- e nanoplásticos (MNPs) secundários. Existem também os micro- e nanoplásticos primários, que são partículas propositadamente produzidas pela indústria.

A intensa produção, utilização e descarte destes materiais resultam na disseminação de partículas de plástico por todo o ambiente. Estas partículas podem ser encontradas nos oceanos, praias, neve, ar, solos, diversas espécies e até mesmo em órgãos humanos. De facto, os efeitos de micro- e nanoplásticos já foram observados em diversas espécies marinhas, como bivalves (*Mytillus galloprovincialis*), crustáceos (*Macrobrachium niponense)* e peixes (*Danio rerio* e *Oreochromis niloticus*), entre outras. Nestas espécies, os MNPs têm sido facilmente internalizados, afetando o metabolismo e a expressão de vários genes, incluindo genes relacionados com a atividade antioxidante que podem levar à apoptose celular. A presença de MNPs nos solos pode ainda alterar o pH, estimular a biodisponibilidade de metais pesados como o cádmio e provocar alterações nas comunidades microbiotas, com consequências no seu proteoma.

Os seres humanos estão expostos aos MNPs através de três vias principais: ingestão, através do consumo de alimentos contaminados; inalação, por exposição a aerossóis contendo partículas; e absorção, através da pele, pelo uso de produtos cosméticos que contêm MNPs. Estudos realizados em várias linhas celulares humanas têm demonstrado que os MNPs têm a capacidade de penetrar nas células, reduzir a viabilidade celular, induzir a produção de espécies reativas de oxigénio e respostas inflamatórias e até mesmo provocar efeitos genotóxicos.

Sendo a inalação uma das principais vias de exposição, faz sentido que vários microplásticos de polipropileno e polietileno tereftalato tenham sido identificados em amostras de tecido de pulmão humano. É, portanto, necessário estudar o efeito destas partículas em células de pulmão. Nesse contexto, as células A549, derivadas de células alveolares epiteliais de tipo II, são frequentemente utilizadas para avaliar os efeitos dos MNPs. De facto, foi demonstrado que estas células conseguem internalizar as partículas através de endocitose mediada por caveolina e/ou clatrina e fagocitose, para nanoplásticos de menor e maior dimensão, respetivamente. Consequentemente, a presença destas partículas resultou na redução da viabilidade celular, com efeitos adversos e genotóxicos nas mitocôndrias. Por sua vez, a ingestão de MNPs pode ser avaliada recorrendo às células Caco-2, que são células epiteliais de adenocarcinoma do colón. Estas células foram expostas a micro- e nanoplásticos de diferentes dimensões, que demonstraram a capacidade destas partículas de entrar nas células e reduzir a viabilidade celular de forma dependente da concentração. Além disso, estes microplásticos (MPs) também causaram a disrupção do potencial de membrana mitocondrial e provocaram danos genotóxicos.

Apesar da crescente atenção que esta problemática tem recebido nos últimos anos, existe ainda uma lacuna de conhecimento em relação aos efeitos dos MNPs em células humanas, sendo que a maioria utiliza concentrações de partículas que não correspondem à real exposição a que estamos sujeitos. Nesse sentido, este trabalho teve como objetivo principal investigar os efeitos de micro- e nanoplásticos de poliestireno (50, 500 e 1000 *n*m) em células humanas A549 e Caco-2, na viabilidade, proliferação, migração celular, stress oxidativo e adesão celular. Em primeiro lugar, foi realizada uma caracterização das duas linhas celulares que seriam utilizadas, tendo em consideração as curvas de crescimento e a morfologia celular, incluindo o núcleo, actina, tubulina e mitocôndrias. Em segundo lugar, realizou-se o estudo da viabilidade celular na presença de MNPs, que revelou um efeito citotóxico dependente do tamanho e concentração das partículas em ambas as linhas celulares. Relativamente à proliferação celular, nas células A549, observou-se um efeito estimulatório no crescimento, mas sem uma relação clara com o tamanho ou concentração dos MNPs. No entanto, nas células Caco-2, houve uma redução da proliferação nas concentrações mais elevadas das partículas de maior dimensão (500 e 1000 *n*m). No estudo da migração celular, foi utilizado o ensaio *scratch*, no qual as células de pulmão expostas a MNPs migraram mais rapidamente do que as células não expostas. Por outro lado, nas células Caco-2 expostas a partículas de 50 e 1000 *n*m, a capacidade migratória foi afetada, levando mais tempo a recuperar do *scratch*. A produção de espécies reativas de oxigénio parece

ser afetada tanto nas células de pulmão quanto nas células de intestino, mas de formas diferentes. Enquanto os nanoplásticos (NPs) de 50 e 500 *n*m levaram a um aumento da produção com o aumento da concentração, o contrário foi observado para os microplásticos, nas células A549. Nas células Caco-2, apenas foram observados aumentos na produção para algumas concentrações de todos os tamanhos. Quanto à morfologia das células, não foram observadas alterações visíveis no citoesqueleto, mitocôndrias e núcleos das células tratadas com MNPs. Relativamente à adesão celular, as células de pulmão expostas a NPs de 50 e 500 *n*m aderiram mais rapidamente que o controlo, assim como as células de intestino tratadas com 500 e 1000 *n*m. Por sua vez, no ensaio de recuperação de uma ferida feita eletricamente, enquanto as A549 expostas às partículas recuperaram mais rapidamente relativamente às células controlo, as Caco-2 tratadas demoraram mais tempo e não voltaram a adquirir a resistência inicial. Os estudos realizados demonstraram que os micro- e nanoplásticos de poliestireno provocam alterações no comportamento e viabilidade de células A549 e Caco-2, para as concentrações estudadas. Futuramente, serão realizados mais ensaios, incluindo uma análise metabolómica, estudos enzimáticos, como a fosfatase e estudos eletrofisiológicos mais detalhados. Adicionalmente estão a ser considerados ensaios com longos períodos de exposição aos MNPs e outros tipos de plásticos.

Palavras-chave: microplástico, nanoplástico, poliestireno, células de pulmão, células do intestino

Abstract

Plastics are synthetic materials that result from the combination of polymers and have several industrial applications. However, they represent an emerging global threat to the environment and humanity. One particular concern is the presence of micro- and nanoplastics (MNPs), which are particles that result from the degradation of plastic debris. Reports have already described the presence of MNPs in bivalves, fish, and even humans. Despite the growing awareness about this issue, there are still few studies investigating the effects of MNPs on human cells. Moreover, most of the existing studies use particles' concentrations that do not accurately reflect the current environment reality. In an attempt to fill this gap, the present project investigated the effects of MNPs on human lung adenocarcinoma cells (A549) and human colon adenocarcinoma cells (Caco-2). These cell lines were chosen since they represent organs that are directly exposed to MNPs in organisms. The results showed that in both cell lines polystyrene MNPs exhibited a size and concentration-dependent cytotoxic effect. In Caco-2 cells treated with 500 and 1000 *n*m particles, cell proliferation was reduced. Furthermore, an increase in cell migration was observed in A549 cells compared to the control cells. Caco-2 cells exposed to 50 and 1000 *n*m took more time to recover from a scratch, indicating MNPs impaired cellular migration. MNPs appeared to affect the mechanism of ROS production but no effect was observed on the structural integrity of key cellular components (nuclei, actin, mitochondria, or tubulin) in both cell lines. Electrophysiological assays revealed that the presence of MNPs enhanced cell adhesion for both cell lines but significantly reduced the wound recovery capacity of Caco-2 cells. The assays performed revealed that MNPs altered cell behaviour and viability in A549 and Caco-2 cells, but further studies are necessary to comprehend the mechanisms underlying such effects.

Keywords: microplastic, nanoplastic, polystyrene, lung cells, gut cells

Table of contents

Acknowledgements ..... **iv**
Resumo ..... **v**
Abstract ..... **viii**
List of Figures ..... **xi**
List of abbreviations ..... **xviii**
1. Introduction **1**
1.1 Plastics in the environment 1
1.2 Micro- and nanoplastics effects in the environment 2
1.2.1 Micro- and nanoplastics effects on marine species 3
1.2.2 Micro- and nanoplastics effects in soil and microorganisms 4
1.3 Micro- and nanoplastics effects on human cell lines 5
1.4 Plastics in human lung adenocarcinoma cells A549 6
1.4.1 Micro- and nanoplastics uptake by A549 cells 7
1.4.2 Micro- and nanoplastics effects on A549 cells 8
1.5 Plastics in human colon adenocarcinoma cells Caco-2 9
1.5.1 Micro- and nanoplastics uptake by Caco-2 cells 10
1.5.2 Micro- and nanoplastics effects on Caco-2 cells 10
2. Objectives **13**
3. Materials and methods **14**
3.1 Cell lines 14
3.2 Polystyrene micro- and nanoparticles 14
3.3 Cell culture maintenance 14
3.4 Growth curve of A549 and Caco-2 cells 14
3.5 Characterization of cell morphology of A549 and Caco-2 15
3.6 PSMNP uptake by A549 and Caco-2 cells 16
3.7 PSMNP effects on cell viability 17
3.8 PSMNP effects on cell migration 18
3.9 PSMNP effects on cell proliferation 18
3.10 PSMNP effects on oxidative stress 18
3.11 PSMNP effects on cell morphology 19
3.12 PSMNP effects on cell adhesion assessed using ECIS 19
3.13 PSMNP effects on wound recovery assessed using ECIS 20
3.14 Statistical analysis 21
4. Results **22**
4.1 A549 cells **22**
4.1.1 Characterization of A549 cells 22

4.1.2 Uptake of PSMNPs by A549 cells 24
4.1.3 PSMNP effects on A549 cell viability 25
4.1.4 PSMNP effects on A549 cell proliferation 26
4.1.5 PSMNP effects on A549 migration 27
4.1.6 PSMNP effects on A549 cells oxidative stress 29
4.1.7 PSMNP effects on A549 cells morphology 30
4.1.8 PSMNP effects on cell adhesion assessed using ECIS 31
4.1.9 PSMNP effects on wound recovery assessed using ECIS 32
4.2 Caco-2 cells 33
4.2.1 Characterization of Caco-2 cells 33
4.2.2 Uptake of PSMNPs by Caco-2 cells 35
4.2.3 PSMNP effects on Caco-2 cell viability 36
4.2.4 PSMNP effects on Caco-2 cell proliferation 37
4.2.5 PSMNP effects on Caco-2 migration 38
4.2.6 PSMNP effects on Caco-2 oxidative stress 39
4.2.7 PSMNP effects on Caco-2 morphology 40
4.2.8 PSMNP effects on cell adhesion assessed using ECIS 42
4.2.9 PSMNP effects on wound recovery assessed using ECIS **..... 43**
5. Discussion 44
6. Conclusion and future perspectives 49
References 50
Annexes 60

List of Figures

Figure 1 - Image of adherent A549 cells. The scale bar represents 50 μm. Photo was taken with a Leica DM IL microscope coupled to a Visicam Pro 20C digital camera (ampliation x100).. 7

Figure 2 - Image of adherent Caco-2 cells. The scale bar represents 50 μm. Photo was taken with a Leica DM IL microscope coupled to a Visicam Pro 20C digital camera (ampliation x100)..... 10

Figure 3 – Representative images of adherent A549 cells at low density (A) and high density (B). The scale bar represents 100 μm. Photos were taken with a Leica DM IL microscope coupled to a Visicam PRO 20C digital camera (ampliation x 100). 22

Figure 4 – Representative images of adherent A549 cells at different ampliations: 40x (A), 100x (B), 200x (C) and 400x (D). Scales bars represents 50 μm. Photos were taken with a Leica DM IL microscope coupled to a Visicam PRO 20C digital camera. 22

Figure 5 - Growth curve of A549 cells. Data is represented as a smooth fit of the average of the number of cells per well (the assay was performed with 4 replicates)..... 23

Figure 6 – Representative images of A549 cells. Nuclei is always represented in blue. In (A) and (C), the red colour represents mitochondria, in (D) and (F) the green colour represents alpha-tubulin and in (G) and (H) the red colour represents actin. Scale bars represent 50 μm. Photos were taken with a Zeiss Axio Vert. A1 with a Axiocam 202 mono camera (ampliation 400x) and were analysed with ImageJ version 1.53t using ImageJ software for image overlay. 23

Figure 7 – Representative images of A549 cells after 72h exposure to 1000 nm regular PSMPs at a concentration of 0 (A) and 1 μg/mL (B) and 1000 nm green-fluorescent PSMPs at a concentration of 0 (C) and 1 μg/mL (D). Co-localization of nuclei (blue) and actin (red). The scale bar represents 50 μm. Photos were taken with a Leica DM IL microscope coupled to a Visicam PRO 20C digital camera (ampliation 400x) using ImageJ software for image overlay. 24

Figure 8 – Representative orthogonal view of A549 cells exposed to 0 (A and B) and 1 μg / mL green-fluorescent 1000 *n*m PSMPs for 72 hours. Co-localization of actin (red), nuclei (blue) and PSMPs (green) is evident. Scale bars represent 20 *n*m. Z-stack 3D pictures were taken with a Zeiss 1 LSM 710 confocal microscope with Airyscan and analysed with Zeiss Zen 8 Lite (orthogonal view). 25

Figure 9 - Cell viability of A549 cells after the exposure to 50, 500 and 1000 *n*m PSMNPs at concentrations ranging from 0 to 10 μg/mL after 72 h of exposure. Data is represented as the

percentage of living cells relative to the untreated control ± SEM (the assay was performed with 4 replicates and 3 independent experiments). A one-way ANOVA with a Tukey's Multiple Comparison test was used for the statistical analysis. Statistical analysis was performed with GraphPad Prism 8.4.2 and significance is indicated in the graph by *$p < 0.05$, **$p < 0.01$, ***$p < 0.001$ and ****$p < 0.0001$..... 26

Figure 10 - A549 cell proliferation after the exposure to 50 (A), 500 (B) and 1000 *n*m (C) PSMNPs at concentrations ranging from 0.01 to 1 μg/mL for 72 hours. Data is represented as the number of cells per well ± SEM (the assay was performed with 3 replicates and 3 independent experiments). A two-way ANOVA with Tukey's Multiple Comparison test was used for the statistical analysis. Statistical analysis was performed with GraphPad Prism 8.4.2 and significance is indicated in the graphs by *$p < 0.05$, **$p < 0.01$, ***$p < 0.001$ and ****$p < 0.0001$..... 27

Figure 11 - A549 cells scratch assay: (A), (C) and (E) represent the scratch recovery area (percentage) of A549 cells after the exposure to 50, 500 and 1000 nm PSMNPs, respectively, at concentrations ranging from 0 to 1 μg/mL, measured at 0, 4, 8, 12, 24, 28 and 48 hours in relation to the area immediately after the scratch (100 %). Data is represented as the percentage of scratch wound relative to the initial scratch ± SEM (the assay was performed with 3 replicates and 3 independent experiments). A two-way ANOVA with Tukey's Multiple Comparison test was used for the statistical analysis. Statistical analysis was performed with GraphPad Prism 8.4.2 and significance is indicated in the graph as *p < 0.05, **p < 0.01. (B), (D) and (F) are representative images showing the progression of the scratch recovery from 0 to 24 hours in control cells and in cells exposed 50, 500 and 1000 nm, respectively. Scale bars represent 100 μm. Photos were taken with a Leica DM IL microscope coupled to a Visicam PRO 20C digital camera (ampliation 40x) using ImageJ measurement tool..... 28

Figure 12 - Images of the scratch area provoked in a A549 cells monolayer and exposed for 72 hours to regular PSMNPs at concentrations of 0 (A-D) and 1 (E-H for 50 *n*m and I-L for 1000 *n*m particles). Co-localization of alpha-tubulin (green), actin (red) and nuclei (blue) is evident. Images are representative of control cells and 50 and 1000 *n*m treated cells at 12 h after scratching the confluent cell layer. Scale bars represent 50 *n*m. Photos were taken with a Zeiss Axio Vert. A1 coupled to a Axiocam 202 mono camera (ampliation 400x) and analysed with ImageJ 1.53t using ImageJ software for image overlay..... 29

Figure 13 - ROS formation by A549 cells after their exposure to 0, 50, 500 and 1000 *n*m PSMNPs at a concentration of 0 to 10 μg/mL after 72 h of exposure time. Data is represented as the percentage of living cells relative to the untreated control ± SEM (the assay was

performed with 3 replicates and 2 independent experiments). A one-way ANOVA with Tukey's Multiple Comparison test was used for the statistical analysis. Statistical analysis was performed with GraphPad Prism 8.4.2 and significance is indicated in the graph by *$p < 0.05$ and ****$p < 0.0001$. 30
Figure 14 – Representative images of A549 control and 1000 *n*m treated cells at 400x (A-C and D-F, respectively) and 1000x ampliation (G-I and J-L, respectively). Co-localization of mitochondria (red) and nuclei (blue) is evident. Scale bars represent 50 μm. Photos were taken with a Zeiss Axioscope 5 coupled to an Axiocam 202 mono camera and analysed with ImageJ version 1.53t using ImageJ software for image overlay. 31
Figure 15 – Representative images of A549 control and 1000 *n*m treated cells at 400x (A-C and D-F, respectively) and 1000x ampliation (G-I and J-L, respectively). Co-localization of alpha-tubulin (green) and nuclei (blue) is evident. Scale bars represent 50 μm. Photos were taken with a Zeiss Axioscope 5 coupled to an Axiocam 202 mono camera and analysed with ImageJ version 1.53t using ImageJ software for image overlay. 31
Figure 16 - Electrical resistance of a confluent A549 cell monolayer exposed to 50, 500 and 1000 nm PSMNPs at concentrations ranging from 0 to 1 μg / mL, measured at 4000 Hz. Data is represented as the average resistance of one experiment with two replicates for each treatment group. A one-way ANOVA with Tukey's Multiple Comparison test was used for the statistical analysis of the first 24 hours of the assay. Statistical analysis was performed with GraphPad Prism 8.4.2 and significant differences are indicated in the graph as ****p < 0.0001. 32
Figure 17 – Electrical resistance of a confluent A549 cell monolayer exposed to 50, 500 and 1000 *n*m PSMNPs at concentrations of 0 or 1 μg / mL after an electrical wound was inflicted. Data is represented as the average resistance of one experiment with two replicates for each treatment group. A one-way ANOVA with Tukey's Multiple Comparison test was used for the statistical analysis of between the timepoints 24-36 hours. Statistical analysis was performed with GraphPad Prism 8.4.2 and significant difference are noted in the graph by **$p < 0.1$ and ****$p < 0.0001$. 33
Figure 18 – Representative images of adherent Caco-2 cells at low density (A) and high density (B). The scale bar represents 100 μm. Photos were taken with a Leica DM IL microscope coupled to a Visicam PRO 20C digital camera (ampliation x 100). 33
Figure 19 – Representative images of adherent Caco-2 cells at different ampliations: 40x (A), 100x (B), 200x (C) and 400x (D). Scale bars represent 50 μm. Photos were taken with a Leica DM IL microscope coupled to a Visicam PRO 2. 33

Figure 20 - Growth curve of Caco-2 cells. Data is represented as a smooth fit of the average of the number of cells per well (the assay was performed with 4 replicates)..... 34
Figure 21 – Representative images of Caco-2 cells. Nuclei is always represented in blue. In (A) and (C), the red colour represents mitochondria, in (D) and (F) the green colour represents alpha-tubulin and in (G) and (H) the red colour represents actin. Scale bars represent 50 μm. Photos were taken with a Zeiss Axio Vert. A1 with a Axiocam 202 mono camera (ampliation 400x) and were analysed with ImageJ version 1.53t using ImageJ software for image overlay. 35
Figure 22 – Representative images of Caco-2 cells after 72h exposure to 1000 *n*m regular PSMPs at a concentration of 0 (A) and 1 μg/mL (B) and 1000 *n*m green-fluorescent PSMPs at a concentration of 0 (C) and 1 μg/mL (D). Co-localization of nuclei (blue) and actin (red). The scale bar represents 50 μm. Photos were taken with a Leica DM IL microscope coupled to a Visicam PRO 20C digital camera (ampliation 400x) using ImageJ software for image overlay. 35
Figure 23 – Representative orthogonal view of the confocal microscopy images of Caco-2 cells exposed to 0 (A and B) and 1 μg / mL green-fluorescent 1000 *n*m PSMPs for 72 hours. Co-localization of actin (red), nuclei (blue) and PSMPs (green) is evident. Scale bars represent 20 *n*m. Z-stack 3D pictures were taken with a Zeiss 1 LSM 710 confocal microscope with Airyscan and analysed with Zeiss Zen 8 Lite (orthogonal view). 36
Figure 24 - Cell viability of Caco-2 cells after the exposure to 50, 500 and 1000 *n*m PSMNPs at concentrations ranging from 0 to 10 μg/mL after 72 h of exposure. Data is represented as the percentage of living cells relative to the untreated control ± SEM (the assay was performed with 4 replicates and 3 independent experiments). A one-way ANOVA with a Tukey's Multiple Comparison test was used for the statistical analysis. Statistical analysis was performed with GraphPad Prism 8.4.2 and significance is indicated in the graph with * and denotes $p < 0.05$. 37
Figure 25 – Caco-2 cell proliferation after the exposure to 50 (A), 500 (B) and 1000 *n*m (C) PSMNPs at concentrations ranging from 0.01 to 1 μg/mL for 72 hours. Data is represented as the number of cells per well ± SEM (the assay was performed with 3 replicates and 3 independent experiments). A two-way ANOVA with Tukey's Multiple Comparison test was used for the statistical analysis. Statistical analysis was performed with GraphPad Prism 8.4.2 and significance is indicated in the graphs by *$p < 0.05$, **$p < 0.01$, ***$p < 0.001$ and ****$p < 0.0001$. 38

Figure 26 – Caco-2 cells scratch assay: (A), (C) and (E) represent the scratch recovery area (percentage) of Caco-2 cells after the exposure to 50, 500 and 1000 *n*m PSMNPs, respectively, at concentrations ranging from 0 to 1 μg/mL, measured at 0, 6, 12, 24, 30 and 48 hours in relation to the area immediately after the scratch (100 %). Data is represented as the percentage of the repaired scratch area relative to the initial scratch area ± SEM (the assay was performed with 3 replicates and 3 independent experiments). A two-way ANOVA with Tukey's Multiple Comparison test was used for the statistical analysis. Statistical analysis was performed with GraphPad Prism 8.4.2 and significance is indicated in the graphs as *$p < 0.05$, **$p < 0.01$. (B), (D) and (F) are representative images showing the progression of the scratch recovery from 0 to 24 hours in control cells and in cells exposed to 50, 500 and 1000 *n*m, respectively. Scale bars represent 100 μm. Photos were taken with a Leica DM IL microscope coupled to a Visicam PRO 20C digital camera (ampliation 40x) using the ImageJ measurement tool. 39

Figure 27 - ROS formation by Caco-2 cells after their exposure to 0, 50, 500 and 1000 *n*m PSMNPs at concentrations ranging from 0 to 10 μg/mL after 72 h of exposure time. Data is represented as the percentage of living cells relative to the untreated control ± SEM (the assay was performed with 3 replicates and 2 independent experiments). A one-way ANOVA with Tukey's Multiple Comparison test was used for the statistical analysis. Statistical analysis was performed with GraphPad Prism 8.4.2 and significantly different groups are identified with ***** and correspond to $p < 0.05$. 40

Figure 28 – Representative images of Caco-2 control and 1000 nm treated cells at 400x (A-C and D-F, respectively) and 1000x ampliation (G-I and J-L, respectively). Co-localization of mitochondria (red) and nuclei (blue) is evident. Scale bars represent 50 μm. Photos were taken with a Zeiss Axioscope 5 coupled to an Axiocam 202 mono camera and analysed with ImageJ version 1.53t using ImageJ software for image overlay..... 41

Figure 29 – Representative images of Caco-2 control and 1000 *n*m treated cells at 400x (A-C and D-F, respectively) and 1000x ampliation (G-I and J-L, respectively). Co-localization of alpha-tubulin (green) and nuclei (blue) is evident. Scale bars represent 50 μm. Photos were taken with a Zeiss Axioscope 5 coupled to an Axiocam 202 mono camera and analysed with ImageJ version 1.53t using ImageJ software for image overlay. 42

Figure 30 - Electrical resistance of a confluent Caco-2 cell monolayer exposed to 50, 500 and 1000 *n*m PSMNPs at concentrations ranging from 0 to 1 μg / mL, measured at 4000 Hz. Data is represented as the average resistance of one experiment with two replicates for each treatment group. A one-way ANOVA with Tukey's Multiple Comparison test was used for the statistical

analysis of the first 48 hours of the assay. Statistical analysis was performed with GraphPad Prism 8.4.2 and significant differences are indicated in the graph as *$p < 0.0001$. 43
Figure 31 – – Electrical resistance of a confluent Caco-2 cell monolayer exposed to 50, 500 and 1000 *n*m PSMNPs at concentrations of 0 or 1 μg / mL after an electrical wound was inflicted. Data is represented as the average resistance of one experiment with two replicates for each treatment group. A one-way ANOVA with Tukey's Multiple Comparison test was used for the statistical analysis between the timepoints 24-36 hours of the assay. Statistical analysis was performed with GraphPad Prism 8.4.2 and significantly different treatments are indicated in the graph using ** or **** for a $p < 0.1$ and $p < 0.0001$, respectively. 43
Supplementary figure 1 – Representative images of A549 cells after 72h exposure to 500 nm regular PSMPs at a concentration of 0 (A), 1 (B) and 10 μg/mL (C) and 500 nm green-fluorescent PSMPs at a concentration of 0 (D), and 1 μg/mL (E). Co-localization of actin (red) and nuclei (blue). Scale bars represent 50 μm. Photos were taken with a Leica DM IL microscope coupled to a Visicam PRO 20C digital camera (ampliation 400x) and analysed with ImageJ version 1.53t using ImageJ software for image overlay..... 60

Supplementary figure 2 – Representative images of A549 cells after 72h exposure to 1000 nm regular PSMPs at a concentration of 0 (A), 1 (B), 10 (C) and 100 μg/mL (D) and 1000 nm green-fluorescent PSMPs at a concentration of 0 (E), 1 (F), 10 (G) and 100 μg/mL (H). Co-localization of actin (red) and nuclei (blue). Scale bars represent 50 μm. Photos were taken with a Leica DM IL microscope coupled to a Visicam PRO 20C digital camera (ampliation 400x) and analysed with ImageJ version 1.53t using ImageJ software for image overlay..... 60

Supplementary figure 3 – Representative images of A549 cells treated with 50 nm at 400x ampliation (A-C). Co-localization of mitochondria (red) and nuclei (blue) is evident. The scale bar represents 50 μm. Photos were taken with a Zeiss Axioscope 5 coupled to a Axiocam 202 mono camera and analysed with ImageJ version 1.53t using ImageJ software for image overlay.....61

Supplementary figure 4 – Representative images of A549 cells treated with 50 nm at 400x ampliation (A-C). Co-localization of alpha-tubulin (green) and nuclei (blue) is evident. The scale bar represents 50 μm. Photos were taken with a Zeiss Axioscope 5 coupled to a Axiocam 202 mono camera and analysed with ImageJ version 1.53t using ImageJ software for image overlay.....61

Supplementary figure 5 – Representative images of Caco-2 cells after 72h exposure to 500 nm green-fluorescent PSMPs at a concentration of 0 (A), 1 (B), 10 (C) and 100 μg/mL (D). Co-localization of actin (red) and nuclei (blue). The scale bar represents 50 μm. Photos were taken with a Leica DM IL microscope coupled to a Visicam PRO 20C digital camera (ampliation 400x) and analysed with ImageJ version 1.53t using ImageJ software for image overlay.……..62

Supplementary figure 6 – Representative images of Caco-2 cells after 72h exposure to 1000 nm regular PSMPs at a concentration of 0 (A), 1 (B), 10 (C) and 100 μg/mL (D) and 1000 nm green-fluorescent PSMPs at a concentration of 0 (E), 1 (F), 10 (G) and 100 μg/mL (H). Co-localization of actin (red) and nuclei (blue). The scale bar represents 50 μm. Photos were taken with a Leica DM IL microscope coupled to a Visicam PRO 20C digital camera (ampliation 400x) and analysed with ImageJ version 1.53t using ImageJ software for image overlay.……..62

Supplementary figure 7 - Representative images of Caco-2 cells treated with 50 nm at 400x ampliation (A-C). Co-localization of mitochondria (red) and nuclei (blue) is evident. The scale bar represents 50 μm. Photos were taken with a Zeiss Axioscope 5 coupled to a Axiocam 202 mono camera and analysed with ImageJ version 1.53t using ImageJ software for image overlay.……..63

Supplementary figure 8 – Representative images of Caco-2 cells treated with 50 nm at 400x ampliation (A-C). Co-localization of alpha-tubulin (green), actin (red) and nuclei (blue) is evident. The scale bar represents 50 μm. Photos were taken with a Zeiss Axioscope 5 coupled to a Axiocam 202 mono camera and analysed with ImageJ version 1.53t using ImageJ software for image overlay.…….....63

List of abbreviations

ABC	ATP-binding cassette
AgNP	Silver nanoparticle
AMX	Amoxicillin
ATP	Adenosine triphosphate
BPA	Bisphenol A
BSA	Bovine serum albumin
C3G	Cyanidin-3-*O*-glucoside
CIP	Ciprofloxacin
CPF	Chloropyrifos
DBP	Dibutyl phthalate
DEHP	Di (2-ethyl) hexyl phthalate
DINP	Di-iso-nonyl phthalate
DNA	Deoxyribonucleic acid
ECIS	Electrical cell-substrate impedance system
EIS	Electrical impedance spectroscopy
EMT	Epithelial-to-mesenchymal transition
GSH	Glutathione
Hb	Hemoglobin
IL-1	Interleukin-1
LD-IR	Laser direct infrared spectroscopy
MDA	Malondialdehyde
MP	Microplastic
MNP	Micro- and nanoplastic
NOX4	NADPH Oxidase 4

NP	Nanoplastic
OA	Okadaic acid
PBAT	Poly-butylene-adipate-*co*-terephthalate
PBS	Phosphate buffer saline
PE	Polyethylene
PEMP	Polyethylene microplastic
PET	Polyethylene terephthalate
PLA	Poly-lactic acid
PMMA	Polymethyl methacrylate
PP	Polypropylene
PPNP	Polypropylene nanoplastic
PS	Polystyrene
PSMP	Polystyrene microplastic
PSMNP	Polystyrene micro- and nanoplastic
PSNP	Polystyrene nanoplastic
PO	Polyolefin
POM	Polyoxymethylene
PU	Polyurethane
PVC	Polyvinylchloride
PVP	Polyvinylpyrrolidone
RBC	Red blood cell
ROS	Reactive oxygen species
SERS	Surface-enhanced Raman spectroscopy
SVM	Support vector machine

TBBPA	Tetrabromobisphenol A
TC	Tetracyclin
TCA	Tricarboxylic acid
UV	Ultraviolet
WWTP	Wastewater treatment plant

1. Introduction

1.1 Plastics in the environment

Plastics are synthetic macromolecular end products made of polymers with appealing properties such as low production cost, thermo-mechanical properties, high chemical resistance and versatility, which make them the golden material of the last century (Desidery & Lanotte, 2022). This means that plastics have diverse applications and are used for medical tools, electronic devices, food and beverage containers and others (Khan & Jia, 2023).

The first plastic ever produced was made of cellulose and was called "Parkesine" by Alexander Parkes in 1862 and it was followed by the development of the first synthetic plastic in 1907 by Dr. Leo Bakeland who called it "Bakelite". The exponential development of different types of plastics took place during World War II and by 1950 its production was mainly directed for consumer products (Napper & Thompson, 2020). Since then, plastic production has not slowed down and has increased from 1.5 to 390.7 million metric tons, from 1950 to 2021 (Tiseo, 2022). The main plastics produced are polyethylene (PE, 36 %), polypropylene (PP, 21 %) and polyvinylchloride (PVC, 21 %), followed by polyethylene terephthalate (PET, < 10 %), polyurethane (PU, < 10 %) and polystyrene (PS, < 10 %) (Geyer *et al.*, 2017). After disposal, plastic waste can be degraded by several factors including ultraviolet (UV) radiation, rain, waves, oxidation, and mechanical degradation which eventually generates particles or microplastics with a size range of 1 μm to 5 mm and nanoplastics with a diameter ranging from 1 to 1000 *n*m. These end-products are named secondary micro- and nanoplastics and they can also result from the production of textile fibres and sea-salt aerosols. Micro- and nanoplastics are also deliberately synthesised for a diversity of products such as toothpaste, cosmetics, or fabric softener, and in this case they are classified as primary micro- and nanoplastics (Bengalli *et al.*, 2022; Frias & Nash, 2019; Gigault *et al.*, 2018).

The ubiquity of plastic's in the environment is already well known and it is estimated that a minimum of 5.25 trillion plastic particles weighing 268940 tons are floating in the oceans (Eriksen *et al.*, 2014). Microplastics are detected in a city atmospheric fallout, with an average of 118 particles / m^2 / day, raw wastewater contains from 260 x 10^3 to 320 x 10^3 particles / m^3 and after treatment in wastewater treatment plants (WWTPs) 14 x 10^3 to 50 x 10^3 particles / m^3 have been reported (Dris *et al.*, 2015). Moreover, in ambient air 1-1000 microplastics / m^3 have been reported, 2-477 microplastics / g in road dust and 0.1-30 000 microplastics / L in snow

(O'Brien *et al.*, 2023). The presence of microplastics was also detected in plastic bottled water, 72.32 ± 44.64 particles / L, and in tap water, 49.67 ± 17.49 particles / L, using laser direct infrared spectroscopy (LD-IR) (H. Li *et al.*, 2023).

One of the main problems related to plastic pollution is how to accurately detect and quantify plastics in the environment and determine their effects on ecosystems and human health. In that regard laser-induced breakdown spectroscopy was developed for the *in situ* detection of both plastic and its combustion products, with an identification accuracy of 92.73 % and 77.42 %, respectively (Wan *et al.*, 2023). Also, surface-enhanced Raman spectroscopy (SERS) has been used to efficiently detect 350 *n*m PS particles at concentrations ranging from 6.5 μg / mL to 100 μg / mL (Mikac *et al.*, 2023). Electrical impedance spectroscopy (EIS) coupled to a classifier based on a support vector machine (SVM) method is being developed for *in situ* detection of microplastics, and it has been applied to detect PP and polyolefin (PO) microplastics in deionized water (Bifano *et al.*, 2022). Similarly, a microfluidic sensor with microwire electrodes was developed for the detection and extraction of polystyrene microplastics in water, at concentrations ranging from 5 to 100 ppm and further tests for applications in other types of plastics are being considered (Zabihihesari *et al.*, 2023).

1.2 Micro- and nanoplastics effects in the environment

Plastic debris are spread through the marine environment, from coastlines to the deep sea, and are easily transported across the environment and transferred through the trophic chains in the food web. In fact, ingestion of plastics by various marine animals such as fishes, sea turtles and bivalves, that are planktivorous and filter feeding species readily accumulate microplastics (Law, 2017; Ozturk & Altinok, 2020; Peng *et al.*, 2020). Plastic pollution causes modifications in marine ecosystems with socio-economics consequences for fishing, aquaculture, and tourism. Aquaculture is affected by the problem but also contributes to plastic pollution, for example, 70 % of plastic litter collected on beaches may originate from aquaculture (Bringer *et al.*, 2021; Thushari & Senevirathna, 2020; Tian *et al.*, 2022).

Besides the aquatic environment, soils can also be contaminated by MNPs through sewage sludge, irrigation, littering along roads and illegal waste dumping, where it is assumed that they will remain for decades due to interactions with soil constituents (Bläsing & Amelung, 2018). As consequence, MNPs accumulated throughout time affect the microbiota and other species

present including soil invertebrates, rhizosphere communities and plants, which also contribute to their transfer through trophic chains to humans (Hurley & Nizzetto, 2018; Meng *et al.*, 2023).

1.2.1 Micro- and nanoplastics effects on marine species

Several reports exist concerning the effects of micro- and nanoplastics (MNPs) on marine species, in the bivalve *Mytillus galloprovincialis*, polystyrene micro- and nanoplastics (PSMNPs) of 50 *n*m, 100 *n*m and 1 μm were internalized and translocated to the hemolymph and taken up by haemocytes (Sendra *et al.*, 2020). In the water flea *Daphnia pulex* exposure for 21 days to 75 *n*m PSNPs caused downregulation of several key genes, involved in trehalose transport or chitinase and upregulation of some others, which eventually led to reduced growth and a change in the sex ratio (W. Zhang *et al.*, 2020). A study also showed that the presence of 100 *n*m PSNPs increased the infection rate in *Daphnia magna* of two pathogens, a fungal parasite *Metschnikowia bicuspidate* and a gut microsporidium *Ordospora colligate*, except at the concentration of 50 mg / mL due to high mortality rates (Manzi *et al.*, 2023). In crustaceans, such as *Macrobrachium nipponense*, an oriental river prawn, 75 *n*m PSNPs affected energy metabolism and exposure for different durations to different concentrations of nanoplastics (5, 10, 20, and 40 mg / L) decreased the survival rate in a dose- and time dependent manner and altered enzyme activity as well as gene expression (Y. Li *et al.*, 2021). In sediment-rooted macrophytes, namely, *Myriophyllum spicatum* and *Elodea* sp. the effect of polystyrene MNPs was not concentration-dependent but was suggested to be size-dependent as nanoplastics induced greater effects than microplastics and decreased the shoot length of *M. spicatum* and shoot to root ratio for both macrophytes (van Weert *et al.*, 2019).

In zebrafish (*Danio rerio)* the exposure route influences the effects of PSNPs and exposure through water and microinjection (to mimic maternal transfer) led to their accumulation, although the aqueous route led to greater PSNPs accumulation in the brain, reduced antioxidant gene expression, hypoactivity and developmental abnormalities (R. Zhang *et al.*, 2020). By comparing the uptake of 86 and 185 *n*m NPs, the smaller NPs had a greater accumulation in the intestine, liver, and muscle in tilapia (*Oreochromis niloticus*), although particle uptake in the stomach and gill was not size-dependent (Hao *et al.*, 2023). The ingestion of polypropylene microplastics for 4 to 14 days in the tilapia, *Oreochromis mossambicus*, altered homeostasis and antioxidants levels, increased reactive oxygen species (ROS) and the oxidation of lipid molecules and 14 days increased cell apoptosis and induced DNA (deoxyribonucleic acid)

damage (Jeyavani *et al.*, 2023). In korean bullhead fish (*Pseudobagrus fulvidraco*), exposure to polyethylene microplastics (PEMPs) at concentrations over 5000 mg / L, caused accumulation in the gut, gills and liver and decreased red blood cell (RBC) count, hemoglobin (Hb) and calcium for concentrations (Lee *et al.*, 2023).

1.2.2 Micro- and nanoplastics effects in soil and microorganisms

The effect of polymer-coated fertilizers in acid-contaminated soils was simulated with the addition of 0.1 % and 1 % (*w / w*) polyethylene (PE) and polyurethane (PU) in acid soil. The presence of these microplastics decreased the soil pH and increased cadmium bioavailability by enhancing DTPA (cadmium extracted by diethylenetriamine-pentaacetic acid-Cd) contents. Moreover, it induced changes in the fungi community present and altered soil enzymatic activities (Diao *et al.*, 2023). The presence of polyethylene and a biodegradable microplastic of poly-butylene-adipate-*co*-terephthalate (PBAT) mixed with poly-lactic acid (PLA) also altered the composition and diversity of rhizosphere bacterial communities (Meng *et al.*, 2023). In earthworm (*Lumbricus terrestris*), the combination of PE and biodegradable microplastics with a pesticide, chlorpyrifos (CPF), had greater toxic effects than the exposition to only microplastics. Furthermore, this combination resulted in an increase of the bioaccumulation of PE and its distribution in the soil and in an inhibition of the CPF degradation (Ju *et al.*, 2023).

The toxicity of several microplastics (PS, PVC, PE, and PP) and the additives that arise from their UV-aging were also evaluated. The results showed that the release of the additives, namely, di (2-ethyl) hexyl phthalate (DEHP) increased the toxicity of the MPs in *Escherichia coli*. However, when polystyrene microplastics (PSMPs) were combined with antibiotics, such as amoxicillin (AMX), ciprofloxacin (CIP) or tetracyclin (TC), their toxicity decreased, contrary to what happened for PVC microplastics (H. Yang *et al.*, 2023). A proteomic analysis of macrophages exposed to polystyrene micro- and nanoplastics (PSMNPs) revealed that one third of proteins had a significant change in their abundance, namely, mitochondrial, lysosomal, and cytoskeletal proteins. It was also observed the secretion of tumour necrosis factor and interleukin 6 in response to lipopolysaccharides challenge, but not in inflammatory responses (Collin-faure *et al.*, 2022).

1.3 Micro- and nanoplastics effects on human cell lines

Humans are exposed to micro- and nanoplastics by different routes: via inhalation, of plastic-containing aerosols in indoor and outdoor environments; via ingestion, by consuming MNP contaminated food or water and via absorption, by the skin from personal care products containing nanoplastics (Lehner *et al.*, 2019). Microplastics particularly abundant polyvinylchloride, and polypropylene (PP) have been detected in human breast milk and in the human placenta (Ragusa *et al.*, 2022; Zhu *et al.*, 2023). Microplastics such as PS, PVC, PET, polymethyl methacrylate (PMMA), polyoxymethylene (POM) and PP, have been detected in the liver and peripheral blood of humans with liver cirrhosis (Horvatits *et al.*, 2022; Salvia *et al.*, 2023).

Several studies have assessed the effects of MNPs in human cells and have shown that the size and surface charge of the particles are important factors for cellular uptake (Banerjee *et al.*, 2021; He *et al.*, 2020). In gastric cells, SNU-1, the uptake of PSNPs was not only size-dependent with particles with a lower size (50 and 100 *n*m) having a higher uptake than the bigger ones (1000 *n*m) but uptake was also dependent of the surface charge of the nanoparticles, and particles with carboxyl groups more easily internalized than the amino or neutral charge ones (Banerjee *et al.*, 2021). In human hepatocellular carcinoma cells (HepG2), PSNPs with carboxyl or amino groups were more easily taken up compared to non-functionalized PSNPs. Charged nanoparticles reduce cell viability (reduction of 46 % at 100 μg / mL of PSNPs) and induce the production of reactive oxygen species, ROS (He *et al.*, 2020). A study comparing the effect of PSNPs of 50 *n*m diameter in different leukocytic cell lines – Raji-B, TK6 and THP-1 – respond differently to MNPs exposure. Monocytes (THP-1) had the highest internalization rate, but no toxicity while in the other two cell lines, Raji-B and TK6, MNPs were mildly toxic at 200 μg / mL, and increased ROS production and genotoxic damage (Rubio *et al.*, 2020). PSNPs have a genotoxic effect on human skin fibroblast cells (Hs27) and concentrations of 25 and 75 μg / mL induced DNA damage and the formation of micronuclei, and 5 μg / mL increased ROS production (Poma *et al.*, 2019). Polyethylene microplastics (PEMPs) of 6.2 and 30.5 μm diameter reduced cell viability and increased the nitric oxide content in a concentration-dependent manner in THP-1, U937 and A549 cells. These microparticles induced the formation of ROS and pro-inflammatory cytokines in monocytes (THP-1 and U937), but not in A549 cells (Gautam *et al.*, 2022). PSNPs with 80 *n*m of diameter caused damages to mitochondria in hepatic (L02) and lung (BEAS-2B) cells in a concentration-dependent manner, leading to overproduction of mitochondrial ROS, alterations in the mitochondrial membrane potential and

suppression of mitochondrial respiration. A metabolomic analysis revealed that 80 *n*m PSNPs affected mitochondrial related pathways, such as the tricarboxylic acid (TCA) cycle, glutathione (GSH) metabolism and purine metabolism, which are pathways related to mitochondrial functions (Lin *et al.*, 2022).

MNPs are exposed to the most diverse environmental factors and thus their effects may be altered. To understand how environmental factors could affect MNPs structure and interaction with organisms, the effects of nanoplastics previously subjected to oxidation exposure were evaluated on the growth of *Scenedesmus obliquus*, a green alga, in the viability of A549 cells and in the formation of chlorinated by-products such as dibutyl phthalate (DBPs). The results showed that the treated PSNPs had a lower toxicity in *S. obliquus*, a higher toxicity in A549 cells and caused an increase in the formation of hydroxylated and carboxylated precursors DBPs (Zhou *et al.*, 2022). Furthermore, the interaction between microplastics and a common pollutant, DEHP, induced an inflammatory response in primary skin fibroblast cells from mice and inhibited fibrosis (X. Shi *et al.*, 2023). In another study the plasticizers DEHP and di-iso-nonyl phthalate (DINP) reduced the expression of tight/adherent junction genes in human enterocyte cells (HT-29) and of anti-inflammatory genes in murine macrophage cells (RAW264.7) (Shum *et al.*, 2023).

1.4 Plastics in human lung adenocarcinoma cells A549

Inhalation is one of the main routes of human exposure to MNPs. The presence of 39 identified microplastics was reported in several human lung tissue samples with polypropylene (PP, 23 %), polyethylene terephthalate (PET, 18 %) and resin (15 %) most abundant. MPs had a higher accumulation in the lower region of the lung when compared with the upper and middle regions (Jenner *et al.*, 2022). The presence of nanoplastics in the lungs can contribute to a variety of diseases, such as tumours or pulmonary fibrosis. PSNP exposure induces epithelial-to-mesenchyme transition (EMT), a pre-stage of pulmonary fibrosis by increasing EMT markers and the production of ROS and NADPH oxidase 4 (NOX4) (Halimu *et al.*, 2022). Similarly, 50 and 500 *n*m PSNPs were internalized by human primary nasal epithelial cells (HNEpCs) and accumulated in the cell cytoplasm, increased ROS production, decreased the mitochondrial membrane potential and affected the autophagy pathway (Annangi *et al.*, 2023). PSNP exposure causes ferroptosis in bronchial epithelial cells, decreasing the levels of glutathione (GSH) and increasing the levels of Fe^{2+}, malondialdehyde (MDA) and ROS. This

phenotype was triggered by the activation of the HIF-1α / HO-1 signalling pathway, due to enhanced HIF-1α / *Hmox1* (gene that codes HO-1) binding, ultimately, leading to a regulated cell death phenomenon dependent of ferrous-iron, ferroptosis (Y. Wu *et al.*, 2023).

A549 (figure 1) is a cell line originated from type II alveolar epithelial cells isolated from lung tissue from a 58-years-old Caucasian male with lung adenocarcinoma (Foster *et al.*, 1998; Giard *et al.*, 1973). This cell line is widely used as an *in vitro* lung model and is used for studies of cell biology, cell morphology, cytotoxicity, oxidative stress, and the inflammatory responses (Barosova *et al.*, 2021).

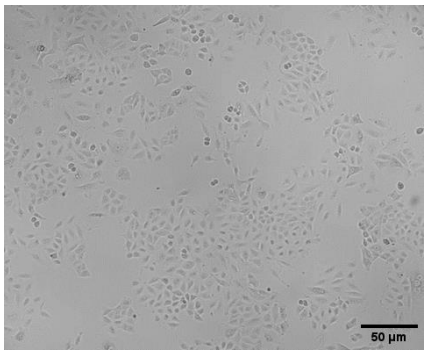

Figure 1 - Image of adherent A549 cells. The scale bar represents 50 μm. Photo was taken with a Leica DM IL microscope coupled to a Visicam Pro 20C digital camera (ampliation x100).

1.4.1 Micro- and nanoplastics uptake by A549 cells

A549 cells internalize nanoplastics in a size-dependent manner, and smaller particles (25 *n*m) accumulate faster, induce changes in the transcription of pro-inflammatory cytokines (IL-8, NF-KB, and TNF-A) and pro-apoptotic proteins (DR5, caspase-3, caspase-8, caspase-9, and cytochrome c) (M. Xu *et al.*, 2019). Lung cells accumulate PMMA up to 400 *n*m, which modifies the intracellular thiol content and cytokine secretion (da Silva Brito *et al.*, 2023). PET nanoparticles can also enter A549 cells, reducing cell viability, enhancing the oxidative stress responses and inducing cell apoptosis in a dose dependent-manner (H. Zhang *et al.*, 2022).

The mechanisms of uptake of MNPs by A549 cells remained unclear until recently, when it was shown that nanoplastics with diameters of 200 and 500 *n*m could enter human lung cells by phagocytosis, while the smaller ones with 70 *n*m of diameter could also be internalized by clathrin- and caveolae-mediated endocytosis, which are particularly relevant uptake mechanisms for particles with a size range between 50 and 80 *n*m. After internalization, nanoplastics accumulated in lysosomes and around the cell membrane The exocytosis of

particles occurs through lysosomes and small PSNPs are more easily eliminated than large particles (Liu *et al.*, 2023; X. Shi *et al.*, 2022; Y.-X. Zhang *et al.*, 2022).

1.4.2 Micro- and nanoplastics effects on A549 cells

The presence of bigger PSMPs (1 and 10 μm) was also reported to have a negative effect on A549 cell proliferation, affecting their metabolic activity and causing morphological changes in their cellular cytoskeletal (Goodman *et al.*, 2021). Polypropylene nanoplastics (PPNPs) in concentrations ranging from 1 to 4 mg / mL induce depolarisation of the mitochondrial membrane potential, decrease adenosine triphosphate (ATP) levels and ROS production, and decrease cell viability (Woo *et al.*, 2023).

The surface charge is also an important factor for the toxicity of particles. A549 cells exposed to PSNPs with neutral, carboxyl and amino groups revealed negatively charged particles had a greater effect on cell viability compared to positive and neutral particles. However, the overall toxicity of PSNPs was reduced when aggregated with a protein corona, simulating the interactions of NPs with proteins present in biological fluids (Hou *et al.*, 2023). In another study a protein corona reduced the cytotoxic effects of PSNPs and 20 *n*m PSNPs were found near chromosomes without a nuclear membrane, which was not verified for the larger 200 *n*m PSNPs (Kihara *et al.*, 2021).

One of the biggest problems of the nanoplastic inhalation is their association with other substances or additives, because of their colloidal properties (Pradel *et al.*, 2023). The effects of nanoplastics combined with two common plasticizers, dibutyl phthalate (DBP) and di-(2-ethylhexyl) phthalate (DEHP), were evaluated in the viability, oxidative stress and inflammatory responses of A549 cells and the results showed that in the groups treated with DBP or DEHP together with the nanoplastics, the cell viability was higher in the groups with the lower concentration of PSNPs (20 μg / mL), compared with the groups treated only with DBP or DEHP. In contrast, cell viability was lower when the concentration of the nanoplastics was higher (200 μg / mL) compared to the groups treated only with the plasticizers (Q. Shi, Tang, Wang, *et al.*, 2021). In addition to additives, nanoplastics can also be carriers of metals, such as silver, which is commonly used in consumer products and medical applications. In fact, polyvinylpyrrolidone (PVP)-coated AgNPs (silver nanoparticles) and ions Ag^{+} where shown to induce cellular toxicity in a dose-dependent manner in A549 cells, as well as causing

mitochondrial damage, early apoptosis, and DNA damage, including the formation of DNA adducts that could eventually lead to cancer (Foldbjerg *et al.*, 2011).

To investigate the effects that environmental factors such as UV radiation could have in MNPs structures and subsequent effects in A549 cells, PSNPs were aged through photodegradation by ultraviolet irradiation, which led to an increase in oxygen-containing groups on their surfaces. These aged particles showed a greater toxicity in A549 cells, when compared to regular particles and induced changes in gene expression (Q. Shi *et al.*, 2021). Similarly, photoaged PSNPs caused greater morphological changes, reduced monolayer integrity, and decreased wound recovery in A549 cells (El Hayek *et al.*, 2023).

It is also relevant to consider that the real MNPs to which humans are exposed in their daily lives are not perfectly regular in size and shape. The effect of microplastics derived from real waste plastics was evaluated in A549 in different concentrations (0.1 μg / mL to 100 μg / mL). The physico-chemical characterization of the particles showed that the most common component was polyethylene (PE) and the experimental results showed that the MNPs only presented significant effects for the highest concentration in cell viability, inducing inflammatory and genotoxic responses (Bengalli *et al.*, 2022). It is also necessary to consider the effects of aerosols resulting from the plastic combustion at the time of energetic recovery or recycling. In fact, PE combustion-generated aerosols decreased cell viability, induced genotoxicity and transcriptional alterations, in lung cells, and also enhanced inflammatory responses (Hufnagel *et al.*, 2021).

1.5 Plastics in human colon adenocarcinoma cells Caco-2

Ingestion is another of the main gateways for the entry of MNPs into the human body. It is estimated that humans annually ingest 39000 to 52000 plastic nanoparticles, plus 4000 or 90000 microplastics resulting from the consumption of tap water and bottled water, respectively (Cox *et al.*, 2019).

Caco-2 cells (figure 2) are epithelial cells isolated from the colon of a 72-years-old Caucasian male with colon adenocarcinoma with the capacity to spontaneously differentiate into enterocytes after confluence (Fogh *et al.*, 1977). These cells have been widely used as a model of the intestinal epithelium to study the absorption of drugs and other compounds (Engle *et al.*, 1998; Lea, 2015).

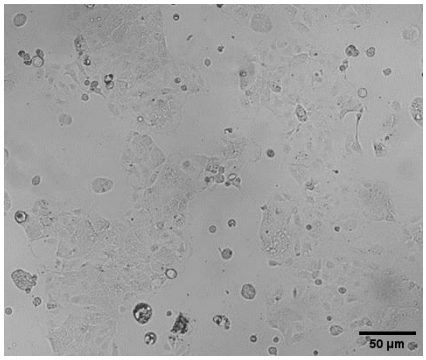

Figure 2 - Image of adherent Caco-2 cells. The scale bar represents 50 μm. Photo was taken with a Leica DM IL microscope coupled to a Visicam Pro 20C digital camera (ampliation x100).

1.5.1 Micro- and nanoplastics uptake by Caco-2 cells

The effects of PSNPs (50 *n*m) in concentrations ranging from 1 to 200 μg / mL were analysed in Caco-2 cells and the results showed that although PSNPs accumulated in Caco-2 cells, there were only mild toxic and genotoxic effects registered for concentrations above 100 μg / mL (Cortés *et al.*, 2020). However, accumulation of nanoparticles resulted in the presence of dark and dense structures within cells at all concentrations and for 50 and 100 μg / mL, mitochondrial cristae were swollen, which showed that nanoplastics could trigger subcellular responses. These results were supported by the demonstration that PSNPs were able to enter Caco-2 / HT29 and Caco-2 / HT29 + Raji-B co-cultures with no negative effects to their permeability, and with neither genotoxic nor oxidative DNA damage observed (Domenech *et al.*, 2020). In another study, Caco-2 cells were exposed to PSMPs with 1, 4 and 10 μm diameter, where only the smallest particles significantly reduced the cell viability. It was also evaluated the PSMPs uptake with three different models: Caco-2 monolayer, a M cell model (Caco-2 / Raji-B co-culture) and a mucus model (Caco-2 / HT29-MTX co-culture), where the particles were easily taken up by all models, apart from the 10 μm microplastics that had 0.07 % uptake (Stock *et al.*, 2019). Caco-2 cells internalize PSNPs through micropinocytosis and clathrin-mediated endocytosis, and this uptake is easier for functionalized PSNPs, PS-NH_2 and PS-COOH, meaning that the surface charge is an important parameter when studying the effects of MNPs in Caco-2 cells (D. Xu *et al.*, 2021). These results were supported by the demonstration that nanoplastics with diameters of 200 and 500 *n*m entered Caco-2 cells by phagocytosis, while the smaller ones with 70 *n*m of diameter were internalized by clathrin- and caveolae-mediated endocytosis (Y.-X. Zhang *et al.*, 2022).

1.5.2 Micro- and nanoplastics effects on Caco-2 cells

One of the concerns related with the human exposure to micro- and nanoplastics is that they can be carriers of other substances, like metals or toxins. PSNPs were reported to be able to function as carriers of silver and silver nitrate nanoparticles, and these complexes could modulate cellular uptake in Caco-2 cells, reaching the cell nucleus and inducing genotoxic and oxidative DNA damage. Nonetheless, metal complexed PSNPs do not significantly reduce cell viability (Domenech, Cortés, *et al.*, 2021). However, the presence of PSNPs led to a greater cytotoxicity of okadaic acid (OA, a neurotoxin associated with seafood poisoning) in Caco-2 cells compared to complexes formed with PSMPs. The combination of the nanoparticles with OA caused oxidative stress, mitochondrial membrane depolarization and induced endoplasmic reticulum stress-mediated apoptosis (Yan *et al.*, 2023). MNPs can also interact with other components in the environment and become carriers of heavy metals or even organic pollutants. For example, it was shown that the conjugation of tetrabromobisphenol A (TBBPA) with polyethylene microplastics (PEMPs) decreased the viability of Caco-2 cells, increased ROS production and disrupted the mitochondrial membrane potential (Huang *et al.*, 2021). Additionally, these complexes also induced some changes in the gut microbiota promoting the growth of gram-negative bacteria, as *Escherichia* and *Bacteroides*, and gram-positive bacteria as *Clostridium*. Similarly, PSMNPs with adsorbed bisphenol A (BPA) caused depolarization of mitochondria, decreasing Caco-2 cell viability and increasing cellular oxidative stress. It was also demonstrated that smaller particles (300 and 500 *n*m) were more uptaken than larger ones (1, 3 and 6 μm) and adsorbed more BPA in its surface (Wang *et al.*, 2020).

Polyethylene microplastics reduced the cell viability in a concentration-dependent manner, and enhanced oxidative stress, namely the mitochondrial superoxide production in Caco-2 cells, after a 48 hours exposure (Herrala *et al.*, 2023). An *in vitro* triple culture model composed by Caco-2 / HT29-MTX-E12 / THP-1 was exposed to PS and PVC micro- and nanoparticles to assess their effects in a healthy and inflamed human intestine. The results revealed that PVC particles increased the release of interleukin-1 β (IL-1β) and led to a loss of epithelial cells, during inflammatory responses, while no effects were observed for the presence of PSMNPs (Busch *et al.*, 2021).

Despite the low toxicity of polystyrene micro- and nanoplastics in Caco-2 cells it was reported that particles with a size of 0.1 and 5 μm could disrupt the mitochondrial membrane potential in a size-dependent manner, as well as inhibit plasma membrane ATP-binding cassette (ABC) transporter and increase arsenic toxicity (a substrate of the ABC transporter) (B. Wu *et al.*, 2019). Another study demonstrated that cyanidin-3-*O*-glucoside (C3G) during PS exposure,

reduced the effects induced in ABC transporters by activating the AMPK / SIRT1 / PGC-1α signalling pathway (Chen *et al.*, 2022). It was also demonstrated that the uptake of spherical and fibre / fragmented PSMPs by Caco-2 cells triggered a mitochondrial stress responses, by decreasing H_2O_2 levels, increasing mitochondrial DNA content and enhancing the expression of related genes such as *HMOX1*, *CAT* and *GPX1* (Saenen *et al.*, 2023). Moreover, PVC and PE particles can also interfere with cell apoptosis by affecting the caspase activity and PE showed to be more efficiently transported through an intestinal barrier model with Caco-2 than PS particles (Stock *et al.*, 2021).

Micro- and nanoplastics are exposed to different environmental conditions that could alter their properties and therefore, their effects on the cells. Indeed, the photo-transformation of polystyrene microplastics (PSMPs) by ultraviolet light resulted in changes in size and shape and in the transformation of some carbon-containing functional groups into oxygen-containing functional groups. The exposition of Caco-2 cells to 500 μg / mL of these PSMPs decreased the cell viability and damaged cellular membranes (Yu *et al.*, 2022). Similarly, 100 *n*m PET nanoplastics obtained by laser ablation were internalised in Caco-2 endolysosomes with high biopersistence (Magrì *et al.*, 2018). Polycarbonate and polyethylene terephthalate nanoplastics also obtained by laser ablation decreased the Caco-2 cells viability at concentrations ranging from 10 to 80 μg / mL and reduced mitochondrial activity (Tolardo *et al.*, 2022). In nanoplastic particles obtained from food containers, PET and PP particles increased DNA strand breaks in a dose-dependent manner in Caco-2 cells, but no effects on ROS production or changes in cell cycle distribution were registered (Roursgaard *et al.*, 2022).

Most studies expose cells continuously to MNPs for a short period of time, which does not accurately represent what happens in the environment. For that reason, some studies have considered long-term exposure of Caco-2 cells to 50 *n*m diameter PSNPs at different concentrations. This revealed that PSNPs accumulated in Caco-2 cells in a concentration-dependent manner and caused structural and molecular changes such as ultrastructural alterations in mitochondria (Domenech, de Britto, *et al.*, 2021). However, no significant cytotoxicity, genotoxicity neither oxidative stress effects were observed.

2. Objectives

Micro- and nanoplastics are ubiquitous in the environment and, consequently, humans are exposed daily to them via inhalation, ingestion with food or water and absorption through the skin. Despite the growing number of studies of MNPs, there are major knowledge gaps about the potential consequences of environmental contamination because most studies use high particles concentrations that do not reflect real exposure levels.

The main goal of this project was to study the effects of MNPs on human lung A549 and intestine Caco-2 cells since both cell lines are widely used as *in vitro* models of tissues directly exposed to MNPs. The aim was to use low doses of MNP exposure to obtain a more realistic assessment of the consequences of environmental exposure to polystyrene particles. This was achieved through the following specific objectives:

1) Characterization of A549 and Caco-2 growth and cellular morphology (nucleus, cytoskeleton, and mitochondria) under normal conditions;
2) Demonstrate MNP uptake by confocal microscopy;
3) Evaluate the effects of MNPs in cell viability, proliferation, migration, oxidative stress, and morphology for both cell lines;
4) Characterization of the effects of NPs on cell adhesion and wound recovery using standard imaging approaches and electrical cell-substrate impedance (ECIS) measurements.

3. Materials and methods

3.1 Cell lines

Human colon adenocarcinoma cells, Caco-2 (HTB-37) and human lung adenocarcinoma cells, A549 (CCL-85), were purchased from American Type Culture Collection (Virginia, USA).

3.2 Polystyrene micro- and nanoparticles

Regular polystyrene nanoparticles with diameters 50 and 500 *n*m and green-fluorescent microparticles with a diameter of 1000 *n*m were purchased from Phosphorex (Massachusetts, USA). Regular microparticles with a diameter of 1000 *n*m were obtained from Sigma-Aldrich (Missouri, USA).

3.3 Cell culture maintenance

A549 cells were maintained in culture with F12-K Medium (Cytiva, Danaher Corporation, Washington, USA), supplemented with 10 % (*v / v*) inactivated Fetal Bovine Serum (FBS, Sigma-Aldrich, Missouri, USA), 1 % (*v / v*) penicillin-streptomycin antibiotic solution (Lonza, Basel, Switzerland) and 1 % (*v / v*) Amphotericin-B fungicide solution (Sigma-Aldrich, Missouri, USA). Caco-2 cells were maintained in culture with Dulbecco's Modified Eagle Medium with high glucose (Sigma-Aldrich, Missouri, USA), supplemented with 10 % (*v / v*) inactivated FBS, 1 % (*v / v*) penicillin-streptomycin antibiotic solution and 1 % (*v / v*) MEM Non-essential aminoacids solution (Sigma-Aldrich, Missouri, USA). Both cell cultures were incubated at 37 ºC in a humidified atmosphere with 5 % CO_2 (Thermo Fisher Scientific, New York, USA). Confluent cells were enzymatically detached with Tryple-select-EDTA (Gibco, Thermo Fisher Scientific, New York, USA), counted using a hemocytometer (Marienfeld Superior, Marienfeld, Germany) and cell solutions were prepared according to the assay.

3.4 Growth curve of A549 and Caco-2 cells

To characterize both cell lines, their growth curves were firstly established.

A549 and Caco-2 cells were plated in 96-wells plate (10 000 cells / well) and maintained in optimal conditions for counting, being the cell medium renewed every 48 hours.

For cell counting, cells were fixed with absolute ethanol for 15 minutes, washed with phosphate buffer saline (PBS) 1X, stained with 4',6-diamidino-2-phenylindole (DAPI) (300 *n*M) for 20 minutes and washed again with PBS 1X. Pictures were taken every 24 hours to monitor cell proliferation. A Leica DM IL microscope coupled to a Visicam PRO 20C digital camera was used. Cells were counted from the pictures taken using ImageJ software, version 1.53t, with the trainable weka segmentation Plugin based on a previously prepared model (Abràmoff *et al.*, 2004).

3.5 Characterization of cell morphology of A549 and Caco-2

For the characterization of cell morphology, immunofluorescence assays (IFA) were performed. A Mitotracker dye was used to stain the mitochondria, by binding to the thiol groups present (Chazotte, 2011a). A primary antibody-monoclonal anti alpha-tubulin which binds to the alpha-tubulin conjugated with a secondary antibody-Alexa fluor 488 Goat anti-mouse IgG was used to stain the alpha-tubulin. Phalloidin Texas Red dye to stain the actin structure and DAPI dye to stain the nucleus of cells. Phalloidin Texas Red is a dye that binds preferentially to F-actin, which are linear polymers of globular actin monomers (G-actin), while DAPI associates with the minor groove of double-stranded DNA, preferring the adenine-thymine clusters (Chazotte, 2011b; Fujino *et al.*, 2010). All the reagents used were added in a volume enough to cover the cells on the coverslips.

A549 and Caco-2 cells were plated in 24-wells plate previously prepared with glass coverslips (80 000 cells / well and 100 000 cells / well, respectively). For the mitochondria staining, 72 hours after incubation, the medium was removed and cells were stained with Mitotracker™ Deep Red FM (Thermo Fisher Scientific, New York, USA) at 250 *n*M for 20 minutes at 37 ºC, 5 % CO_2, followed by washes with PBS 1X. Cells were fixed with absolute ethanol for 15 minutes, washed with PBS 1X, permeabilized with 0.1 % Triton X-100 / PBS 1X for 15 minutes, and washed again. Finally, cells were stained with DAPI (300 *n*M) for 20 minutes and washed with PBS 1X. The coverslips were placed in a lamina with polyvinylpyrrolidone (PVP) mounting medium and images were taken with a Leica DM IL microscope coupled to a Visicam PRO 20C digital camera. Images were analysed with ImageJ software, version 1.53t using image overlay (Abràmoff *et al.*, 2004).

For the tubulin staining, a specific antibody was used to stain alpha-tubulin, monoclonal anti – alpha – tubulin antibody produced in mouse (Thermo Fisher Scientific, New York, USA).

Briefly, cells were fixed with paraformaldehyde (PFA) 4 % for 15 minutes, washed with PBS 1X, followed by cell permeabilization with 0.1 % Triton X-100 / PBS 1X for 15 minutes, and washed again. Cells were then incubated with 3% BSA (bovine serum albumin) / PBS 1X for 30 minutes to avoid unspecific binding of the antibody, followed by incubation with primary antibody-monoclonal anti alpha-tubulin (1:400) for 1 hour in the dark. Cells were then washed with PBS 1X and incubated with secondary antibody-Alexa fluor 488 Goat anti-mouse IgG (1:1000, Invitrogen, Massachusetts, USA) for 1 hour in the dark, washed again and stained with Phalloidin Texas-Red (1:40) for 20 minutes. Cells were washed with PBS 1X, stained with DAPI (300 *n*M) for 20 minutes and washed with PBS 1X. The coverslips were placed in a lamina with PVP mounting medium. Images were taken with a Zeiss Axioscope 5 with a fluorescence LED illumination Colibri 7 coupled to a Axiocam 202 mono camera and a Zeiss Axio Vert. A1 with a Axiocam 202 mono camera. Images were analysed with ImageJ software, version 1.53t using the image overlay tool (Abràmoff *et al.*, 2004).

For the Phalloidin Texas-Red staining, 72 hours after incubation, cells were fixed with absolute ethanol for 15 minutes, washed with PBS 1X, stained with Phalloidin Texas-Red (1:40) for 20 minutes and washed again with PBS 1X before being incubated with DAPI (300 *n*M) for 20 minutes and washed with PBS 1X. The coverslips were placed in a lamina with PVP Mounting medium. Images were taken with a Leica DM IL microscope coupled to a Visicam PRO 20C digital camera and images were analysed with ImageJ 1.53t (Abràmoff *et al.*, 2004).

3.6 PSMNP uptake by A549 and Caco-2 cells

To study the uptake of micro- and nanoplastics by the cells, an assay was performed using regular and fluorescent MNPs, Phalloidin Texas Red dye to stain the actin structure and DAPI dye to stain the nucleus of cells. All the reagents used were added in a volume enough to cover the cells on the coverslips.

A549 and Caco-2 cells were plated in 24-wells plate previously prepared with glass coverslips (80 000 cells / well and 100 000 cells / well, respectively). After 24 hours, regular and green-fluorescent 500 and 1000 *n*m PSMPs at concentrations of 1, 10 and 100 μg / mL were added to the respective wells and cell normal medium was added to the control wells and cells were incubated in optimal conditions for 72 hours. Following incubation, cells incubated with regular PSMPs were fixed with absolute ethanol for 15 minutes, washed with PBS 1X, stained

with DAPI (300 *n*M) for 20 minutes and washed again with PBS 1X. Cells treated with green-fluorescent PSMPs were fixed with absolute ethanol for 15 minutes, washed with PBS 1X, stained with Phalloidin Texas-Red (1:40) for 20 minutes and washed again with PBS 1X before being incubated with DAPI (300 *n*M) for 20 minutes and washed with PBS 1X. The coverslips were placed in a lamina with PVP Mounting medium. Images were taken with a Leica DM IL microscope coupled to a Visicam PRO 20C digital camera and images were analysed with ImageJ 1.53t (Abràmoff *et al.*, 2004). Confocal microscopy images were also taken with the prepared coverslips. Pictures were taken with a Zeiss 1 LSM 710 confocal microscope with Airyscan and analysed with Zeiss Zen 8 Lite.

3.7 PSMNP effects on cell viability

To evaluate the effect of PMNPs in cell viability, the MTT (3 [4,5-dimethylthiazol-2-y1]-2,5 diphenyl tetrazolium bromide) assay was used. This assay is based on the principle that MTT can be reduced to formazan by mitochondria, and the mitochondrial activity by the conversion of MTT in formazan can be related with the number of living cells. It's a colorimetric-based measurement, where the formazan's formation can be measured by its optical density at a wavelength around 540-570 *n*m (Ghasemi *et al.*, 2021; van Meerloo *et al.*, 2011).

For the experimental assay, A549 and Caco-2 cells were plated in 96-wells plate (25 000 cells / well and 50 000 cells / well, respectively) and incubated under optimal conditions. After 24 hours, 50, 500 and 1000 *n*m PSMPs at concentrations of 0.01, 0.1, 1 and 10 μg / mL were added to the respective wells and cell medium to the control wells and cells were incubated in optimal conditions for 72 hours. On the assay day, cells were incubated with a MTT solution at 12 mM for 4 hours at 37 ºC with 5 % CO_2. After the incubation period, 85 μL of medium was removed and 50 μL of dimethyl sulfoxide (DMSO) was added to dissolve the formazan crystals. The plates were then incubated at 37 ºC for 10 minutes and incubated with agitation for 10 minutes (Heidolph Unimax 1010, Heidolph instruments, Schwabach, Germany). Absorbance was measured at wavelength (λ) 540 *n*m in a microplate reader (Tecan Infinite M200, Tecan, Männedorf, Swiss).

3.8 PSMNP effects on cell migration

To study cell migration in the presence of PMNPs, *in vitro* scratch assays were performed. Cell migration is an important process for many physiological activities, and it relies on the actin cytoskeleton and depolymerization of microtubules, in case of fibroblasts and tumour cells. In a scratch assay, it is evaluated the migration of cells into a wounded area created physically in a confluent monolayer, by measuring the cell-free area during a period of time (Gough *et al.*, 2011; Kauanova *et al.*, 2021).

A549 and Caco-2 cells were plated in 24-wells plate (80 000 cells / well and 100 000 cells / well, respectively) incubated overnight at 37 ºC with 5 % CO_2. The next day regular 50, 500 and 1000 *n*m PSMPs at concentrations of 0.1 and 1 μg / mL were added to the respective wells and cell medium to the control wells. Forty-eight hours after MNPs incubation, a scratch was made using a 1000 μL pipette tip in the cell monolayer, cells were washed with PBS 1X and fresh medium was added. Pictures were taken periodically to monitor the cell migration with a Leica DM IL microscope coupled to a Visicam PRO 20C digital camera and images were analysed with ImageJ 1.53t (Abràmoff *et al.*, 2004). Results were analysed taking the time zero as the 100 % of the wound area.

3.9 PSMNP effects on cell proliferation

Proliferation is the cell growth resulting from cellular division and it's a complex and essential physiological process. To assess the effects of PSMNPs in A549 and Caco-2 cell proliferation, it was used DAPI to stain the cell nuclei, followed by nuclei counting.

A549 and Caco-2 cells were plated in 24-wells plate (300 000 cells / well) and incubated with regular 50, 500 and 1000 *n*m PSMPs at concentrations of 0.01, 0.1, 1 and 10 μg / mL. Seventy-two hours later, cells were harvested by Tryple select digestion, counted, and redistributed in 96-wells plate. From this point, for cell counting, the same procedure described for the growth curves counting was used.

3.10 PSMNP effects on oxidative stress

To evaluate the oxidative stress caused by the presence of MNPs, a DCFH-DA ROS assay kit (BQCKit, Bioquochem, Asturias, Spain) was used to access the formation of ROS, through the measurement of the fluorescence of 2'-7'dichlorofluorescein (DCF), which is a

compound that results from the oxidation of 2'-7'dichlorofluorescein diacetate (DCFH-DA) by ROS.

A549 and Caco-2 cells were plated in 96-wells plate (25 000 cells / well and 50 000 cells / well, respectively). After 24 hours, regular 50, 500 and 1000 *n*m PSMNPs at concentrations of 0.01, 0.1, 1 and 10 μg / mL were added to the respective wells and cell medium was added to the control wells and cells were incubated in optimal conditions for 72 hours. ROS formation was then measured with a DCFH-DA ROS assay kit (BQCKit, Bioquochem, Asturias, Spain). Briefly, cells were incubated with 100 μL of the dilution buffer 1X for 5 minutes, followed by 100 μL of the DCFH-DA at 25 μM for 45 minutes in the dark. The probe solution was removed, and 100 μL of PBS 1X was added. The fluorescence was measured at λ_{exc} = 485 *n*m and λ_{em} = 535 *n*m in a microplate reader (Tecan Infinite M200, Tecan, Männedorf, Swiss). Results were analysed with the following formula: $[(F_{sample} - F_{blank}) / (F_{control} - F_{blank})] \times 100$, being F the signal of fluorescence measured.

3.11 PSMNP effects on cell morphology

To study the effect of micro- and nanoplastics on cell morphology, immunofluorescence assays (IFA) were performed. It was used a Mitotracker dye to stain mitochondria and DAPI dye to stain the nucleus of cells. It was also used a primary antibody-monoclonal anti alpha-tubulin which binds to the alpha-tubulin conjugated with a secondary antibody-Alexa fluor 488 Goat anti-mouse IgG to stain the alpha-tubulin. All the reagents used were added in a volume enough to cover the cells on the coverslips.

A549 and Caco-2 cells were plated in 24-wells plate previously prepared with glass coverslips (80 000 cells / well and 100 000 cells / well, respectively). After 24 hours, regular 50 and 1000 *n*m PSMNPs at 1 μg / mL were added to the respective wells and cell medium was added to control wells. For the mitochondria and tubulin stainings, the same procedure as in the characterization of cell morphology was used.

3.12 PSMNP effects on cell adhesion assessed using ECIS

An Electric Cell-Substrate Impedance system (ECIS) was used to study the impact of nano- and microplastics in the cell adhesion. ECIS is an *in vitro* system based on the detection of a chosen frequency of cell impedance, allowing the study of several properties of cells cultured in chips with gold electrodes as adhesion, migration and even differentiation. The

adherent cells will work as insulators to the current flow and, thus, it will be measured the current between the electrodes. It's a non-optical and non-invasive method and it provides a real time measurement of the phenomena being studied (Cavallini & Tarantola, 2019; Iwakura *et al.*, 2021).

A549 and Caco-2 cells were plated in 24-wells plate (300 000 cells / well) and incubated with regular 50, 500 and 1000 *n*m PSMNPs at a concentration of 1 μg / mL an incubated in optimal conditions. Seventy-two hours later, cells were harvested by Tryple select digestion, counted, and 75 000 cells / well and 150 000 cells / well, respectively were plated in an 8W10E+ chip (Applied Biophysics, NY, USA) previously coated with cysteine (10 mM) for 30 minutes. The cell adhesion was monitored in both chips. The data was analysed using the Applied Biophysics Z-theta Analysis Software v1.2.92.0 and impedance was measured at a multi-frequency approach, being 4000 Hz the frequency chosen for data analysis.

3.13 PSMNP effects on wound recovery assessed using ECIS

To study the impact of nano- and microplastics in wound recovery, it was also used ECIS. In this system, a pulse is applied, causing pores in the cell membrane, and leading to cell lysis, resulting in an area of dead cells. The cells around the wound will migrate, leading to variations in the impedance. By being a real-time measurement, it is possible to monitor the different phases of the process as the cell transition, migration, and re-establishment of cell impedance.

A549 and Caco-2 cells were plated in an 8W1E chip (Applied Biophysics, NY, USA) previously coated with cysteine (60 000 cells / well and 128 000 cells / well, respectively). After 72 hours, the medium was removed and it was added regular 50, 500 and 1000 *n*m PSMNPs at a concentration of 1 μg / mL to the respective wells. After 48 hours, it was made the electric wound (wound time – 10 seconds (A549) and 20 seconds (Caco-2), wound current – 1200 uA and frequency – 40 000 Hz). The wells of the chip were washed with cell medium, fresh medium was added, and cell migration was monitored. The data was analysed using the Applied Biophysics Z-theta Analysis Software v1.2.92.0 and impedance was measured at a multi-frequency approach, being 4000 Hz the frequency chosen for data analysis.

3.14 Statistical analysis

Statistical analysis was performed with GraphPad Prism 8.4.2. One-way ANOVA analysis was used for the data obtained in the cell viability, oxidative stress and ECIS assays. Two-way ANOVA was used to analyse the data from the cell migration and cell proliferation assays. Statistical analysis is indicated in the graphs as $*p < 0.05$, $**p < 0.01$, $***p < 0.001$ and $****p < 0.0001$.

4. Results

4.1 A549 cells

4.1.1 Characterization of A549 cells

A549 is a cell line originated from type II alveolar epithelial cells, which is adherent and grows into a cell monolayer. These cells are relatively small and have a triangle-like shape, as illustrated in figures 3 and 4.

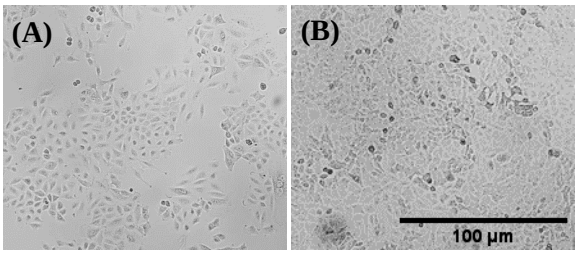

Figure 3 – Representative images of adherent A549 cells at low density (A) and high density (B). The scale bar represents 100 μm. Photos were taken with a Leica DM IL microscope coupled to a Visicam PRO 20C digital camera (ampliation x 100).

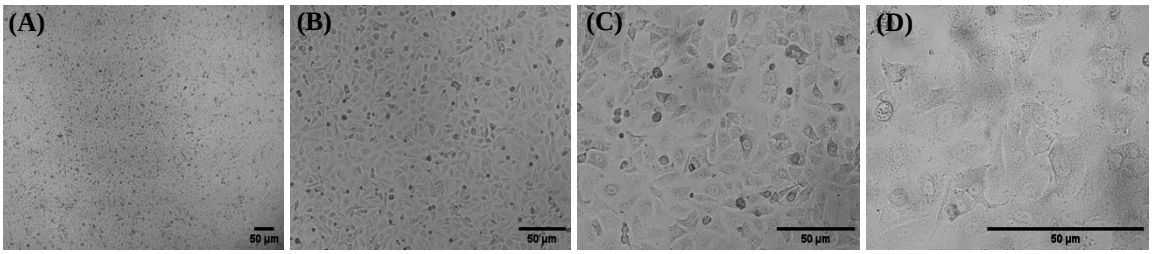

Figure 4 – Representative images of adherent A549 cells at different ampliations: 40x (A), 100x (B), 200x (C) and 400x (D). Scales bars represents 50 μm. Photos were taken with a Leica DM IL microscope coupled to a Visicam PRO 20C digital camera.

The growth rate of A549 cells was characterized. The growth curve (figure 5) shows that A549 cells duplicate within 48 hours, displaying exponential growth during the first 72 hours. After that, cell growth stabilizes until 120 hours.

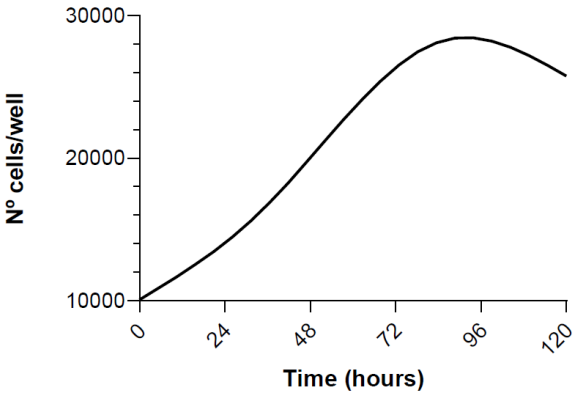

Figure 5 - Growth curve of A549 cells. Data is represented as a smooth fit of the average of the number of cells per well (the assay was performed with 4 replicates).

Mitochondria are usually elongated organelles ranging from 400 to 500 *n*m. The morphological analyses (figure 6) showed that, in A549 cells, mitochondria appear in a more swollen and spherical form around cell nuclei. Alpha-tubulin is one of the five subunits of tubulin, and it was found around the nuclei and in the cytoplasm, presenting a fibrous morphology, while actin was dense and reticulated, and interlinked the cell monolayer.

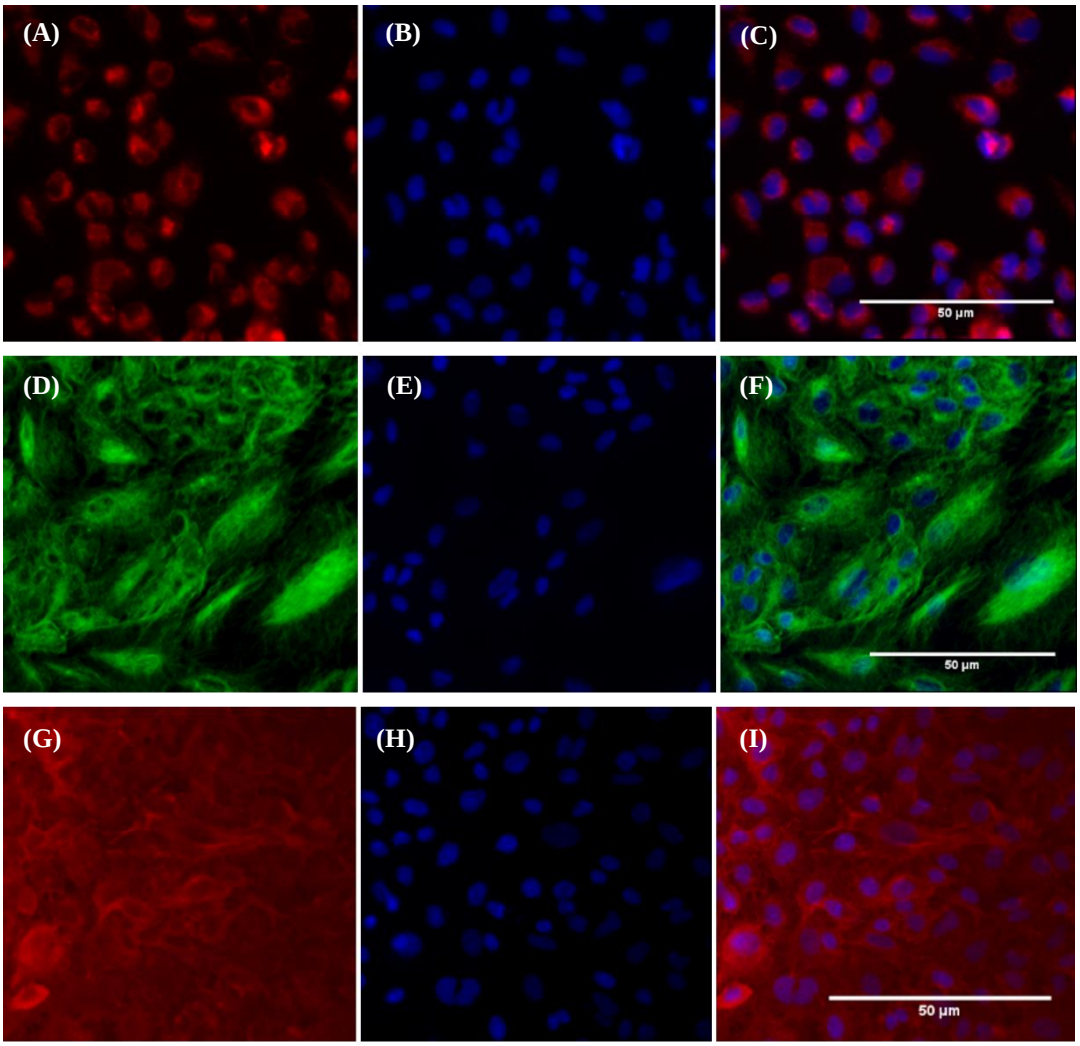

Figure 6 – Representative images of A549 cells. Nuclei is always represented in blue. In (A) and (C), the red colour represents mitochondria, in (D) and (F) the green colour represents alpha-tubulin and in (G) and (H) the red colour represents actin. Scale bars represent 50 μm. Photos were taken with a Zeiss Axio Vert. A1 with a Axiocam 202 mono camera (ampliation 400x) and were analysed with ImageJ version 1.53t using ImageJ software for image overlay.

4.1.2 Uptake of PSMNPs by A549 cells

A549 cells were exposed to 500 and 1000 *n*m regular and green-fluorescent PSMNPs at concentrations ranging from 0 to 100 μg / mL. Results showed that cells can take up 1000 *n*m polystyrene particles in 72 hours, and the particles accumulate around the nuclei (figure 7). Non-labelled particles were more easily internalized than fluorescent ones. In annex 1, the uptake of 500 and 1000 *n*m particles by lung cells for all concentrations tested is illustrated (supplementary figures 1 and 2).

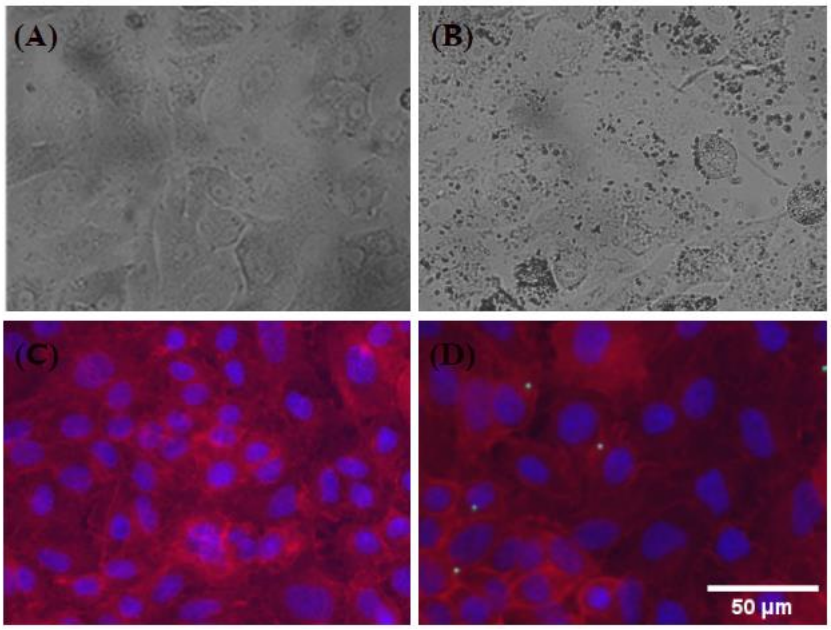

Figure 7 – Representative images of A549 cells after 72h exposure to 1000 nm regular PSMPs at a concentration of 0 (A) and 1 µg/mL (B) and 1000 nm green-fluorescent PSMPs at a concentration of 0 (C) and 1 µg/mL (D). Co-localization of nuclei (blue) and actin (red). The scale bar represents 50 µm. Photos were taken with a Leica DM IL microscope coupled to a Visicam PRO 20C digital camera (ampliation 400x) using ImageJ software for image overlay.

Confocal microscopy was used to further confirm the presence of 1000 *n*m microplastics inside lung cells (figure 8). Results showed that microparticles were inside the cells, namely, close to the cell nucleus, similarly to what has been previously observed in inverted microscopy images.

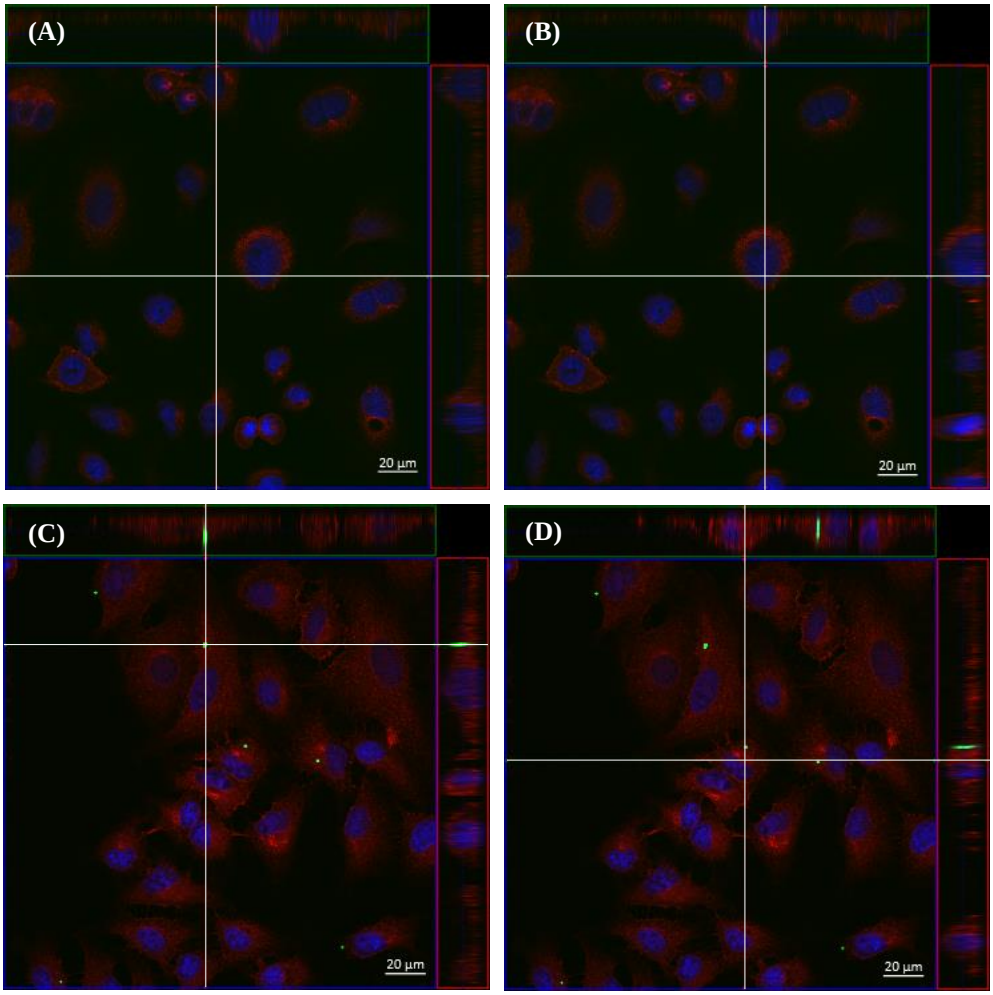

Figure 8 – Representative orthogonal view of A549 cells exposed to 0 (A and B) and 1 μg / mL green-fluorescent 1000 *n*m PSMPs for 72 hours. Co-localization of actin (red), nuclei (blue) and PSMPs (green) is evident. Scale bars represent 20 *n*m. Z-stack 3D pictures were taken with a Zeiss 1 LSM 710 confocal microscope with Airyscan and analysed with Zeiss Zen 8 Lite (orthogonal view).

4.1.3 PSMNP effects on A549 cell viability

The effect of PSMNPs on A549 cell viability was evaluated using an MTT assay. This assay revealed that smaller particles didn't have any significative effect on cell viability, while 500 *n*m PSNPs at a concentration of 1 and 10 μg/mL decreased the cell viability compared to the control group (non-treated cells), with $p < 0.05$ and $p < 0.01$, respectively. Likewise, the exposure to 1000 *n*m PSMPs at concentrations of 0.1, 1 and 10 μg/mL significantly reduced the cell viability, by $p < 0.001$, $p < 0.001$ and $p < 0.0001$, respectively (figure 9).

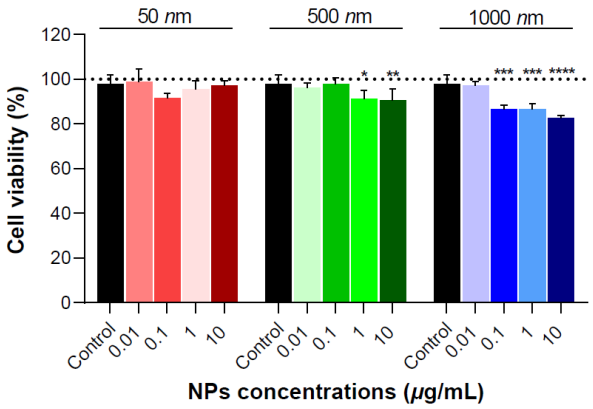

Figure 9 - Cell viability of A549 cells after the exposure to 50, 500 and 1000 *n*m PSMNPs at concentrations ranging from 0 to 10 μg/mL after 72 h of exposure. Data is represented as the percentage of living cells relative to the untreated control ± SEM (the assay was performed with 4 replicates and 3 independent experiments). A one-way ANOVA with a Tukey's Multiple Comparison test was used for the statistical analysis. Statistical analysis was performed with GraphPad Prism 8.4.2 and significance is indicated in the graph by *$p < 0.05$, **$p < 0.01$, ***$p < 0.001$ and ****$p < 0.0001$.

4.1.4 PSMNP effects on A549 cell proliferation

The effect of PSMNPs on A549 cell proliferation was evaluated by counting the stained cell nucleus (figure 10). This assay showed that 50 *n*m nanoparticles at 10 μg/mL increased the cell growth at 48 hours ($p < 0.0001$), while the lowest concentration significantly reduced the cell proliferation at 48 and 72 hours ($p < 0.01$ and $p < 0.001$, respectively). With regards to 500 *n*m nanoplastics, at 24 hours, the lowest concentration increased the cell number ($p < 0.01$), and the opposite occurred at 48 hours ($p < 0.0001$). Also, at 0.1 μg/mL, the cell number was reduced at 48 hours and at 10 μg/mL ($p < 0.05$), it increased at 72 hours ($p < 0.05$). For the largest particles, there was a reduction in the cell growth in the first 24 hours at 1 μg/mL ($p < 0.05$) and an increase at 48 hours for both 0.1 and 10 μg/mL ($p < 0.01$ and $p < 0.05$, respectively). By 72 hours of proliferation, the 1000 *n*m particles at 0.1 μg/mL increased the cell proliferation ($p < 0.0001$).

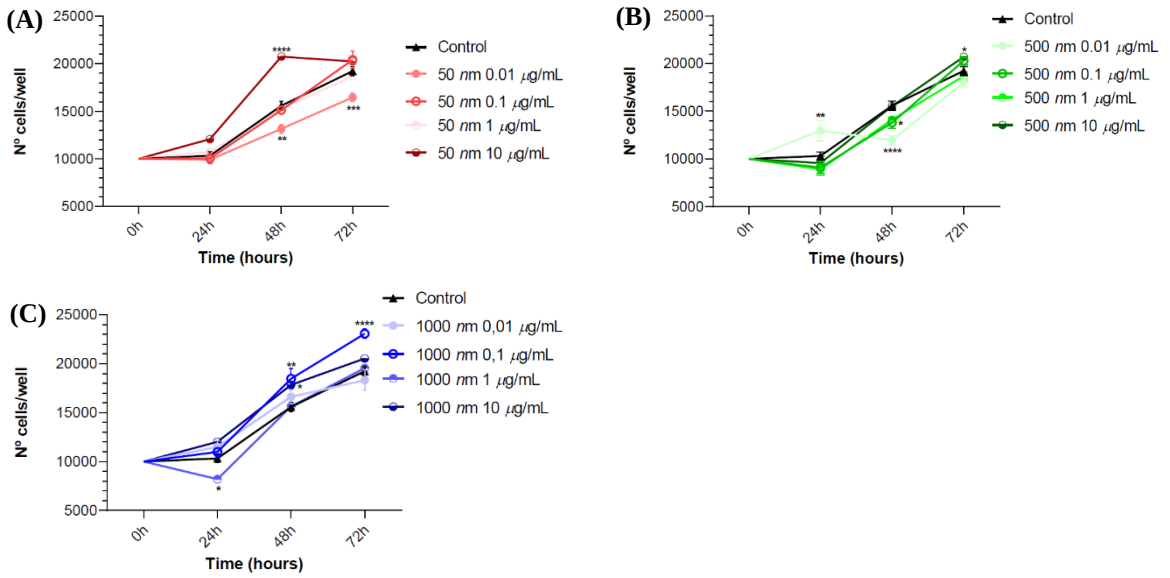

Figure 10 - A549 cell proliferation after the exposure to 50 (A), 500 (B) and 1000 *n*m (C) PSMNPs at concentrations ranging from 0.01 to 1 μg/mL for 72 hours. Data is represented as the number of cells per well ± SEM (the assay was performed with 3 replicates and 3 independent experiments). A two-way ANOVA with Tukey's Multiple Comparison test was used for the statistical analysis. Statistical analysis was performed with GraphPad Prism 8.4.2 and significance is indicated in the graphs by *$p < 0.05$, **$p < 0.01$, ***$p < 0.001$ and ****$p < 0.0001$.

4.1.5 PSMNP effects on A549 migration

The effects of PSMNPs on A549 cell migration was evaluated in a scratch assay. This assay showed that, the presence of PSMNPs promoted scratch recovery faster than in the untreated cells, and the difference was most significant at 12h after the scratch (figure 11). In the presence of 50 *n*m nanoplastics, cells recovered significantly faster for both 0.1 and 1 μg/mL concentrations ($p < 0.05$ and $p < 0.01$, respectively). On the other hand, cells incubated with 500 *n*m particles recovered more easily than control cells ($p < 0.01$), and a similar situation occurred for the larger particles ($p < 0.05$).

Alpha-tubulin antibody and Phalloidin Texas-red was used to evaluate the cell morphology in the scratch area and results showed that cells appeared to stretch to migrate and fill the empty zone, as illustrated in the figure 12. It appears that there were no significant differences in the cell cytoskeleton morphology, with both actin filaments and tubulin microtubules spreading and forming a network between the cells close to the wound area.

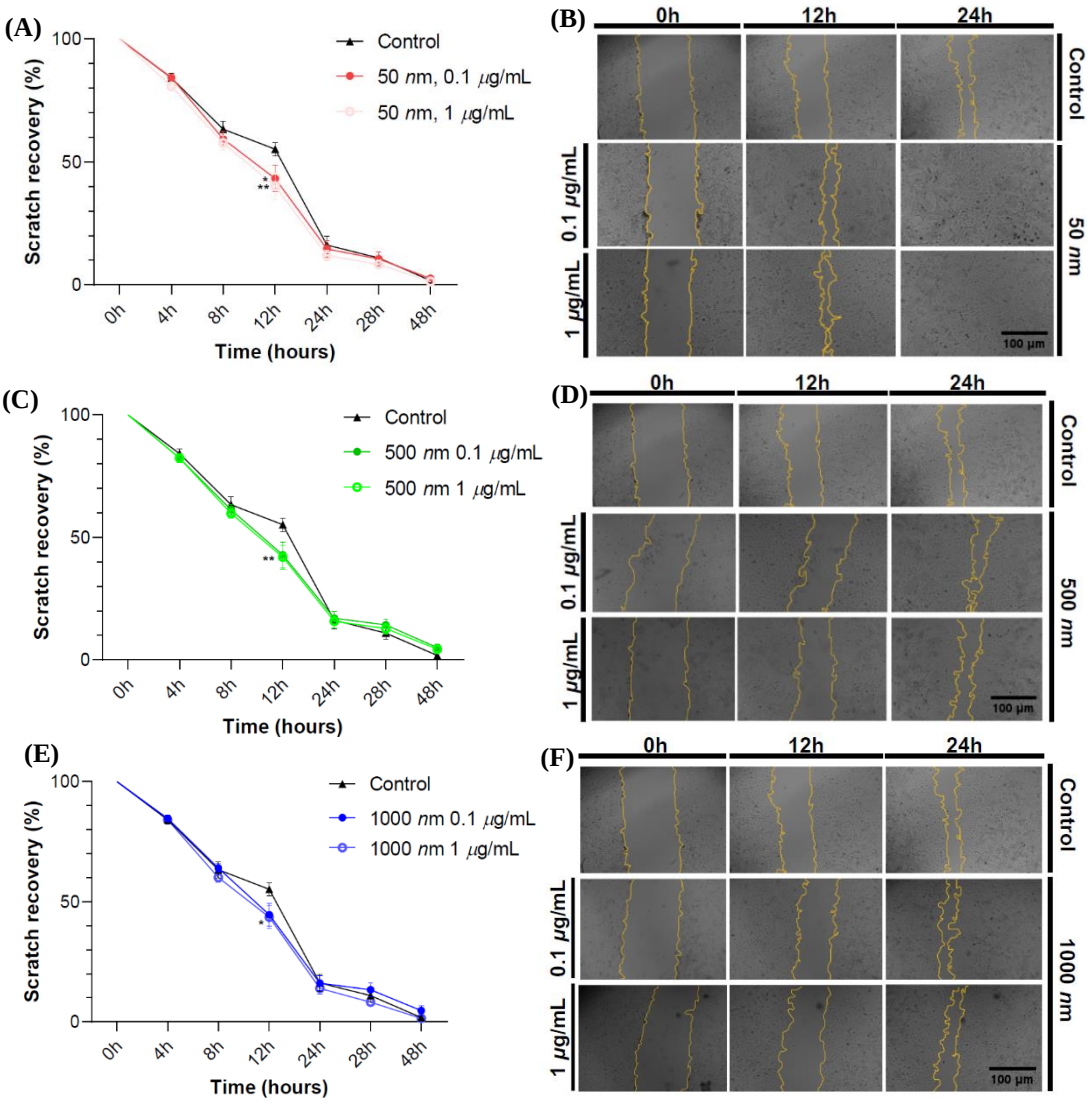

Figure 11 - A549 cells scratch assay: (A), (C) and (E) represent the scratch recovery area (percentage) of A549 cells after the exposure to 50, 500 and 1000 nm PSMNPs, respectively, at concentrations ranging from 0 to 1 µg/mL, measured at 0, 4, 8, 12, 24, 28 and 48 hours in relation to the area immediately after the scratch (100 %). Data is represented as the percentage of scratch wound relative to the initial scratch ± SEM (the assay was performed with 3 replicates and 3 independent experiments). A two-way ANOVA with Tukey's Multiple Comparison test was used for the statistical analysis. Statistical analysis was performed with GraphPad Prism 8.4.2 and significance is indicated in the graph as *$p < 0.05$, **$p < 0.01$. (B), (D) and (F) are representative images showing the progression of the scratch recovery from 0 to 24 hours in control cells and in cells exposed 50, 500 and 1000 nm, respectively. Scale bars represent 100 µm. Photos were taken with a Leica DM IL microscope coupled to a Visicam PRO 20C digital camera (ampliation 40x) using ImageJ measurement tool.

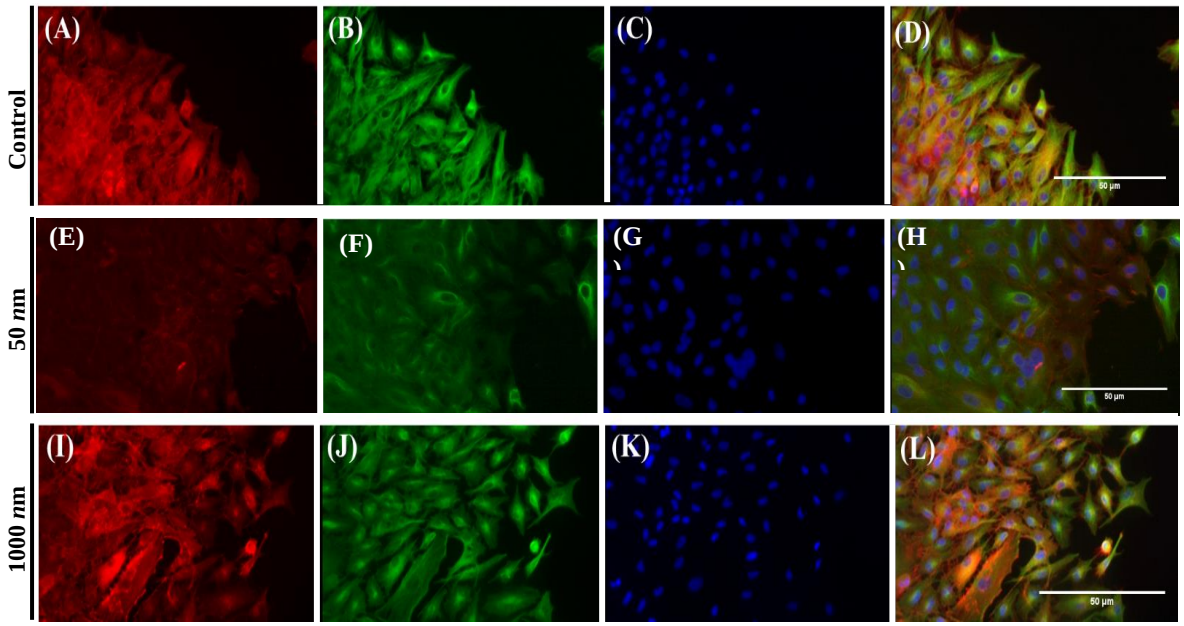

Figure 12 - Images of the scratch area provoked in a A549 cells monolayer and exposed for 72 hours to regular PSMNPs at concentrations of 0 (A-D) and 1 (E-H for 50 *n*m and I-L for 1000 *n*m particles). Co-localization of alpha-tubulin (green), actin (red) and nuclei (blue) is evident. Images are representative of control cells and 50 and 1000 *n*m treated cells at 12 h after scratching the confluent cell layer. Scale bars represent 50 *n*m. Photos were taken with a Zeiss Axio Vert. A1 coupled to a Axiocam 202 mono camera (ampliation 400x) and analysed with ImageJ 1.53t using ImageJ software for image overlay.

4.1.6 PSMNP effects on A549 cells oxidative stress

The effects of PSMNPs on A549 cells oxidative stress was evaluated by the assessment of ROS formation. This assay revealed that 50 *n*m PSNPs at a concentration of 0.01 μg/mL decreased the formation of ROS compared to the control group (non-treated cells) with a $p < 0.05$, as well as 500 *n*m PSNPs at 0.01 and 0.1 μg/mL ($p < 0.0001$ and $p < 0.05$, respectively) and 1000 *n*m PSMPs at 1 and 10 μg/mL with $p < 0.05$ (figure 13).

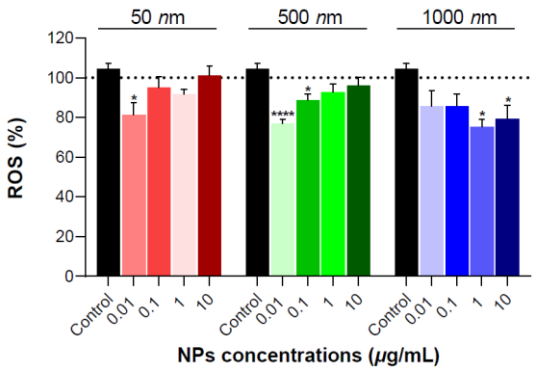

Figure 13 - ROS formation by A549 cells after their exposure to 0, 50, 500 and 1000 *n*m PSMNPs at a concentration of 0 to 10 μg/mL after 72 h of exposure time. Data is represented as the percentage of living cells relative to the untreated control ± SEM (the assay was performed with 3 replicates and 2 independent experiments). A one-way ANOVA with Tukey's Multiple Comparison test was used for the statistical analysis. Statistical analysis was performed with GraphPad Prism 8.4.2 and significance is indicated in the graph by $*p < 0.05$ and $****p < 0.0001$.

4.1.7 PSMNP effects on A549 cells morphology

The effects of PSMNPs on A549 cell morphology were evaluated. Immunofluorescence assays (IFA) showed that neither 50 or 1000 *n*m microplastics affected the morphology of the nuclei and mitochondria of the cell (figure 14). Additionally, IFA assays targeting alpha-tubulin revealed that the presence of microplastics did not cause alterations in the morphology of these structures (figure 15). IFA pictures of cells exposed to 50 *n*m PSNPs are represented in annex 2 (supplementary pictures 3 and 4).

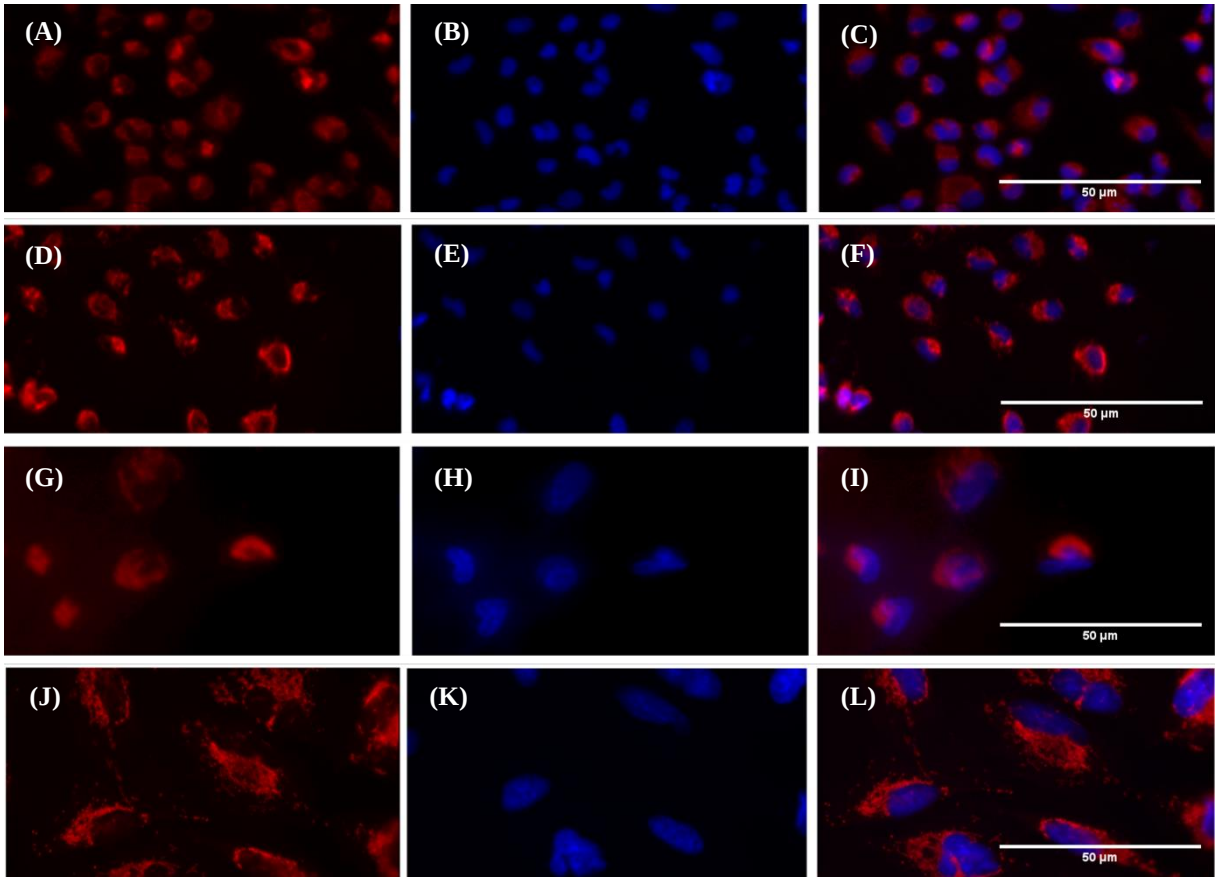

Figure 14 – Representative images of A549 control and 1000 *n*m treated cells at 400x (A-C and D-F, respectively) and 1000x ampliation (G-I and J-L, respectively). Co-localization of mitochondria (red) and nuclei (blue) is evident. Scale bars represent 50 μm. Photos were taken with a Zeiss Axioscope 5 coupled to an Axiocam 202 mono camera and analysed with ImageJ version 1.53t using ImageJ software for image overlay.

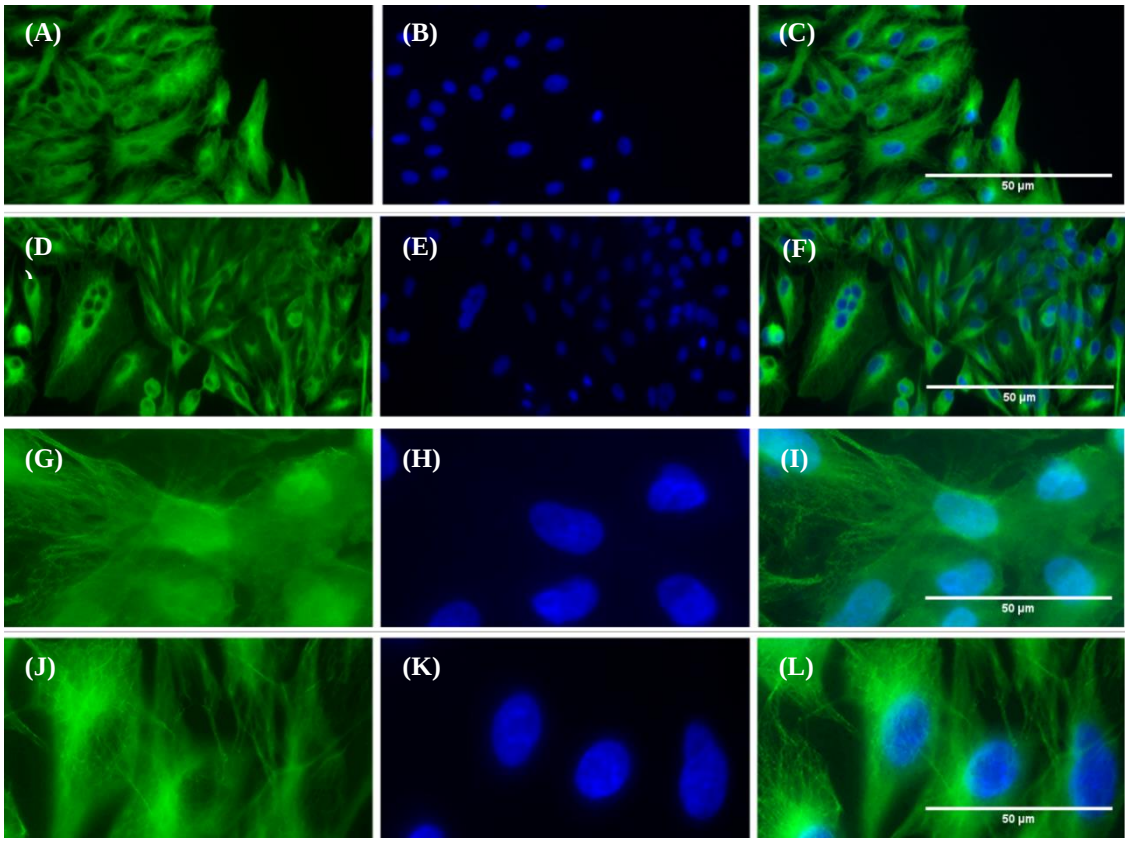

Figure 15 – Representative images of A549 control and 1000 *n*m treated cells at 400x (A-C and D-F, respectively) and 1000x ampliation (G-I and J-L, respectively). Co-localization of alpha-tubulin (green) and nuclei (blue) is evident. Scale bars represent 50 μm. Photos were taken with a Zeiss Axioscope 5 coupled to an Axiocam 202 mono camera and analysed with ImageJ version 1.53t using ImageJ software for image overlay.

4.1.8 PSMNP effects on cell adhesion assessed using ECIS

ECIS was used to evaluate the effects of PSMNPs on cell adhesion through the measurement of the resistance. Results showed that cells treated with 50 and 500 *n*m nanoplastics had a greater adhesion capacity in the first 24 hours ($p < 0.0001$), and by 48 hours after plating the cells completely adhered to the microchip (figure 16).

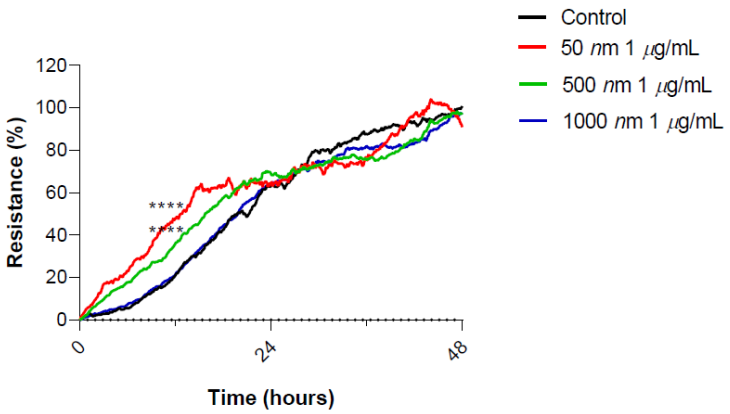

Figure 16 - Electrical resistance of a confluent A549 cell monolayer exposed to 50, 500 and 1000 nm PSMNPs at concentrations ranging from 0 to 1 µg / mL, measured at 4000 Hz. Data is represented as the average resistance of one experiment with two replicates for each treatment group. A one-way ANOVA with Tukey's Multiple Comparison test was used for the statistical analysis of the first 24 hours of the assay. Statistical analysis was performed with GraphPad Prism 8.4.2 and significant differences are indicated in the graph as ****p < 0.0001.

4.1.9 PSMNP effects on wound recovery assessed using ECIS

ECIS was also used to evaluate the effects of PSMNPs on wound recovery through the measurement of changes in the resistance. Results showed that cells treated with the largest particles recovered significantly faster in the first 12 hours after damage ($p < 0.01$ and $p < 0001$, respectively). Cells took approximately 24 hours to repair the damage and achieve a confluent monolayer but did not achieve the starting resistance (figure 17).

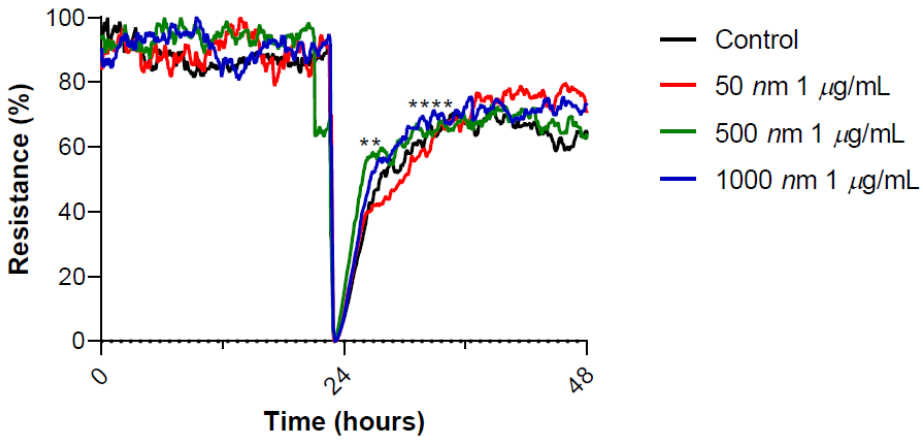

Figure 17 – Electrical resistance of a confluent A549 cell monolayer exposed to 50, 500 and 1000 *n*m PSMNPs at concentrations of 0 or 1 μg / mL after an electrical wound was inflicted. Data is represented as the average resistance of one experiment with two replicates for each treatment group. A one-way ANOVA with Tukey's Multiple Comparison test was used for the statistical analysis of between the timepoints 24-36 hours. Statistical analysis was performed with GraphPad Prism 8.4.2 and significant difference are noted in the graph by $**p < 0.1$ and $****p < 0.0001$.

4.2 Caco-2 cells

4.2.1 Characterization of Caco-2 cells

Caco-2 cells are adherent epithelial cells isolated from colon tissue which grow into a cell monolayer. Caco-2 cells are small and rounded in shape and have a variable morphology, as illustrated in the figures 18 and 19.

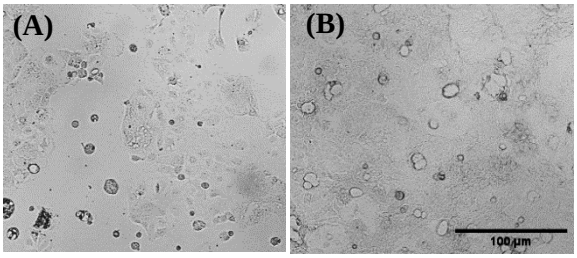

Figure 18 – Representative images of adherent Caco-2 cells at low density (A) and high density (B). The scale bar represents 100 μm. Photos were taken with a Leica DM IL microscope coupled to a Visicam PRO 20C digital camera (ampliation x 100).

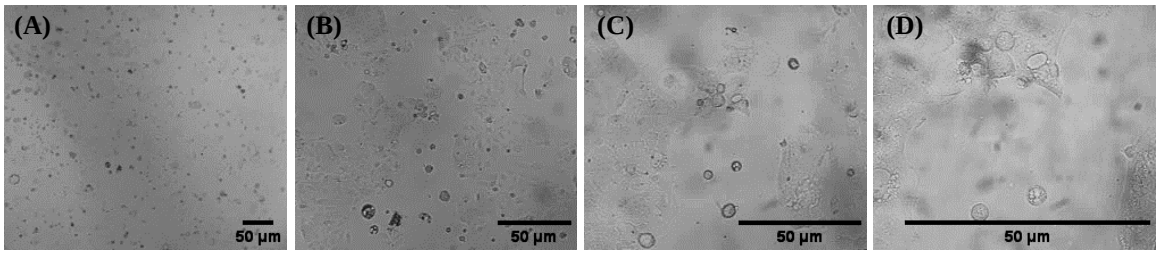

Figure 19 – Representative images of adherent Caco-2 cells at different ampliations: 40x (A), 100x (B), 200x (C) and 400x (D). Scale bars represent 50 μm. Photos were taken with a Leica DM IL microscope coupled to a Visicam PRO 2.

Caco-2 cells were characterized regarding their growth rate (figure 20). The cell growth curve shows that Caco-2 cells duplicate their population between 48 and 72 hours, displaying an exponential growth during the first 96 hours. After that, cell growth stabilizes until 192 hours.

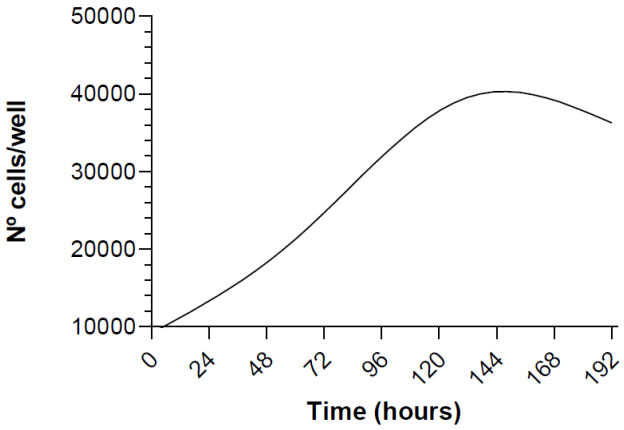

Figure 20 - Growth curve of Caco-2 cells. Data is represented as a smooth fit of the average of the number of cells per well (the assay was performed with 4 replicates).

Mitochondria are usually elongated organelles ranging from 400 to 500 *n*m. Morphological analyses of the Caco-2 cells (figure 21) revealed the presence of mitochondria with an elongated form around the cell nuclei, as has been reported in most cell lines (Nasonovs *et al.*, 2021). Alpha-tubulin was also concentrated around the nuclei and throughout the cytoplasm, where it presented a fibrous morphology, while actin was very dense and reticulated, connecting the cell monolayer.

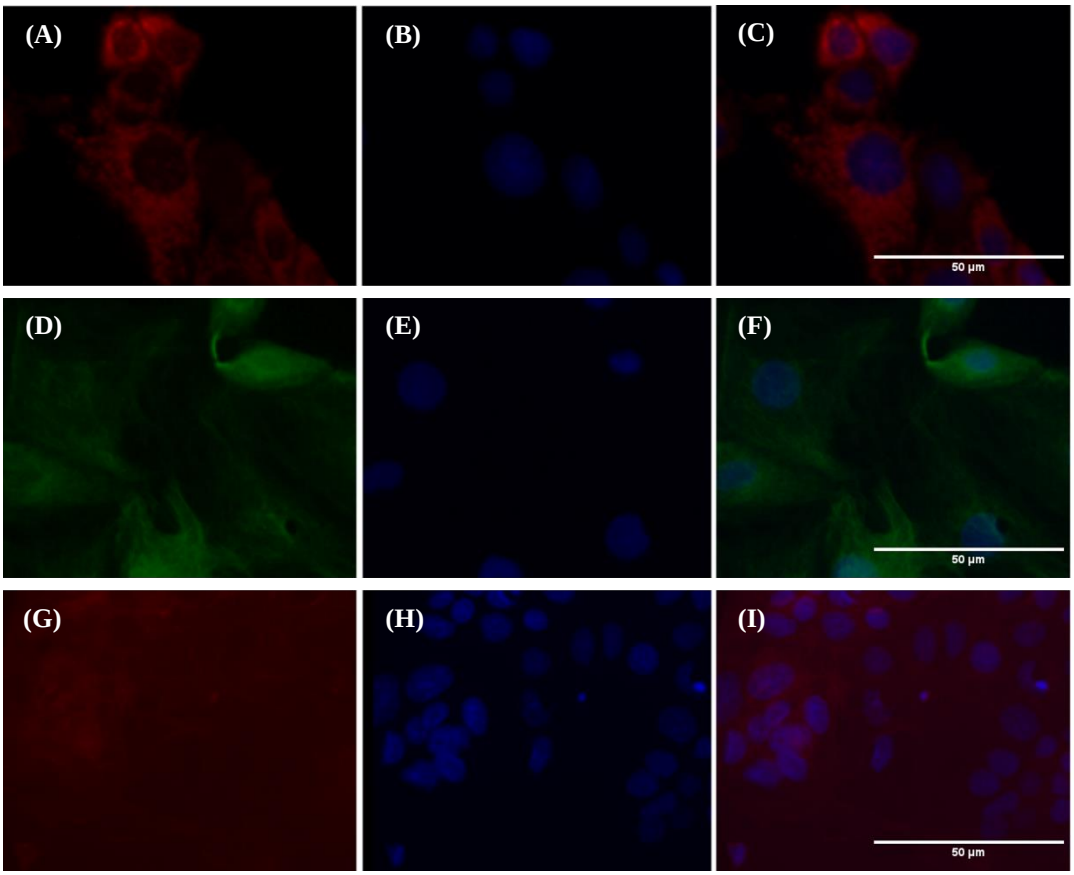

Figure 21 – Representative images of Caco-2 cells. Nuclei is always represented in blue. In (A) and (C), the red colour represents mitochondria, in (D) and (F) the green colour represents alpha-tubulin and in (G) and (H) the red colour represents actin. Scale bars represent 50 μm. Photos were taken with a Zeiss Axio Vert. A1 with a Axiocam 202 mono camera (ampliation 400x) and were analysed with ImageJ version 1.53t using ImageJ software for image overlay.

4.2.2 Uptake of PSMNPs by Caco-2 cells

The uptake capacity of PSNPs by Caco-2 cells was evaluated with regular and green-fluorescent 500 and 1000 *n*m PSMPs at concentrations ranging from 0 to 100 μg/mL. Results showed that cells take up 1000 *n*m polystyrene particles in 72 hours, and then they start to accumulate around nuclei (figure 22). It was observed that the non-fluorescent particles were less easily internalized than the unlabelled particles (regular particles). In annex 3 images of the Caco-2 cells exposed to 500 and 1000 *n*m particles are presented to illustrate MNP uptake when cells are exposed to a concentration range (supplementary figures 5 and 6).

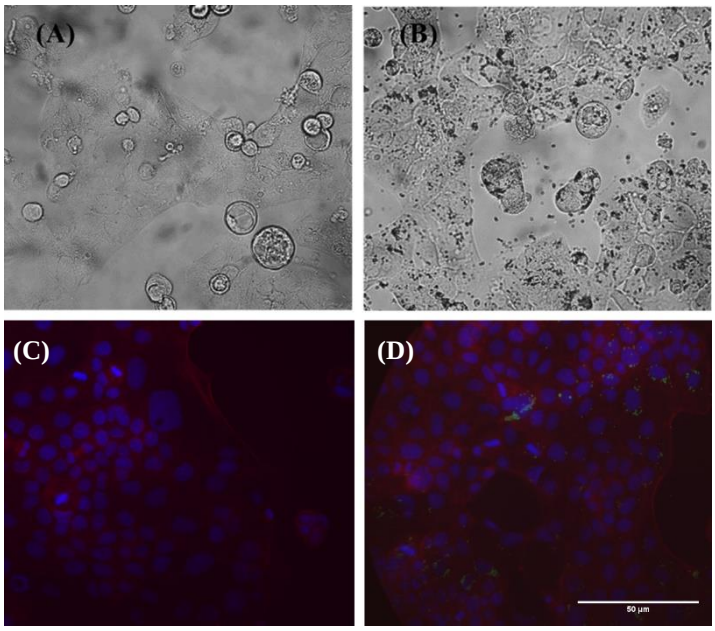

Figure 22 – Representative images of Caco-2 cells after 72h exposure to 1000 *n*m regular PSMPs at a concentration of 0 (A) and 1 μg/mL (B) and 1000 *n*m green-fluorescent PSMPs at a concentration of 0 (C) and 1 μg/mL (D). Co-localization of nuclei (blue) and actin (red). The scale bar represents 50 μm. Photos were taken with a Leica DM IL microscope coupled to a Visicam PRO 20C digital camera (ampliation 400x) using ImageJ software for image overlay.

Confocal microscopy was used to confirm that the 1000 *n*m microplastics were internalized by the Caco-2 gut cells (figure 23). The results showed that microparticles were internalized by the cells and were close to the cell nuclei, which is a similar pattern of PSMP distribution to what was observed in the inverted microscope.

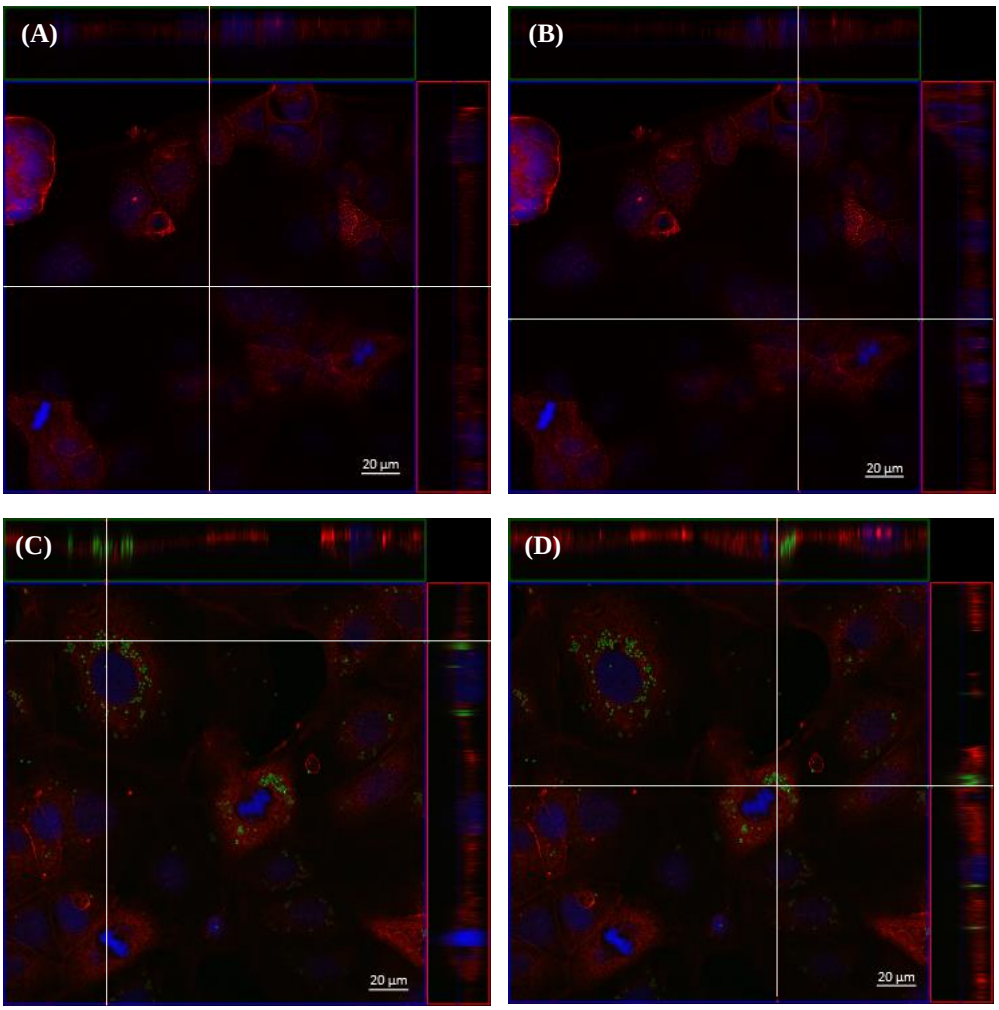

Figure 23 – Representative orthogonal view of the confocal microscopy images of Caco-2 cells exposed to 0 (A and B) and 1 μg / mL green-fluorescent 1000 *n*m PSMPs for 72 hours. Co-localization of actin (red), nuclei (blue) and PSMPs (green) is evident. Scale bars represent 20 *n*m. Z-stack 3D pictures were taken with a Zeiss 1 LSM 710 confocal microscope with Airyscan and analysed with Zeiss Zen 8 Lite (orthogonal view).

4.2.3 PSMNP effects on Caco-2 cell viability

The effect of PSMNPs on Caco-2 cell viability was evaluated using a MTT assay. This assay revealed that 500 *n*m PSNPs at concentrations of 1 and 10 μg/mL decreased the cell viability compared to the control group (non-treated cells). Exposure to 1000 *n*m PSMPs at 1

μg/mL had a similar effect $p < 0.05$ (figure 24). Of note was the observation that the smallest nanoplastics tended to increase the Caco-2 viability, although not significantly.

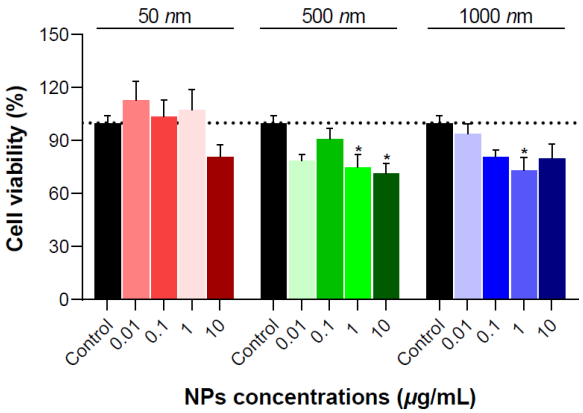

Figure 24 - Cell viability of Caco-2 cells after the exposure to 50, 500 and 1000 *n*m PSMNPs at concentrations ranging from 0 to 10 μg/mL after 72 h of exposure. Data is represented as the percentage of living cells relative to the untreated control ± SEM (the assay was performed with 4 replicates and 3 independent experiments). A one-way ANOVA with a Tukey's Multiple Comparison test was used for the statistical analysis. Statistical analysis was performed with GraphPad Prism 8.4.2 and significance is indicated in the graph with * and denotes $p < 0.05$.

4.2.4 PSMNP effects on Caco-2 cell proliferation

The effect of PSMNPs on Caco-2 cell proliferation was evaluated and it presented a concentration and size-dependent reduction (figure 25). This assay showed that 50 *n*m nanoparticles at 0.01, 0.1 and 1 μg/mL increased the cell growth at 48 hours ($p < 0.05$, $p < 0.0001$ and $p < 0.001$, respectively), while at 72 hours for 0.01 and 1 μg/mL it was significantly reduced ($p < 0.0001$). Regarding 500 *n*m nanoplastics, at 24 hours, the cell growth was reduced at 1 and 10 μg/mL ($p < 0.05$ and $p < 0.0001$). After, 48 hours, the proliferation was enhanced at 0.1 μg/mL ($p < 0.0001$) but reduced for the highest concentration of PSMNPs ($p < 0.0001$). These nanoplastics increased Caco-2 cell proliferation at 72 hours at 0.01 and 1 μg/mL ($p < 0.0001$) and continued to reduce it for the highest dose ($p < 0.0001$). For the largest particles, there was a reduction in the cell growth in the first 24 hours at 0.01 μg/mL ($p < 0.05$) and at 48 hours for both 0.01 and 10 μg/mL ($p < 0.01$ and $p < 0.0001$, respectively). By 72 hours of proliferation, the 1000 *n*m particles at all exposure concentrations had significantly decreased the cell proliferation, compared to the control cells ($p < 0.0001$).

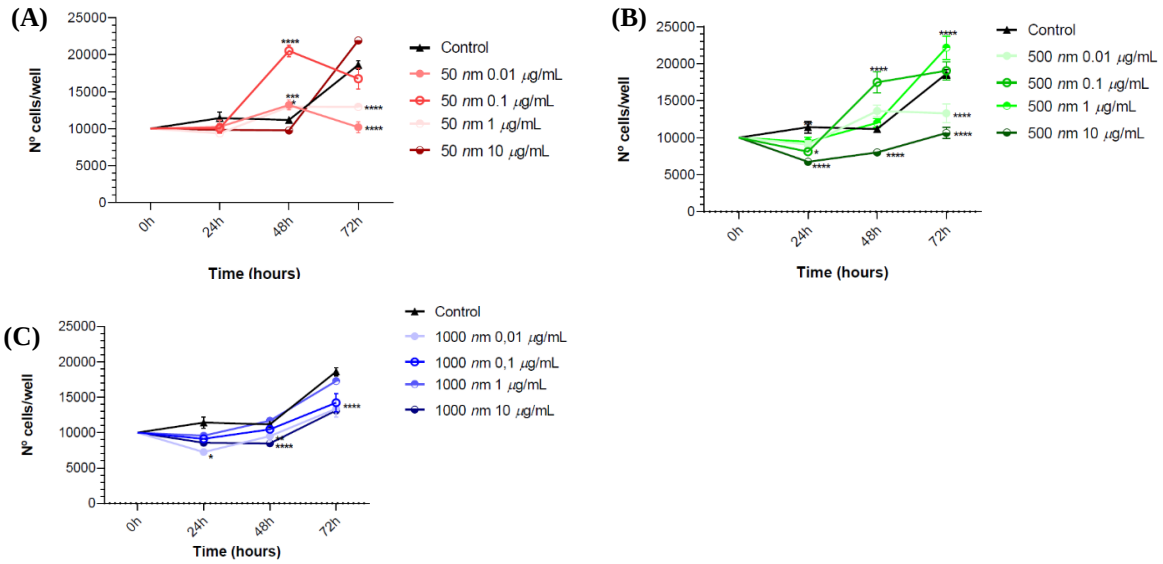

Figure 25 – Caco-2 cell proliferation after the exposure to 50 (A), 500 (B) and 1000 *n*m (C) PSMNPs at concentrations ranging from 0.01 to 1 μg/mL for 72 hours. Data is represented as the number of cells per well ± SEM (the assay was performed with 3 replicates and 3 independent experiments). A two-way ANOVA with Tukey's Multiple Comparison test was used for the statistical analysis. Statistical analysis was performed with GraphPad Prism 8.4.2 and significance is indicated in the graphs by *$p < 0.05$, **$p < 0.01$, ***$p < 0.001$ and ****$p < 0.0001$.

4.2.5 PSMNP effects on Caco-2 migration

The effects of PSMNPs on Caco-2 cell migration was evaluated using a scratch assay. This assay showed that in the presence of PSMNPs the cells took more time to recover from the scratch compared to the untreated cells. The difference in time of recovery for the control versus PSMNP was significant for 50 *n*m at 30 h and 48 h after the scratch was made ($p < 0.01$ and $p < 0.05$, respectively) and for 1000 *n*m at 48h after the scratch was made ($p < 0.0001$) (figure 26).

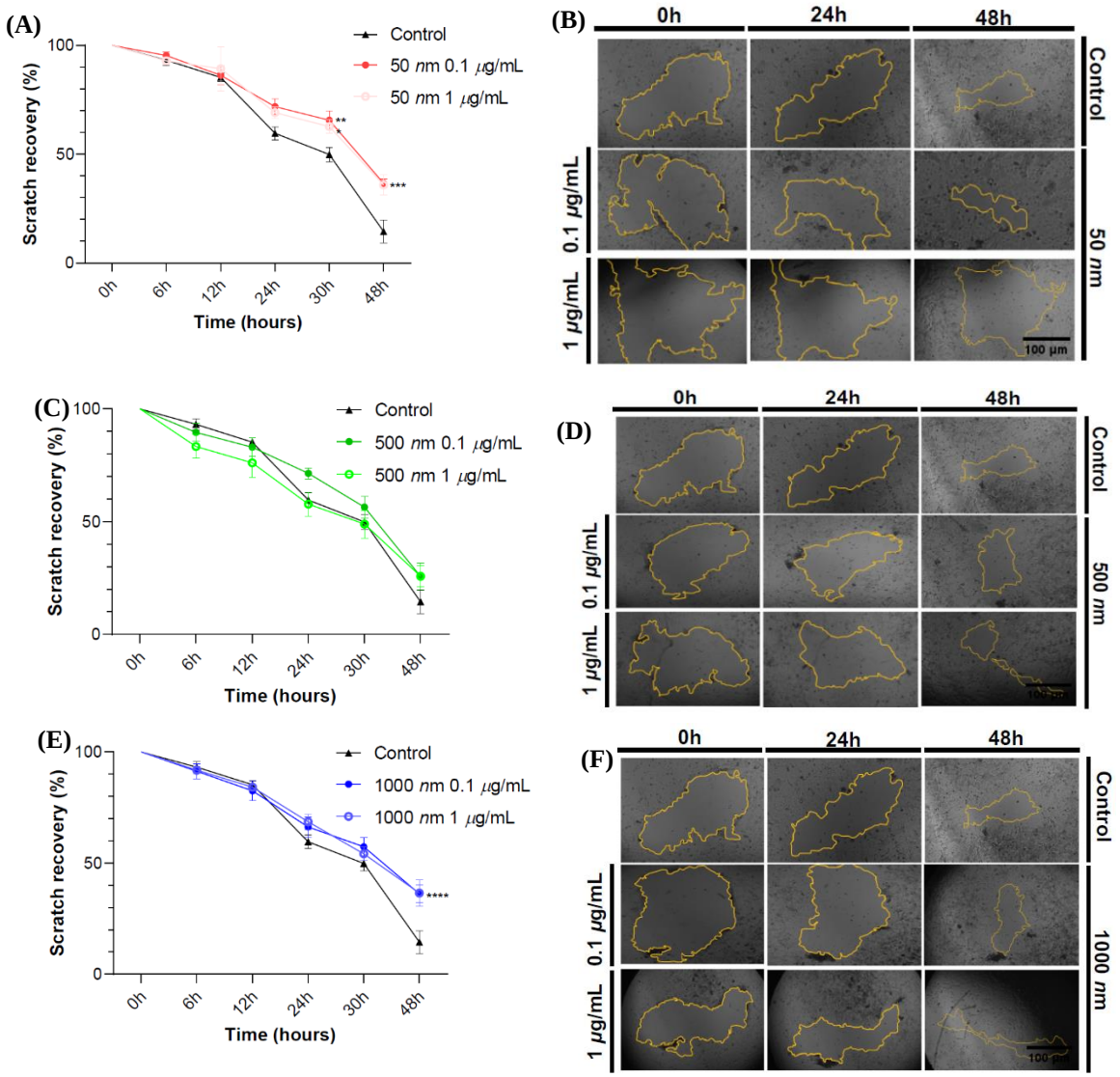

Figure 26 – Caco-2 cells scratch assay: (A), (C) and (E) represent the scratch recovery area (percentage) of Caco-2 cells after the exposure to 50, 500 and 1000 *n*m PSMNPs, respectively, at concentrations ranging from 0 to 1 μg/mL, measured at 0, 6, 12, 24, 30 and 48 hours in relation to the area immediately after the scratch (100 %). Data is represented as the percentage of the repaired scratch area relative to the initial scratch area ± SEM (the assay was performed with 3 replicates and 3 independent experiments). A two-way ANOVA with Tukey's Multiple Comparison test was used for the statistical analysis. Statistical analysis was performed with GraphPad Prism 8.4.2 and significance is indicated in the graphs as $*p < 0.05$, $**p < 0.01$. (B), (D) and (F) are representative images showing the progression of the scratch recovery from 0 to 24 hours in control cells and in cells exposed to 50, 500 and 1000 *n*m, respectively. Scale bars represent 100 μm. Photos were taken with a Leica DM IL microscope coupled to a Visicam PRO 20C digital camera (ampliation 40x) using the ImageJ measurement tool.

4.2.6 PSMNP effects on Caco-2 oxidative stress

The effects of PSMNPs on the oxidative stress of Caco-2 cells was evaluated by the assessment of ROS formation. This assay revealed that 50 and 500 *n*m PSNPs at a concentration of 0.01 μg/mL increased the formation of ROS compared to the control group (non-treated cells), $p < 0.05$ (figure 27). Other PSNP sizes and concentrations did not significantly affect the ROS production in Caco-2 cells.

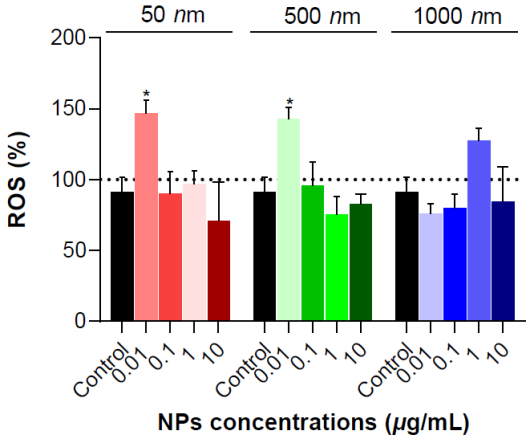

Figure 27 - ROS formation by Caco-2 cells after their exposure to 0, 50, 500 and 1000 *n*m PSMNPs at concentrations ranging from 0 to 10 μg/mL after 72 h of exposure time. Data is represented as the percentage of living cells relative to the untreated control ± SEM (the assay was performed with 3 replicates and 2 independent experiments). A one-way ANOVA with Tukey's Multiple Comparison test was used for the statistical analysis. Statistical analysis was performed with GraphPad Prism 8.4.2 and significantly different groups are identified with ***** and correspond to $p < 0.05$.

4.2.7 PSMNP effects on Caco-2 morphology

The effects of PSMNPs on Caco-2 cell morphology was evaluated with a staining procedure and immunofluorescence assays (IFA). IFA showed that nano- and microplastics did not affected the morphology of the cell, namely the nuclei and mitochondria (figure 28). Furthermore, IFA assays targeting alpha-tubulin and actin showed that the presence of microplastics did not cause alterations in the morphology of these structures (figure 29). IFA pictures of cells exposed to 50 *n*m PSNPs are represented in annex 4 (supplementary figures 7 and 8).

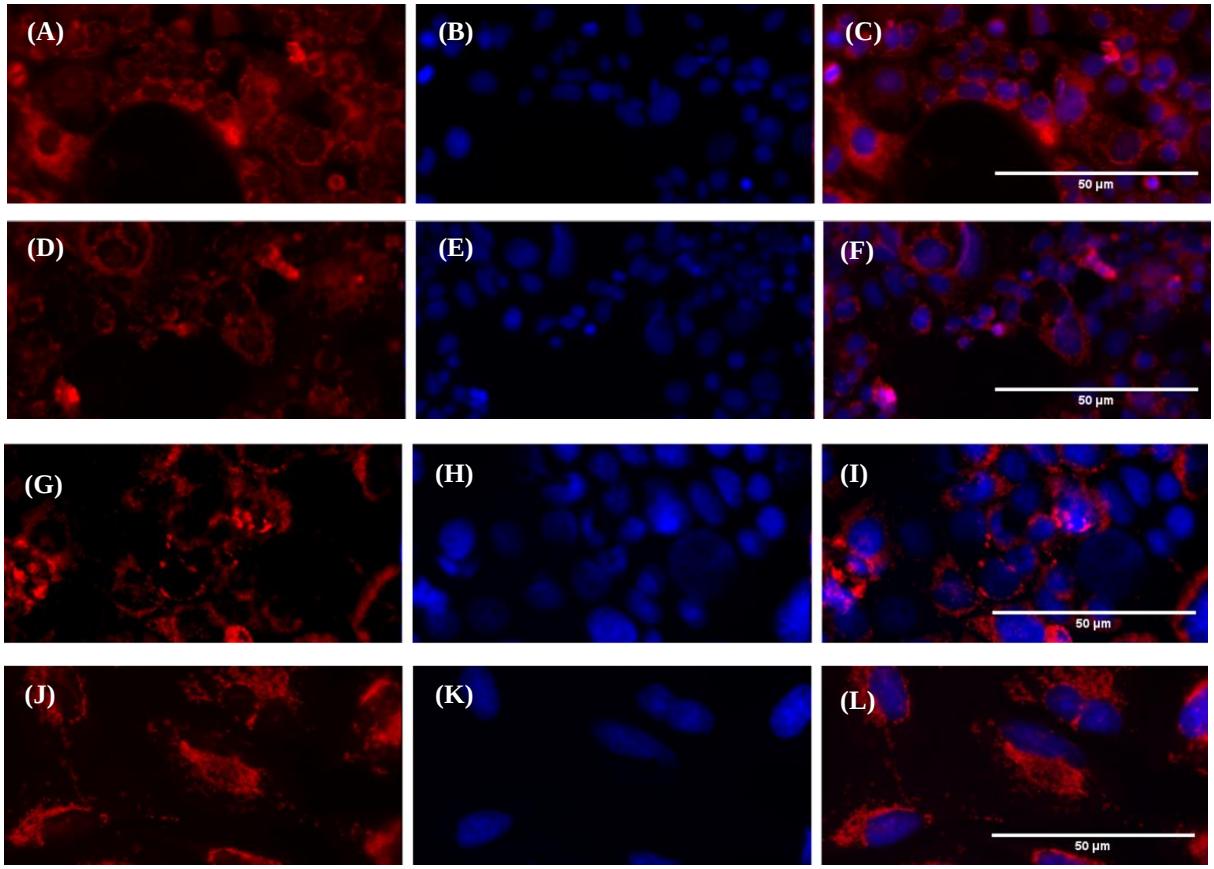

Figure 28 – Representative images of Caco-2 control and 1000 nm treated cells at 400x (A-C and D-F, respectively) and 1000x ampliation (G-I and J-L, respectively). Co-localization of mitochondria (red) and nuclei (blue) is evident. Scale bars represent 50 µm. Photos were taken with a Zeiss Axioscope 5 coupled to an Axiocam 202 mono camera and analysed with ImageJ version 1.53t using ImageJ software for image overlay.

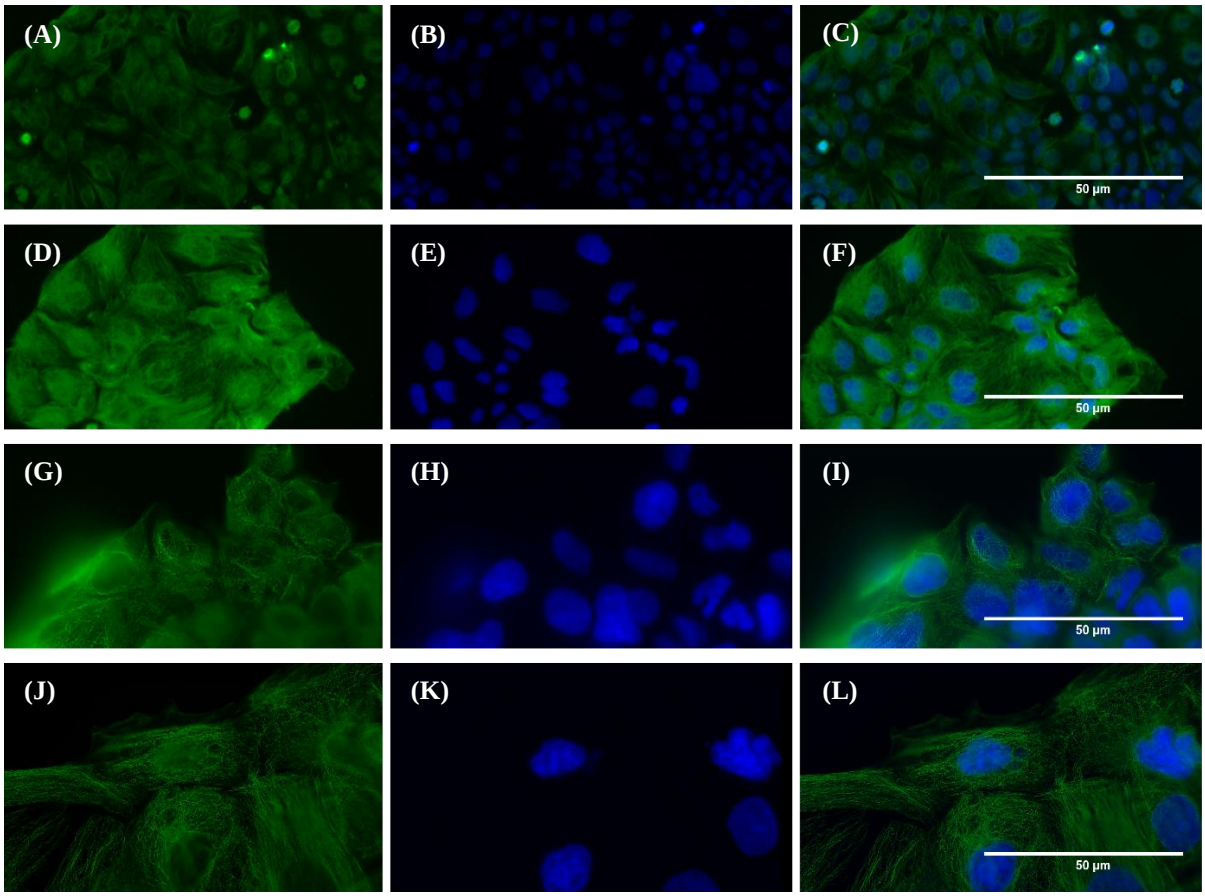

Figure 29 – Representative images of Caco-2 control and 1000 *n*m treated cells at 400x (A-C and D-F, respectively) and 1000x ampliation (G-I and J-L, respectively). Co-localization of alpha-tubulin (green) and nuclei (blue) is evident. Scale bars represent 50 μm. Photos were taken with a Zeiss Axioscope 5 coupled to an Axiocam 202 mono camera and analysed with ImageJ version 1.53t using ImageJ software for image overlay.

4.2.8 PSMNP effects on cell adhesion assessed using ECIS

ECIS was used to evaluate the effects of PSMNPs on cell adhesion through the measurement of the resistance. Results showed that cells treated with 500 and 1000 *n*m particles had a greater adhesion capacity in the first 48 hours ($p < 0.0001$), and 72 hours was the time necessary for cells to completely adhere to the microchip (figure 30).

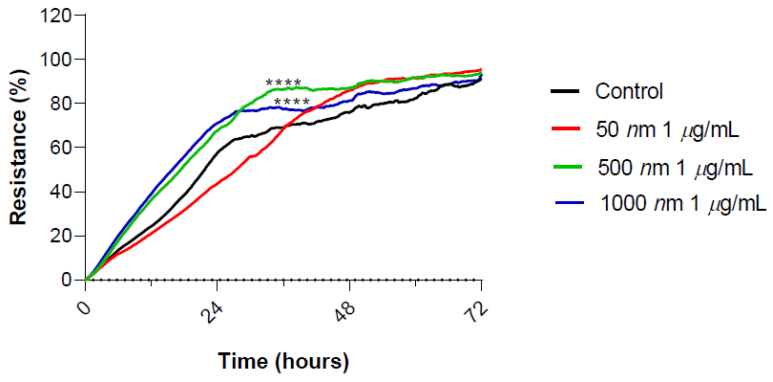

Figure 30 - Electrical resistance of a confluent Caco-2 cell monolayer exposed to 50, 500 and 1000 *n*m PSMNPs at concentrations ranging from 0 to 1 μg / mL, measured at 4000 Hz. Data is represented as the average resistance of one experiment with two replicates for each treatment group. A one-way ANOVA with Tukey's Multiple Comparison test was used for the statistical analysis of the first 48 hours of the assay. Statistical analysis was performed with GraphPad Prism 8.4.2 and significant differences are indicated in the graph as *p < 0.0001.

4.2.9 PSMNP effects on wound recovery assessed using ECIS

ECIS was also used to evaluate the effects of PSMNPs on wound recovery through the measurement of the resistance. Results showed that cells exposed to 50 *n*m, 500 *n*m and 1000 *n*m did not recover as expected in the 24 hours after the cell monolayer was damaged (p < 0.0001). Caco-2 cells treated with smallest size nanoplastics (50 *n*m) only recovered about 40% of the wound area, while Caco-2 cells treated with 1000 *n*m PSMPs were unable to repair the wounded cell monolayer. Caco-2 cells both the control and 500 *n*m PSMNPs took approximately 24 hours to reestablish the cell monolayer and reach the initial resistance (figure 31).

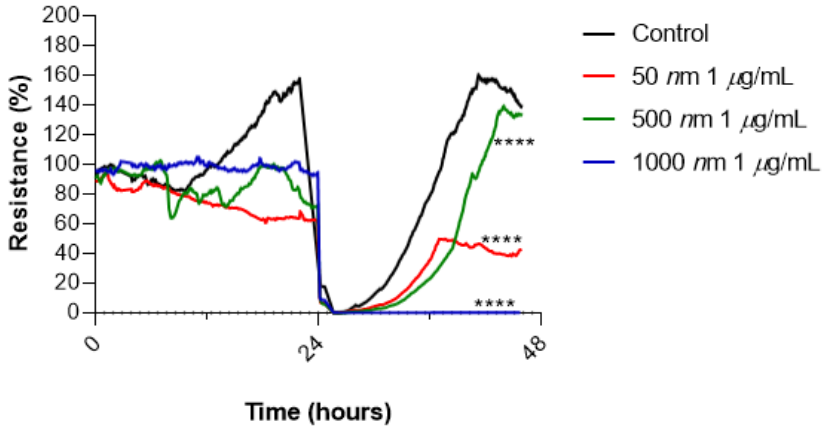

Figure 31 – – Electrical resistance of a confluent Caco-2 cell monolayer exposed to 50, 500 and 1000 *n*m PSMNPs at concentrations of 0 or 1 μg / mL after an electrical wound was inflicted. Data is represented as the average resistance of one experiment with two replicates for each treatment group. A one-way ANOVA with Tukey's Multiple Comparison test was used for the statistical analysis between the timepoints 24-36 hours of the assay. Statistical analysis was performed with GraphPad Prism 8.4.2 and significantly different treatments are indicated in the graph using ** or **** for a p < 0.1 and p < 0.0001, respectively.

5. Discussion

MNPs increase represent an emerging global concern to the environment and humanity, being present in the oceans, soils and even air. There are already reports about the presence of MNPs in several marine species, soil, microorganisms and even humans. However, there are still few studies regarding their effects on human cell lines. To fill this gap, our study focused on the effects of MNPs in two cell lines from tissues directly exposed to the particles in the environment: human lung adenocarcinoma cells (A549) and human gut adenocarcinoma cells (Caco-2).

Firstly, both cell lines were characterized regarding their growth curve and cell morphology. Growth curve results showed that A549 cells take about 48 hours to duplicate, while Caco-2 cells needed 2 to 3 days, a similar behaviour was reported by other studies (Jahn *et al.*, 2010; Leibrock *et al.*, 2019). In lung cells, mitochondria presented a swollen and spherical form around cell nuclei, while for Caco-2, mitochondria was elongated and branched as is typical for most cell lines (Nasonovs *et al.*, 2021). Regarding the cell cytoskeleton, actin filaments and alpha-tubulin microtubules were found around the nuclei and in the cytoplasm with a fibrous and dense morphology in both cell lines.

After experiment with different incubation periods, it was observed that both cell lines efficiently internalized microparticles within 72 hours. *In vivo*, lungs have a thin barrier of 1 μm, and internalized particles can penetrate into the capillary blood system and potentially spread throughout the body (Lehner *et al.*, 2019). Interestingly, non-fluorescent (regular) particles exhibited greater uptake by lung and gut cells compared to fluorescent particles. One possible explanation for this disparity in uptake may be because the green fluorescent protein attached to the particles influenced the particle-cell membrane interaction, potentially due to differences in surface polarity. In this context, regular polystyrene particles, which are hydrophobic, can more easily permeate into the lipidic bilayer. To confirm this hypothesis, further studies investigating the structural properties of fluorescent and regular polystyrene micro- and nanoparticles are required. Confocal microscopy also confirmed there was particle uptake by both cell lines, with Caco-2 internalizing more microplastics than A549 cells, which is likely connected to their intrinsic characteristics and functions. In both cases, 1000 *n*m PSMPs accumulated around the cell nuclei, as has been reported in previous studies (Domenech, Cortés, *et al.*, 2021; X. Shi *et al.*, 2022)

PSMNPs exhibited a size and concentration-dependent impact on A549 cell viability. Higher concentrations and larger particles, such as 500 and 1000 *n*m, showed an increased cell toxicity. In contrast, the cytotoxic effect of smaller nanoplastics was very low, as observed in hematopoietic cell lines, such as Raji-B, TK6 and THP-1, which were exposed to 50 *n*m PSNPs at a range of concentrations from 0 to 200 μg / mL (Rubio *et al.*, 2020). Additionally, A549 cells treated with 100 *n*m PSNPs did not cause changes in cell viability at concentrations up to 20 μg / mL (Q. Shi, Tang, Wang, *et al.*, 2021). Generally, nanoplastics show greater cell toxicity compared to microplastics. However, an ecotoxicological analysis of nanoplastics revealed that larger particles were most toxic and that polystyrene was more toxic than PMMA and PHB (T. Yang & Nowack, 2020).

In Caco-2 cells, the impact of size and concentration effects on cell viability was also observed. Interestingly, the presence of 50 *n*m at low doses seemed to stimulate cell viability, which could potentially be attributed to the phenomenon of hormesis. Hormesis occurs when an agent, known to be toxic at high doses, exhibits a stimulating or beneficial effect at low doses (Calabrese, 2008). Similar stimulation effects on cell viability have been observed in fibroblast cells, Hs27, treated with 100 *n*m PSNPs, suggesting a potential overcompensation response due to disruption of cell homeostasis (Poma *et al.*, 2019). Despite the observed cytotoxicity, the reduction in cell viability was only around 20 to 30 %. The resistance to PSMNPs of Caco-2 cells could be explained by their role as a primary barrier in the human body, and the results observed in the present study corroborate observations in previous studies (Cortés *et al.*, 2020; Domenech, de Britto, *et al.*, 2021; B. Wu *et al.*, 2019). However, it is important to highlight that cells are generally only exposed to PSMNPs for a relatively short duration, and longer-term assays are required to thoroughly evaluate the impact of plastics particles in the human body. This is particularly important because one of the main concerns about MNPs is their potential association with carcinogenesis (Domenech, de Britto, *et al.*, 2021).

PSMNPs didn't present a clear effect on A549 proliferation, as different effects were observed in the micro- and nanoparticles sizes and concentrations tested. This variability could be attributed to an unbalanced homeostasis or the possibility that effects on cell proliferation only manifest at higher concentrations, as reported in other studies (Goodman *et al.*, 2021). A transcriptomic analysis revealed up-regulation of genes involved in cell proliferation (such as CCND coding for cyclin D and Ki678) in A549 cells exposed to PSNPs. This up-regulation may be explained by DNA peroxidation, which can be reverted by delayed cell progression through base excision repair (M. Xu *et al.*, 2019). Regarding Caco-2 proliferation, PSMNPs

appear to have a negative effect in a size and dose-dependent manner. The highest concentration of 500 *n*m and 1000 *n*m particles significantly reduced cell growth. However, the opposite effect was observed at lower concentrations of nanoplastics, suggesting, again, a potential hormesis effect with lower doses of a toxic compound stimulating cell growth. A similar reduction in cell growth with increasing of PSNPs concentrations with 100 *n*m particle size was also observed in others intestinal epithelial cell lines such as HIEC-6, RKO, HT-29 and HTCC116 (X. Xu *et al.*, 2023).

During the scratch recovery assay, the A549 cells treated with PSMNPs showed faster migration compared to untreated cells, particularly at the 12 h time point. In terms of cell morphology, cells in the scratched area appeared to elongate and migrate to fill the empty zone. In the case of Caco-2 cells, the presence of particles affected the migration capacity of cells, particularly with the 50 and 1000 *n*m particles. The scratch assay is commonly used to assess cell migration capacity which is relevant for processes like angiogenesis or wound repair, and it relies on the actin cytoskeleton and microtubules. Thus, it is possible that the reduction in the scratch recovery capacity in Caco-2 cells could result from the interference of nano- and microplastics with the cell cytoskeleton (Kauanova *et al.*, 2021).

The evaluation of ROS production showed that both nanoplastics (50 and 500 *n*m) exhibited an increase in lung cell ROS production with increasing concentration of PSMNPs, although the concentrations of ROS were comparable to the control A549 cells. These findings suggest that nanoplastics may interfere with the production of ROS. In the presence of 1000 *n*m PSMPs, a decrease in ROS production was observed as the particle concentration was increased, suggesting that larger particles may have a different impact on the oxidative stress response compared to smaller PSNPs. In the case of Caco-2 cells, the effect of particles on ROS production was different. Not only was there no significant increase in ROS production with increasing nanoparticle concentration, but there was also no significant decrease in ROS production with the larger plastics. In fact, ROS production increased at 0.01 μg / mL when cells were exposed to particles of 50 and 500 *n*m and at 1 μg / mL of 1000 *n*m, and for the rest of concentrations, it remained relatively similar to the control group. The DCFH-DA method, which we used to detect ROS production, involves a broad spectrum of reactive species, such as H_2O_2, $ONOO^-$, and superoxide, where DCFH-DA is deacetylated by a nonspecific esterase in the cytoplasm and later oxidized to DCF. Other studies have reported non-significant effects on oxidative stress of Caco-2 cells using the DCFA-DH method and have suggested the use of

alternative approaches or the supplementation of this method with genotoxicity evaluation, such as the comet assay (Cortés *et al.*, 2020; Domenech *et al.*, 2020).

From the morphology staining of A549 and Caco-2, no noticeable alterations were observed in mitochondria, actin, or tubulin for both 50 and 1000 *n*m PSMNPs compared to the control group. These findings suggest that any potential effects of micro- and nanoplastics may be manifested more at a molecular or functional level, than by modifying the morphology of the organelles.

Regarding cell adhesion, lung cells exposed to 50 and 500 *n*m nanoplastics showed a faster adhesion compared to control cells, while Caco-2 cells exposed to 500 and 1000 *n*m particles presented an opposite effect. The cell adhesion process occurs through the action of cell adhesion molecules (CAMs) that anchor the cells to an extracellular matrix or to each other. Since the presence of particles affected this process in both cell lines, this may suggest that micro- and nanoplastics can interfere with the molecules involved, such as integrins, selectins or cadherins (Miller *et al.*, 2013; Stachowicz, 2023). Moreover, throughout the wound recovery assessed by ECIS, A549 cells that had been exposed to 500 and 1000 *n*m plastics had a faster recovery than the untreated cells, which agrees with the results obtained from the scratch recovery assay. In Caco-2 cells, all sizes of particles decreased the capacity of these cells to migrate, which is similar to the outcome of the scratch assay in which 50 and 100 *n*m particles affected the migration capacity of the cells. This may suggest that micro- and nanoplastics affect the cell cytoskeleton, particularly in Caco-2 cells of the gut, even though no morphological alterations were observed with the staining assays.

In the environment, micro- and nanoparticles exist in various shapes and sizes and are exposed to different factors that can alter their structure, thereby influencing their interactions with cells. However, it is essential to initially assess the effects of these particles using spherical particles of a specific size, even though they may not precisely reflect real-word exposure conditions. This approach allows comparability between different studies. Once these effects are established, standardization models are required to account for different polymer types, particles sizes and shapes (Busch *et al.*, 2023). Furthermore, if standardized commercial MNPs exhibit negative effects on cells, it is highly likely that the non-standard MNPs in the environment may cause even more and harmful damage to cells (Lin *et al.*, 2022).

It is also important to acknowledged that the results obtained in the present study are based on the use of polystyrene particles, which is the most used material for cell culture studies.

Therefore, extrapolating these results to other types of plastics and even to real samples requires caution (Lehner *et al.*, 2019). Additionally, there is still a significant knowledge gap when it comes to effective detection and identification methods for micro- and nanoplastics in the environment. Consequently, the actual concentrations of these particles that we are currently exposed to remains uncertain and can vary across regions and environments. This gap makes it challenging to establish a concentration range that accurately represents environmental exposure and means that many studies use very high concentrations that do not really reflect the real-life exposure.

Furthermore, while the focus of these data is on the entry and uptake of particles into cells, it is equally important to consider the exocytosis of plastics. Previous studies have reported that smaller nanoplastics can enter A549 and Caco-2 cells through clathrin- and caveolae-mediated endocytosis, whereas larger nanoparticles may be phagocyted (X. Shi *et al.*, 2022; Y.-X. Zhang *et al.*, 2022). Regarding exocytosis, it has been observed that 50 and 100 *n*m PSNPs are excreted through lysosomal vesicles in A549 cells, while actin and microtubule play a role in the process in BEAS-2B lung cells (Liu *et al.*, 2023). Moreover, this study did not consider the aggregation of micro- and nanoparticles and its consequences in their shape and size. The reported spherical shape and sizes considered are based on the information provided in the product information sheets.

6. Conclusion and future perspectives

In conclusion, the internalisation of polystyrene micro- and nanoplastics by A549 and Caco-2 cell lines resulted in various effects on cell viability, oxidative stress, proliferation, and migration. However, further studies are necessary to comprehensively understand the complete range of effects that plastic particles can have on lung and gut cells. This could involve conducting metabolomic and transcriptional analyses, as well as studies of uptake and exocytosis rates of the particles. Additionally, it is also important to consider conducting long-term studies and exploring the use of different types of plastics, such as acrylic particles or even incorporating metals such as silver to better simulate real environmental exposition. Micro- and nanoplastics are already present throughout the environment and are easily transferred through the trophic chains in the food web, affecting socio-economic activities such as aquaculture and, inevitably, human health. Hence, the present cell culture based study has contributed to a more comprehensive understanding of the potential impacts of plastic particles in biological systems.

References

Abràmoff, M. D., Magalhães, P. J., & Ram, S. J. (2004). Image processing with imageJ. *Biophotonics International*, *11*(7), 36–41. https://doi.org/10.1201/9781420005615.ax4

Annangi, B., Villacorta, A., López-Mesas, M., Fuentes-Cebrian, V., Marcos, R., & Hernández, A. (2023). Hazard Assessment of Polystyrene Nanoplastics in Primary Human Nasal Epithelial Cells, Focusing on the Autophagic Effects. *Biomolecules*, *13*(2). https://doi.org/10.3390/biom13020220

Banerjee, A., Billey, L. O., & Shelver, W. L. (2021). Uptake and toxicity of polystyrene micro/nanoplastics in gastric cells: Effects of particle size and surface functionalization. *PLoS ONE*, *16*(12 December), 1–25. https://doi.org/10.1371/journal.pone.0260803

Barosova, H., Meldrum, K., Karakocak, B. B., Balog, S., Doak, S. H., Petri-Fink, A., Clift, M. J. D., & Rothen-Rutishauser, B. (2021). Inter-laboratory variability of A549 epithelial cells grown under submerged and air-liquid interface conditions. *Toxicology in Vitro*, *75*, 105178. https://doi.org/10.1016/j.tiv.2021.105178

Bengalli, R., Zerboni, A., Bonfanti, P., Saibene, M., Mehn, D., Cella, C., Ponti, J., La Spina, R., & Mantecca, P. (2022). Characterization of microparticles derived from waste plastics and their bio-interaction with human lung A549 cells. *Journal of Applied Toxicology*, *July*, 2030–2044. https://doi.org/10.1002/jat.4372

Bläsing, M., & Amelung, W. (2018). Plastics in soil: Analytical methods and possible sources. *Science of the Total Environment*, *612*, 422–435. https://doi.org/10.1016/j.scitotenv.2017.08.086

Bringer, A., Le Floch, S., Kerstan, A., & Thomas, H. (2021). Coastal ecosystem inventory with characterization and identification of plastic contamination and additives from aquaculture materials. *Marine Pollution Bulletin*, *167*(March), 1–10. https://doi.org/10.1016/j.marpolbul.2021.112286

Busch, M., Bredeck, G., Angela, A. M. K., & Schins, R. P. F. (2021). *Investigations of acute effects of polystyrene and polyvinyl chloride micro- and nanoplastics in an advanced in vitro triple culture model of the healthy and inflamed intestine*. *193*(September 2020). https://doi.org/10.1016/j.envres.2020.110536

Busch, M., Brouwer, H., Aalderink, G., Bredeck, G., Kämpfer, A. A. M., Schins, R. P. F., & Bouwmeester, H. (2023). Investigating nanoplastics toxicity using advanced stem cell-based intestinal and lung in vitro models. *Frontiers in Toxicology*, *5*(January), 1–15. https://doi.org/10.3389/ftox.2023.1112212

Calabrese, E. J. (2008). Mild Stress and Healthy Aging. In *Mild Stress and Healthy Aging*. https://doi.org/10.1007/978-1-4020-6869-0

Cavallini, F., & Tarantola, M. (2019). ECIS based wounding and reorganization of cardiomyocytes and fibroblasts in co-cultures. *Progress in Biophysics and Molecular Biology*, *144*, 116–127. https://doi.org/10.1016/j.pbiomolbio.2018.06.010

Chazotte, B. (2011a). Labeling mitochondria with mitotracker dyes. *Cold Spring Harbor Protocols*, *6*(8), 990–992. https://doi.org/10.1101/pdb.prot5648

Chazotte, B. (2011b). Labeling nuclear DNA using DAPI. *Cold Spring Harbor Protocols*, *6*(1), 80–83. https://doi.org/10.1101/pdb.prot5556

Chen, W., Ye, X., Tang, Q., Yu, T., Tu, P., & Zheng, X. (2022). Cyanidin-3-O-glucoside reduces nanopolystyrene-induced toxicity and accumulation: roles of mitochondrial energy metabolism and cellular efflux. *Environ. Sci.: Nano*, *9*(7), 2572–2586. https://doi.org/10.1039/D2EN00254J

Collin-faure, V., Dalzon, B., Devcic, J., Diemer, H., Cianférani, S., & Rabilloud, T. (2022). Does size matter? A proteomics-informed comparison of the effects of polystyrene beads of different sizes on macrophages. *Environmental Science: Nano*, *9*, 2827–2840. https://doi.org/10.1039/d2en00214k

Cortés, C., Domenech, J., Salazar, M., Pastor, S., Marcos, R., & Hernández, A. (2020). Nanoplastics as a potential environmental health factor: Effects of polystyrene nanoparticles on human intestinal epithelial Caco-2 cells. *Environmental Science: Nano*, *7*(1), 272–285. https://doi.org/10.1039/c9en00523d

Cox, K. D., Covernton, G. A., Davies, H. L., Dower, J. F., Juanes, F., & Dudas, S. E. (n.d.). *Human Consumption of Microplastics*. https://doi.org/10.1021/acs.est.9b01517

da Silva Brito, W. A., Singer, D., Miebach, L., Saadati, F., Wende, K., Schmidt, A., & Bekeschus, S. (2023). Comprehensive in vitro polymer type, concentration, and size correlation analysis to microplastic toxicity and inflammation. *Science of the Total Environment*, *854*(September 2022), 158731. https://doi.org/10.1016/j.scitotenv.2022.158731

Desidery, L., & Lanotte, M. (2022). Polymers and plastics: Types, properties, and manufacturing. *Plastic Waste for Sustainable Asphalt Roads*, 3–28. https://doi.org/10.1016/B978-0-323-85789-5.00001-0

Diao, T., Liu, R., Meng, Q., & Sun, Y. (2023). Microplastics derived from polymer-coated fertilizer altered soil properties and bacterial community in a Cd-contaminated soil. *Applied Soil Ecology*, *183*(December 2022), 104694. https://doi.org/10.1016/j.apsoil.2022.104694

Domenech, J., Cortés, C., Vela, L., Marcos, R., & Hernández, A. (2021). Polystyrene nanoplastics as carriers of metals. Interactions of polystyrene nanoparticles with silver nanoparticles and silver nitrate, and their effects on human intestinal caco-2 cells. *Biomolecules*, *11*(6). https://doi.org/10.3390/biom11060859

Domenech, J., de Britto, M., Velázquez, A., Pastor, S., Hernández, A., Marcos, R., & Cortés, C. (2021). Long-term effects of polystyrene nanoplastics in human intestinal Caco-2 cells. *Biomolecules*, *11*(10). https://doi.org/10.3390/biom11101442

Domenech, J., Hernández, A., Rubio, L., Marcos, R., & Cortés, C. (2020). Interactions of polystyrene nanoplastics with in vitro models of the human intestinal barrier. *Archives of Toxicology*, *94*(9), 2997–3012. https://doi.org/10.1007/s00204-020-02805-3

Dris, R., Gasperi, J., Rocher, V., Saad, M., Renault, N., & Tassin, B. (2015). Microplastic contamination in an urban area: A case study in Greater Paris. *Environmental Chemistry*, *12*(5), 592–599. https://doi.org/10.1071/EN14167

El Hayek, E., Castillo, E., In, J. G., Garcia, M., Cerrato, J., Brearley, A., Gonzalez-Estrella, J., Herbert, G., Bleske, B., Benavidez, A., Hsiao, H., Yin, L., Campen, M. J., & Yu, X. (2023). Photoaging of polystyrene microspheres causes oxidative alterations to surface physicochemistry and enhances airway epithelial toxicity. *Toxicological Sciences*, *193*(1), 90–102. https://doi.org/10.1093/toxsci/kfad023

Engle, M. J., Goetz, G. S., & Alpers, D. H. (1998). Caco-2 cells express a combination of

colonocyte and enterocyte phenotypes. *Journal of Cellular Physiology*, *174*(3), 362–369. https://doi.org/10.1002/(SICI)1097-4652(199803)174:3<362::AID-JCP10>3.0.CO;2-B

Eriksen, M., Lebreton, L. C. M., Carson, H. S., Thiel, M., Moore, C. J., Borerro, J. C., Galgani, F., Ryan, P. G., & Reisser, J. (2014). Plastic Pollution in the World's Oceans: More than 5 Trillion Plastic Pieces Weighing over 250,000 Tons Afloat at Sea. *PLoS ONE*, *9*(12), 1–15. https://doi.org/10.1371/journal.pone.0111913

Fogh, J., Wright, W. C., & Loveless, J. D. (1977). Absence of HeLa cell contamination in 169 cell lines derived from human tumors. *Journal of the National Cancer Institute*, *58*(2), 209–214. https://doi.org/10.1093/jnci/58.2.209

Foldbjerg, R., Dang, D. A., & Autrup, H. (2011). Cytotoxicity and genotoxicity of silver nanoparticles in the human lung cancer cell line, A549. *Archives of Toxicology*, *85*(7), 743–750. https://doi.org/10.1007/s00204-010-0545-5

Foster, K. A., Oster, C. G., Mayer, M. M., Avery, M. L., & Audus, K. L. (1998). Characterization of the A549 cell line as a type II pulmonary epithelial cell model for drug metabolism. *Experimental Cell Research*, *243*(2), 359–366. https://doi.org/10.1006/excr.1998.4172

Frias, J. P. G. L., & Nash, R. (2019). Microplastics: Finding a consensus on the definition. *Marine Pollution Bulletin*, *138*(November 2018), 145–147. https://doi.org/10.1016/j.marpolbul.2018.11.022

Fujino, H., Murayama, T., & Regan, J. W. (2010). Assessment of Constitutive Activity in E-Type Prostanoid Receptors. *Methods in Enzymology*, *484*(C), 95–107. https://doi.org/10.1016/B978-0-12-381298-8.00005-8

Gautam, R., Jo, J. H., Acharya, M., Maharjan, A., Lee, D. E., Pramod, P. B., Kim, C. Y., Kim, K. S., Kim, H. A., & Heo, Y. (2022). Evaluation of potential toxicity of polyethylene microplastics on human derived cell lines. *Science of the Total Environment*, *838*(May), 156089. https://doi.org/10.1016/j.scitotenv.2022.156089

Geyer, R., Jambeck, J. R., & Law, K. L. (2017). Production, use, and fate of all plastics ever made. *Science Advances*, *3*(7), 3–8. https://doi.org/10.1126/sciadv.1700782

Ghasemi, M., Turnbull, T., Sebastian, S., & Kempson, I. (2021). The mtt assay: Utility, limitations, pitfalls, and interpretation in bulk and single-cell analysis. *International Journal of Molecular Sciences*, *22*(23). https://doi.org/10.3390/ijms222312827

Giard, D. J., Aaronson, S. A., Todaro, G. J., Arnstein, P., Kersey, J. H., & Parks, W. P. (1973). In vitro cultivation of human tumors: Establishment of cell lines derived from a series of solid tumors. *Journal of the National Cancer Institute*, *51*(5), 1417–1423. https://doi.org/10.1093/jnci/51.5.1417

Gigault, J., Halle, A. ter, Baudrimont, M., Pascal, P. Y., Gauffre, F., Phi, T. L., El Hadri, H., Grassl, B., & Reynaud, S. (2018). Current opinion: What is a nanoplastic? *Environmental Pollution*, *235*, 1030–1034. https://doi.org/10.1016/j.envpol.2018.01.024

Goodman, K. E., Hare, J. T., Khamis, Z. I., Hua, T., & Sang, Q. X. A. (2021). Exposure of Human Lung Cells to Polystyrene Microplastics Significantly Retards Cell Proliferation and Triggers Morphological Changes. *Chemical Research in Toxicology*, *34*(4), 1069–1081. https://doi.org/10.1021/acs.chemrestox.0c00486

Gough, W., Hulkower, K. I., Lynch, R., McGlynn, P., Uhlik, M., Yan, L., & Lee, J. A.

(2011). A quantitative, facile, and high-throughput image-based cell migration method is a robust alternative to the scratch assay. *Journal of Biomolecular Screening*, *16*(2), 155–163. https://doi.org/10.1177/1087057110393340

Halimu, G., Zhang, Q., Liu, L., Zhang, Z., Wang, X., Gu, W., Zhang, B., Dai, Y., Zhang, H., Zhang, C., & Xu, M. (2022). Toxic effects of nanoplastics with different sizes and surface charges on epithelial-to-mesenchymal transition in A549 cells and the potential toxicological mechanism. *Journal of Hazardous Materials*, *430*(February). https://doi.org/10.1016/j.jhazmat.2022.128485

Hao, T., Gao, Y., Li, Z. C., Zhou, X. X., & Yan, B. (2023). Size-Dependent Uptake and Depuration of Nanoplastics in Tilapia (Oreochromis niloticus) and Distinct Intestinal Impacts. *Environmental Science and Technology*, *57*(7), 2804–2812. https://doi.org/10.1021/acs.est.2c08059

He, Y., Li, J., Chen, J., Miao, X., Li, G., He, Q., Xu, H., Li, H., & Wei, Y. (2020). Cytotoxic effects of polystyrene nanoplastics with different surface functionalization on human HepG2 cells. *Science of the Total Environment*, *723*, 138180. https://doi.org/10.1016/j.scitotenv.2020.138180

Herrala, M., Huovinen, M., Järvelä, E., Hellman, J., Tolonen, P., Lahtela-Kakkonen, M., & Rysä, J. (2023). Micro-sized polyethylene particles affect cell viability and oxidative stress responses in human colorectal adenocarcinoma Caco-2 and HT-29 cells. *Science of the Total Environment*, *867*(August 2022). https://doi.org/10.1016/j.scitotenv.2023.161512

Horvatits, T., Tamminga, M., Liu, B., Sebode, M., Carambia, A., Fischer, L., Püschel, K., Huber, S., & Fischer, E. K. (2022). Microplastics detected in cirrhotic liver tissue. *EBioMedicine*, *82*, 1–10. https://doi.org/10.1016/j.ebiom.2022.104147

Hou, Y., Tu, S., Zhao, X., Li, G., Li, N., & Zou, A. (2023). An integrative method for evaluating the biological effects of nanoparticle-protein corona. *Biochimica et Biophysica Acta - General Subjects*, *1867*(3). https://doi.org/10.1016/j.bbagen.2022.130300

Huang, W., Yin, H., Yang, Y., Jin, L., Lu, G., & Dang, Z. (2021). Influence of the co-exposure of microplastics and tetrabromobisphenol A on human gut: Simulation in vitro with human cell Caco-2 and gut microbiota. *Science of the Total Environment*, *778*, 146264. https://doi.org/10.1016/j.scitotenv.2021.146264

Hufnagel, M., May, N., Wall, J., Wingert, N., Garcia-Käufer, M., Arif, A., Hübner, C., Berger, M., Mülhopt, S., Baumann, W., Weis, F., Krebs, T., Becker, W., Gminski, R., Stapf, D., & Hartwig, A. (2021). Impact of nanocomposite combustion aerosols on a549 cells and a 3d airway model. *Nanomaterials*, *11*(7). https://doi.org/10.3390/nano11071685

Hurley, R. R., & Nizzetto, L. (2018). Fate and occurrence of micro(nano)plastics in soils: Knowledge gaps and possible risks. *Current Opinion in Environmental Science and Health*, *1*, 6–11. https://doi.org/10.1016/j.coesh.2017.10.006

Iwakura, T., Marschner, J. A., Zhao, Z. B., Świderska, M. K., & Anders, H. J. (2021). Electric cell-substrate impedance sensing in kidney research. *Nephrology Dialysis Transplantation*, *36*(2), 216–223. https://doi.org/10.1093/ndt/gfz191

Jahn, K. A., Biazik, J. M., & Braet, F. (2010). GM1 expression in Caco-2 c. *Journal of Pharmaceutical Sciences*, *100*(9), 3751–3763. https://doi.org/10.1002/jps

Jenner, L. C., Rotchell, J. M., Bennett, R. T., Cowen, M., Tentzeris, V., & Sadofsky, L. R.

(2022). Detection of microplastics in human lung tissue using μFTIR spectroscopy. *Science of the Total Environment*, *831*(December 2021), 154907. https://doi.org/10.1016/j.scitotenv.2022.154907

Jeyavani, J., Sibiya, A., Stalin, T., Vigneshkumar, G., Al-Ghanim, K. A., Riaz, M. N., Govindarajan, M., & Vaseeharan, B. (2023). Biochemical, Genotoxic and Histological Implications of Polypropylene Microplastics on Freshwater Fish Oreochromis mossambicus: An Aquatic Eco-Toxicological Assessment. *Toxics*, *11*(3). https://doi.org/10.3390/toxics11030282

Ju, H., Yang, X., Osman, R., & Geissen, V. (2023). Effects of microplastics and chlorpyrifos on earthworms (Lumbricus terrestris) and their biogenic transport in sandy soil. *Environmental Pollution*, *316*(October 2022). https://doi.org/10.1016/j.envpol.2022.120483

Kauanova, S., Urazbayev, A., & Vorobjev, I. (2021). The Frequent Sampling of Wound Scratch Assay Reveals the "Opportunity" Window for Quantitative Evaluation of Cell Motility-Impeding Drugs. *Frontiers in Cell and Developmental Biology*, *9*(March), 1–14. https://doi.org/10.3389/fcell.2021.640972

Khan, A., & Jia, Z. (2023). Recent insights into uptake, toxicity, and molecular targets of microplastics and nanoplastics relevant to human health impacts. *IScience*, *26*(2). https://doi.org/10.1016/j.isci.2023.106061

Kihara, S., Ashenden, A., Kaur, M., Glasson, J., Ghosh, S., van der Heijden, N., Brooks, A. E. S., Mata, J. P., Holt, S., Domigan, L. J., Köper, I., & McGillivray, D. J. (2021). Cellular interactions with polystyrene nanoplastics—The role of particle size and protein corona. *Biointerphases*, *16*(4), 041001. https://doi.org/10.1116/6.0001124

Law, K. L. (2017). Plastics in the Marine Environment. *Annual Review of Marine Science*, *9*(1), 205–229. https://doi.org/10.1146/annurev-marine-010816-060409

Lea, T. (2015). Epithelial Cell Models; General Introduction. In K. Verhoeckx, P. Cotter, I. López-Expósito, C. Kleiveland, T. Lea, A. Mackie, T. Requena, D. Swiatecka, & H. Wichers (Eds.), *The Impact of Food Bioactives on Health: in vitro and ex vivo models* (pp. 95–102). Springer International Publishing. https://doi.org/10.1007/978-3-319-16104-4_9

Lee, J.-H., Kang, J.-C., & Kim, J.-H. (2023). Toxic effects of microplastic (Polyethylene) on fish: Accumulation, hematological parameters and antioxidant responses in Korean Bullhead, Pseudobagrus fulvidraco. *Science of The Total Environment*, *877*(March), 162874. https://doi.org/10.1016/j.scitotenv.2023.162874

Lehner, R., Weder, C., Petri-Fink, A., & Rothen-Rutishauser, B. (2019). Emergence of Nanoplastic in the Environment and Possible Impact on Human Health [Review-article]. *Environmental Science and Technology*, *53*, 1748–1765. https://doi.org/10.1021/acs.est.8b05512

Leibrock, L., Wagener, S., Singh, A. V., Laux, P., & Luch, A. (2019). Nanoparticle induced barrier function assessment at liquid-liquid and air-liquid interface in novel human lung epithelia cell lines. *Toxicology Research*, *8*(6), 1016–1027. https://doi.org/10.1039/c9tx00179d

Li, H., Zhu, L., Ma, M., Wu, H., An, L., & Yang, Z. (2023). Occurrence of microplastics in commercially sold bottled water. *Science of the Total Environment*, *867*(January 2023), 161553. https://doi.org/10.1016/j.scitotenv.2023.161553

Li, Y., Liu, Z., Yang, Y., Jiang, Q., Wu, D., Huang, Y., Jiao, Y., Chen, Q., Huang, Y., &

Zhao, Y. (2021). Effects of nanoplastics on energy metabolism in the oriental river prawn (Macrobrachium nipponense). In *Environmental Pollution* (Vol. 268). https://doi.org/10.1016/j.envpol.2020.115890

Lin, S., Zhang, H., Wang, C., Su, X. L., Song, Y., Wu, P., Yang, Z., Wong, M. H., Cai, Z., & Zheng, C. (2022). Metabolomics Reveal Nanoplastic-Induced Mitochondrial Damage in Human Liver and Lung Cells. *Environmental Science and Technology*, *56*(17), 12483–12493. https://doi.org/10.1021/acs.est.2c03980

Liu, Y. Y., Liu, J., Wu, H., Zhang, Q., Tang, X. R., Li, D., Li, C. S., Liu, Y., Cao, A., & Wang, H. (2023). Endocytosis, Distribution, and Exocytosis of Polystyrene Nanoparticles in Human Lung Cells. *Nanomaterials*, *13*(1). https://doi.org/10.3390/nano13010084

Magrì, D., Sánchez-Moreno, P., Caputo, G., Gatto, F., Veronesi, M., Bardi, G., Catelani, T., Guarnieri, D., Athanassiou, A., Pompa, P. P., & Fragouli, D. (2018). Laser ablation as a versatile tool to mimic polyethylene terephthalate nanoplastic pollutants: Characterization and toxicology assessment. *ACS Nano*, *12*(8), 7690–7700. https://doi.org/10.1021/acsnano.8b01331

Manzi, F., Schlösser, P., Owczarz, A., & Wolinska, J. (2023). Polystyrene nanoplastics differentially influence the outcome of infection by two microparasites of the host Daphnia magna. *Philosophical Transactions of the Royal Society B: Biological Sciences*, *378*(1873). https://doi.org/10.1098/rstb.2022.0013

Meng, F., Harkes, P., van Steenbrugge, J. J. M., & Geissen, V. (2023). Effects of microplastics on common bean rhizosphere bacterial communities. *Applied Soil Ecology*, *181*(March 2022), 104649. https://doi.org/10.1016/j.apsoil.2022.104649

Mikac, L., Rigó, I., Himics, L., Tolić, A., Ivanda, M., & Veres, M. (2023). Surface-enhanced Raman spectroscopy for the detection of microplastics. *Applied Surface Science*, *608*(October 2022). https://doi.org/10.1016/j.apsusc.2022.155239

Miller, P. W., Clarke, D. N., Weis, W. I., Lowe, C. J., & Nelson, W. J. (2013). Chapter Eight - The Evolutionary Origin of Epithelial Cell–Cell Adhesion Mechanisms. In V. Bennett (Ed.), *Functional Organization of Vertebrate Plasma Membrane* (Vol. 72, pp. 267–311). Academic Press. https://doi.org/https://doi.org/10.1016/B978-0-12-417027-8.00008-8

Napper, I. E., & Thompson, R. C. (2020). Plastic Debris in the Marine Environment: History and Future Challenges. *Global Challenges*, *4*(6), 1900081. https://doi.org/10.1002/gch2.201900081

Nasonovs, A., Garcia-Diaz, M., & Bogenhagen, D. F. (2021). A549 cells contain enlarged mitochondria with independently functional clustered mtDNA nucleoids. In *PLoS ONE* (Vol. 16, Issue 3 March). https://doi.org/10.1371/journal.pone.0249047

O'Brien, S., Rauert, C., Ribeiro, F., Okoffo, E. D., Burrows, S. D., O'Brien, J. W., Wang, X., Wright, S. L., & Thomas, K. V. (2023). There's something in the air: A review of sources, prevalence and behaviour of microplastics in the atmosphere. *Science of the Total Environment*, *874*(December 2022), 162193. https://doi.org/10.1016/j.scitotenv.2023.162193

Ozturk, R. C., & Altinok, I. (2020). Interaction of plastics with marine species. *Turkish Journal of Fisheries and Aquatic Sciences*, *20*(8), 647–658. https://doi.org/10.4194/1303-2712-v20_8_07

Peng, L., Fu, D., Qi, H., Lan, C. Q., Yu, H., & Ge, C. (2020). Micro- and nano-plastics in

marine environment: Source, distribution and threats — A review. *Science of the Total Environment*, *698*, 134254. https://doi.org/10.1016/j.scitotenv.2019.134254

Poma, A., Vecchiotti, G., Colafarina, S., Zarivi, O., Aloisi, M., Arrizza, L., Chichiriccò, G., & Di Carlo, P. (2019). In vitro genotoxicity of polystyrene nanoparticles on the human fibroblast hs27 cell line. *Nanomaterials*, *9*(9), 1–13. https://doi.org/10.3390/nano9091299

Pradel, A., Catrouillet, C., & Gigault, J. (2023). The environmental fate of nanoplastics: What we know and what we need to know about aggregation. *NanoImpact*, *29*(October 2022), 100453. https://doi.org/10.1016/j.impact.2023.100453

Ragusa, A., Notarstefano, V., Svelato, A., Belloni, A., Gioacchini, G., Blondeel, C., Zucchelli, E., De Luca, C., D'avino, S., Gulotta, A., Carnevali, O., & Giorgini, E. (2022). Raman Microspectroscopy Detection and Characterisation of Microplastics in Human Breastmilk. *Polymers*, *14*(13), 1–14. https://doi.org/10.3390/polym14132700

Roursgaard, M., Rothmann, M. H., Schulte, J., Karadimou, I., Marinelli, E., & Møller, P. (2022). *Genotoxicity of Particles From Grinded Plastic Items in Caco-2 and HepG2 Cells*. *10*(July). https://doi.org/10.3389/fpubh.2022.906430

Rubio, L., Barguilla, I., Domenech, J., Marcos, R., & Hernández, A. (2020). Biological effects, including oxidative stress and genotoxic damage, of polystyrene nanoparticles in different human hematopoietic cell lines. *Journal of Hazardous Materials*, *398*(May), 122900. https://doi.org/10.1016/j.jhazmat.2020.122900

Saenen, N. D., Witters, M. S., Hantoro, I., Tejeda, I., Ethirajan, A., Van Belleghem, F., & Smeets, K. (2023). Polystyrene Microplastics of Varying Sizes and Shapes Induce Distinct Redox and Mitochondrial Stress Responses in a Caco-2 Monolayer. *Antioxidants*, *12*(3), 739. https://doi.org/10.3390/antiox12030739

Salvia, R., Rico, L. G., Bradford, J. A., Ward, M. D., Olszowy, M. W., Martínez, C., Madrid-Aris, Á. D., Grífols, J. R., Ancochea, Á., Gomez-Muñoz, L., Vives-Pi, M., Martínez-Cáceres, E., Fernández, M. A., Sorigue, M., & Petriz, J. (2023). Fast-screening flow cytometry method for detecting nanoplastics in human peripheral blood. *MethodsX*, *10*(February). https://doi.org/10.1016/j.mex.2023.102057

Sendra, M., Saco, A., Yeste, M. P., Romero, A., Novoa, B., & Figueras, A. (2020). Nanoplastics: From tissue accumulation to cell translocation into Mytilus galloprovincialis hemocytes. resilience of immune cells exposed to nanoplastics and nanoplastics plus Vibrio splendidus combination. *Journal of Hazardous Materials*, *388*(October 2019), 121788. https://doi.org/10.1016/j.jhazmat.2019.121788

Shi, Q., Tang, J., Liu, X., & Liu, R. (2021). Ultraviolet-induced photodegradation elevated the toxicity of polystyrene nanoplastics on human lung epithelial A549 cells. *Environ. Sci.: Nano*, *8*(9), 2660–2675. https://doi.org/10.1039/D1EN00465D

Shi, Q., Tang, J., Wang, L., Liu, R., & Giesy, J. P. (2021). Combined cytotoxicity of polystyrene nanoplastics and phthalate esters on human lung epithelial A549 cells and its mechanism. *Ecotoxicology and Environmental Safety*, *213*, 112041. https://doi.org/10.1016/j.ecoenv.2021.112041

Shi, X., Wang, X., Huang, R., Tang, C., Hu, C., Ning, P., & Wang, F. (2022). Cytotoxicity and Genotoxicity of Polystyrene Micro-and Nanoplastics with Different Size and Surface Modification in A549 Cells. *International Journal of Nanomedicine*, *17*(September), 4509–4523. https://doi.org/10.2147/IJN.S381776

Shi, X., Xu, T., Cui, W., Qi, X., & Xu, S. (2023). Combined negative effects of microplastics and plasticizer DEHP: The increased release of Nets delays wound healing in mice. *Science of the Total Environment*, *862*(November 2022), 160861. https://doi.org/10.1016/j.scitotenv.2022.160861

Shum, T. F., Wang, L., & Chiou, J. (2023). Impact of Plasticizer on the Intestinal Epithelial Integrity and Tissue-Repairing Ability within Cells in the Proximity of the Human Gut Microbiome. *International Journal of Environmental Research and Public Health*, *20*(3). https://doi.org/10.3390/ijerph20032152

Stachowicz, K. (2023). Physicochemical Principles of Adhesion Mechanisms in the Brain. *International Journal of Molecular Sciences*, *24*(6), 5070. https://doi.org/10.3390/ijms24065070

Stock, V., Böhmert, L., Lisicki, E., Block, R., Cara, J., Laura, C., Pack, K., Selb, R., Lichtenstein, D., Voss, L., Henderson, C. J., Zabinsky, E., Sieg, H., Braeuning, A., & Lampen, A. (2019). Uptake and effects of orally ingested polystyrene microplastic particles in vitro and in vivo. *Archives of Toxicology*, *93*(7), 1817–1833. https://doi.org/10.1007/s00204-019-02478-7

Stock, V., Laurisch, C., Franke, J., Dönmez, M. H., Voss, L., Böhmert, L., Braeuning, A., & Sieg, H. (2021). Uptake and cellular effects of PE , PP , PET and PVC microplastic particles. *Toxicology in Vitro*, *70*(September 2020), 105021. https://doi.org/10.1016/j.tiv.2020.105021

Thushari, G. G. N., & Senevirathna, J. D. M. (2020). Plastic pollution in the marine environment. *Heliyon*, *6*(8), e04709. https://doi.org/10.1016/j.heliyon.2020.e04709

Tian, Y., Yang, Z., Yu, X., Jia, Z., Rosso, M., Dedman, S., Zhu, J., Xia, Y., Zhang, G., Yang, J., & Wang, J. (2022). Can we quantify the aquatic environmental plastic load from aquaculture? *Water Research*, *219*(April), 118551. https://doi.org/10.1016/j.watres.2022.118551

Tiseo, I. (2022). Annual production of plastics worldwide from 1950 to 2021. *Statista*, https://www.statista.com/statistics/282732/global-production-of-plastics-since-1950/

Tolardo, V., Magrì, D., Fumagalli, F., Cassano, D., Athanassiou, A., Fragouli, D., & Gioria, S. (2022). In Vitro High-Throughput Toxicological Assessment of Nanoplastics. *Nanomaterials*, *12*(12). https://doi.org/10.3390/nano12121947

van Meerloo, J., Kaspers, G. J. L., & Cloos, J. (2011). Cell Sensitivity Assays: The MTT Assay. In I. A. Cree (Ed.), *Cancer Cell Culture: Methods and Protocols* (pp. 237–245). Humana Press. https://doi.org/10.1007/978-1-61779-080-5_20

van Weert, S., Redondo-Hasselerharm, P. E., Diepens, N. J., & Koelmans, A. A. (2019). Effects of nanoplastics and microplastics on the growth of sediment-rooted macrophytes. *Science of the Total Environment*, *654*, 1040–1047. https://doi.org/10.1016/j.scitotenv.2018.11.183

Wan, E., Tian, D., Sun, Z., & Liu, Y. (2023). The online in situ detection of plastic and its combustion smoke via laser-induced breakdown spectroscopy. *Spectroscopy Letters*, *56*(2), 62–72. https://doi.org/10.1080/00387010.2023.2165505

Wang, Q., Bai, J., Ning, B., Fan, L., & Sun, T. (2020). Effects of bisphenol A and nanoscale and microscale polystyrene plastic exposure on particle uptake and toxicity in human Caco-2 cells. *Chemosphere*, *254*, 126788. https://doi.org/10.1016/j.chemosphere.2020.126788

Woo, J. H., Seo, H. J., Lee, J. Y., Lee, I., Jeon, K., Kim, B., & Lee, K. (2023). Polypropylene nanoplastic exposure leads to lung inflammation through p38-mediated NF-κB pathway due to mitochondrial damage. *Particle and Fibre Toxicology*, *20*(1), 1–17. https://doi.org/10.1186/s12989-022-00512-8

Wu, B., Wu, X., Liu, S., Wang, Z., & Chen, L. (2019). Size-dependent effects of polystyrene microplastics on cytotoxicity and efflux pump inhibition in human Caco-2 cells. *Chemosphere*, *221*, 333–341. https://doi.org/10.1016/j.chemosphere.2019.01.056

Wu, Y., Wang, J., Zhao, T., Sun, M., Xu, M., Che, S., Pan, Z., Wu, C., & Shen, L. (2023). Polystyrene Nanoplastics Lead to Ferroptosis in the Lungs. *Journal of Advanced Research*, *xxxx*. https://doi.org/10.1016/j.jare.2023.03.003

Xu, D., Ma, Y., Han, X., & Chen, Y. (2021). Systematic toxicity evaluation of polystyrene nanoplastics on mice and molecular mechanism investigation about their internalization into Caco-2 cells. *Journal of Hazardous Materials*, *417*(March), 126092. https://doi.org/10.1016/j.jhazmat.2021.126092

Xu, M., Halimu, G., Zhang, Q., Song, Y., Fu, X., Li, Y., Li, Y., & Zhang, H. (2019). Internalization and toxicity: A preliminary study of effects of nanoplastic particles on human lung epithelial cell. *Science of the Total Environment*, *694*, 133794. https://doi.org/10.1016/j.scitotenv.2019.133794

Xu, X., Feng, Y., Han, C., Yao, Z., Liu, Y., Luo, C., & Sheng, J. (2023). Autophagic response of intestinal epithelial cells exposed to polystyrene nanoplastics. *Environmental Toxicology*, *38*(1), 205–215. https://doi.org/10.1002/tox.23678

Yan, L., Yu, Z., Lin, P., Qiu, S., He, L., Wu, Z., Ma, L., Gu, Y., He, L., Dai, Z., Zhou, C., Hong, P., & Li, C. (2023). Polystyrene nanoplastics promote the apoptosis in Caco-2 cells induced by okadaic acid more than microplastics. *Ecotoxicology and Environmental Safety*, *249*(October 2022), 114375. https://doi.org/10.1016/j.ecoenv.2022.114375

Yang, H., Li, X., Guo, M. H., Cao, X., Zheng, X., & Bao, D. (2023). UV-induced microplastics (MPs) aging leads to comprehensive toxicity. *Marine Pollution Bulletin*, *189*(November 2022), 114745. https://doi.org/10.1016/j.marpolbul.2023.114745

Yang, T., & Nowack, B. (2020). A Meta-analysis of Ecotoxicological Hazard Data for Nanoplastics in Marine and Freshwater Systems. *Environmental Toxicology and Chemistry*, *39*(12), 2588–2598. https://doi.org/10.1002/etc.488

Yu, X., Lang, M., Huang, D., Yang, C., Ouyang, Z., & Guo, X. (2022). Photo-transformation of microplastics and its toxicity to Caco-2 cells. *Science of the Total Environment*, *806*, 150954. https://doi.org/10.1016/j.scitotenv.2021.150954

Zabihihesari, A., Khalili, A., Farshchi-Heydari, M. J., Eilaghi, A., & Rezai, P. (2023). Simple microfluidic device for simultaneous extraction and detection of microplastics in water using DC electrical signal. *New Journal of Chemistry*. https://doi.org/10.1039/d2nj06268b

Zhang, H., Zhang, S., Duan, Z., & Wang, L. (2022). Pulmonary toxicology assessment of polyethylene terephthalate nanoplastic particles in vitro. *Environment International*, *162*(January), 107177. https://doi.org/10.1016/j.envint.2022.107177

Zhang, R., Silic, M. R., Schaber, A., Wasel, O., Freeman, J. L., & Sepúlveda, M. S. (2020). Exposure route affects the distribution and toxicity of polystyrene nanoplastics in zebrafish. *Science of the Total Environment*, *724*. https://doi.org/10.1016/j.scitotenv.2020.138065

Zhang, W., Liu, Z., Tang, S., Li, D., Jiang, Q., & Zhang, T. (2020). Transcriptional response provides insights into the effect of chronic polystyrene nanoplastic exposure on Daphnia pulex. *Chemosphere*, *238*, 124563. https://doi.org/10.1016/j.chemosphere.2019.124563

Zhang, Y.-X., Wang, M., Yang, L., Pan, K., & Miao, A.-J. (2022). Bioaccumulation of differently-sized polystyrene nanoplastics by human lung and intestine cells. *Journal of Hazardous Materials*, *439*, 129585. https://doi.org/https://doi.org/10.1016/j.jhazmat.2022.129585

Zhou, L., Wang, R., Liu, Y., Zhang, Y., Zhou, J., Qu, G., Tang, S., & Wang, T. (2022). Plasma-induced conversion of polystyrene nanoplastics in water: Intermediates release, toxicity, and disinfection byproducts formation. *Chemical Engineering Journal*, *433*(P1), 134543. https://doi.org/10.1016/j.cej.2022.134543

Zhu, L., Zhu, J., Zuo, R., Xu, Q., Qian, Y., & AN, L. (2023). Identification of microplastics in human placenta using laser direct infrared spectroscopy. *Science of the Total Environment*, *856*(September 2022), 159060. https://doi.org/10.1016/j.scitotenv.2022.159060

Annexes

Annex 1

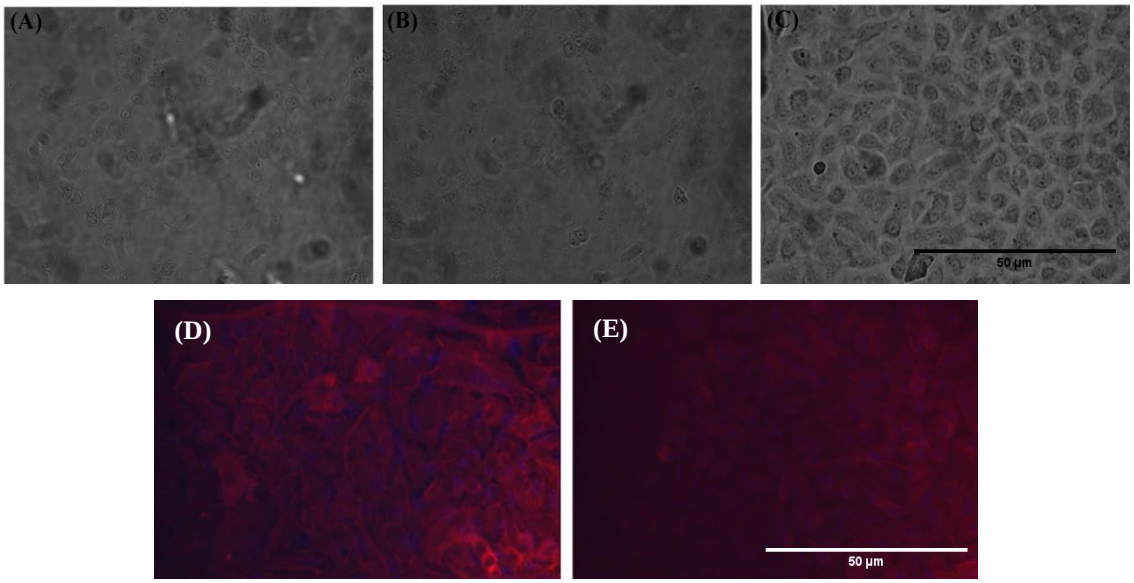

Supplementary figure 1 – Representative images of A549 cells after 72h exposure to 500 *n*m regular PSMPs at a concentration of 0 (A), 1 (B) and 10 μg/mL (C) and 500 *n*m green-fluorescent PSMPs at a concentration of 0 (D), and 1 μg/mL (E). Co-localization of actin (red) and nuclei (blue). Scale bars represent 50 μm. Photos were taken with a Leica DM IL microscope coupled to a Visicam PRO 20C digital camera (ampliation 400x) and analysed with ImageJ version 1.53t using ImageJ software for image overlay.

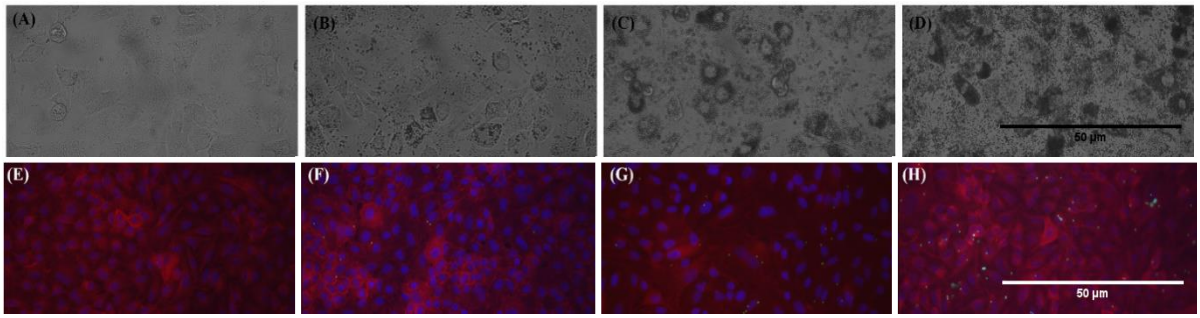

Supplementary figure 2 – Representative images of A549 cells after 72h exposure to 1000 *n*m regular PSMPs at a concentration of 0 (A), 1 (B), 10 (C) and 100 μg/mL (D) and 1000 *n*m green-fluorescent PSMPs at a concentration of 0 (E), 1 (F), 10 (G) and 100 μg/mL (H). Co-localization of actin (red) and nuclei (blue). Scale bars represent 50 μm. Photos were taken with a Leica DM IL microscope coupled to a Visicam PRO 20C digital camera (ampliation 400x) and analysed with ImageJ version 1.53t using ImageJ software for image overlay.

Annex 2

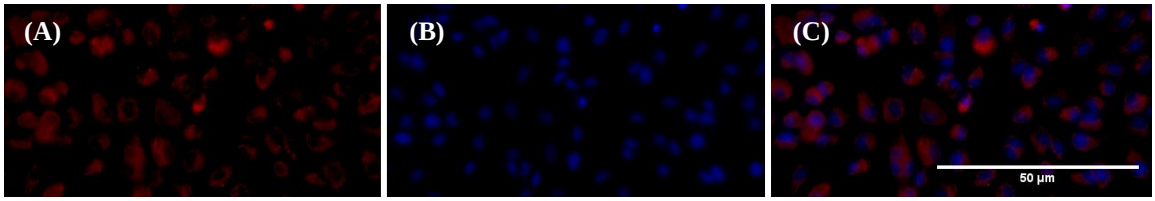

Supplementary figure 3 – Representative images of A549 cells treated with 50 *n*m at 400x ampliation (A-C). Co-localization of mitochondria (red) and nuclei (blue) is evident. The scale bar represents 50 μm. Photos were taken with a Zeiss Axioscope 5 coupled to a Axiocam 202 mono camera and analysed with ImageJ version 1.53t using ImageJ software for image overlay.

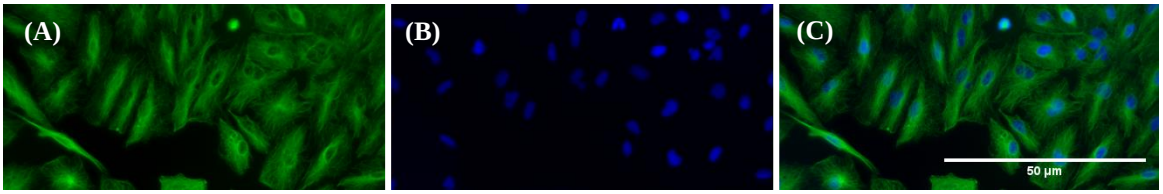

Supplementary figure 4 – Representative images of A549 cells treated with 50 *n*m at 400x ampliation (A-C). Co-localization of alpha-tubulin (green) and nuclei (blue) is evident. The scale bar represents 50 μm. Photos were taken with a Zeiss Axioscope 5 coupled to a Axiocam 202 mono camera and analysed with ImageJ version 1.53t using ImageJ software for image overlay.

Annex 3

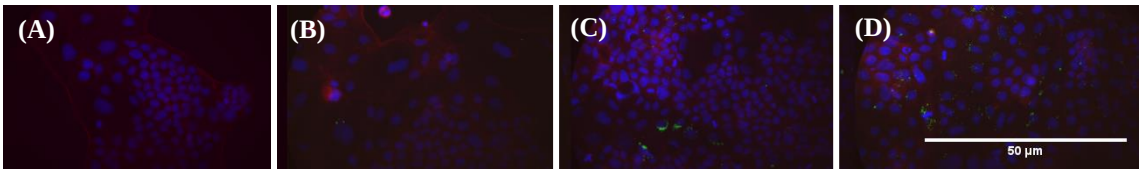

Supplementary figure 5 – Representative images of Caco-2 cells after 72h exposure to 500 *n*m green-fluorescent PSMPs at a concentration of 0 (A), 1 (B), 10 (C) and 100 μg/mL (D). Co-localization of actin (red) and nuclei (blue). The scale bar represents 50 μm. Photos were taken with a Leica DM IL microscope coupled to a Visicam PRO 20C digital camera (ampliation 400x) and analysed with ImageJ version 1.53t using ImageJ software for image overlay.

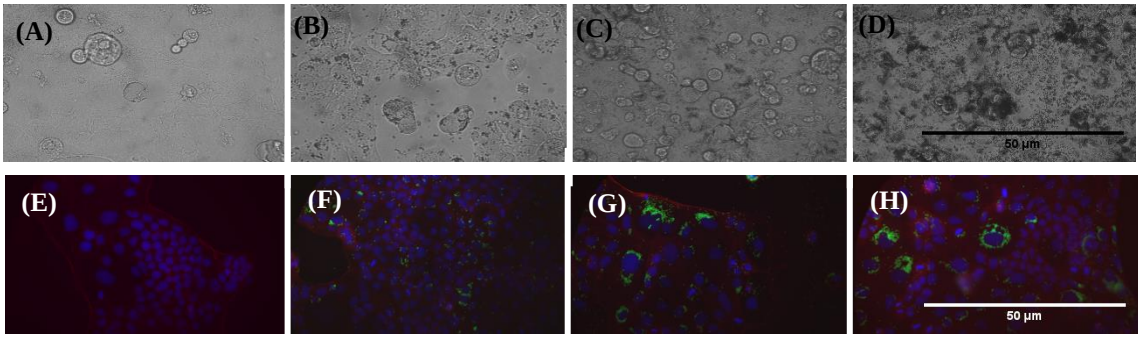

Supplementary figure 6 – Representative images of Caco-2 cells after 72h exposure to 1000 *n*m regular PSMPs at a concentration of 0 (A), 1 (B), 10 (C) and 100 μg/mL (D) and 1000 nm green-fluorescent PSMPs at a concentration of 0 (E), 1 (F), 10 (G) and 100 μg/mL (H). Co-localization of actin (red) and nuclei (blue). The scale bar represents 50 μm. Photos were taken with a Leica DM IL microscope coupled to a Visicam PRO 20C digital camera (ampliation 400x) and analysed with ImageJ version 1.53t using ImageJ software for image overlay.

Annex 4

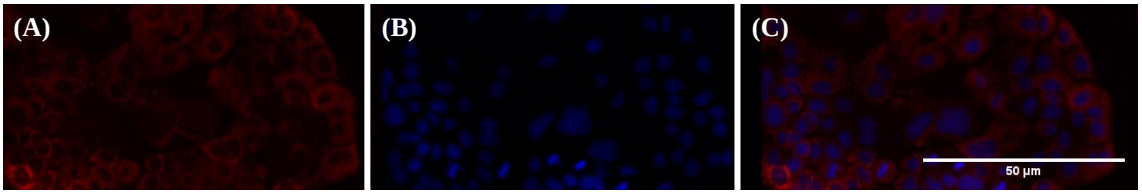

Supplementary figure 7 - Representative images of Caco-2 cells treated with 50 *n*m at 400x ampliation (A-C). Co-localization of mitochondria (red) and nuclei (blue) is evident. The scale bar represents 50 μm. Photos were taken with a Zeiss Axioscope 5 coupled to a Axiocam 202 mono camera and analysed with ImageJ version 1.53t using ImageJ software for image overlay.

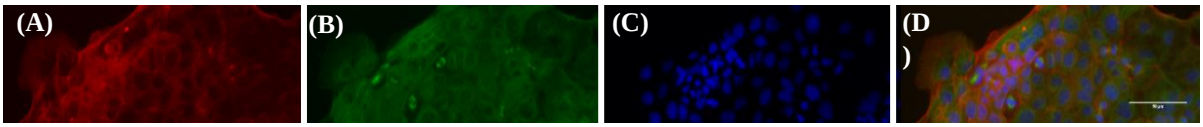

Supplementary figure 8 – Representative images of Caco-2 cells treated with 50 *n*m at 400x ampliation (A-C). Co-localization of alpha-tubulin (green), actin (red) and nuclei (blue) is evident. The scale bar represents 50 μm. Photos were taken with a Zeiss Axioscope 5 coupled to a Axiocam 202 mono camera and analysed with ImageJ version 1.53t using ImageJ software for image overlay.